

POLITECNICO DI MILANO

Scuola di Ingegneria Industriale

Corso di Laurea Specialistica in
Ingegneria Energetica



Study of a High-Temperature Thermal
Energy Storage for a Hybrid Solar-Gas Power Plant

Relatore: Prof. Carlo ORTOLANI

Co-relatore: Ing. Vincenzo CASAMASSIMA

Tesi di Laurea di:

Cristian ZANABONI Matr. 755288

Anno Accademico 2011 - 2012

Index

Index of Figures.....	IV
Index of Tables.....	VIII
Abstract.....	IX
Sommario.....	X
Chapter 1	
Electricity production from the sun.....	1
1.1 Electricity generation in the world.....	1
1.2 Non concentrating solar power systems.....	3
1.2.1 Photovoltaic system.....	3
1.2.2 Solar pond.....	6
1.2.3 Solar updraft tower.....	7
1.3 Concentrating solar power systems.....	9
1.3.1 Parabolic trough.....	10
1.3.2 Linear Fresnel reflector.....	12
1.3.3 Parabolic dish.....	13
1.3.4 Solar power tower.....	15
1.4 Perspectives for CSP plants.....	18
1.4.1 CSP plants installed.....	19
1.4.2 CSP plants under construction.....	21
1.4.3 Announced CSP plants.....	22
Chapter 2	
Design of the reference plant.....	25
2.1 Description of the hybrid solar-gas technology.....	25
2.1.1 Comparison with a solar Rankine cycle.....	26
2.2 Operating hybrid solar-gas power plants.....	26
2.2.1 SOLGATE project.....	27
2.2.2 AORA's solar flower tower.....	28
2.2.3 THEMIS solar power plant.....	30
2.2.4 SOLUGAS project.....	31
2.3 The HYCOSOL proposal.....	32
2.4 Power plant components.....	33
2.4.1 Gas turbine.....	33
2.4.2 Solar receiver.....	35

2.4.3 Solar field and solar power tower.....	39
2.4.4 Thermal energy storage.....	47

Chapter 3

Thermal storage overview.....49

3.1 Introduction.....	49
3.2 Heat storage media.....	50
3.2.1 Sensible heat storage: concrete.....	51
3.2.2 Sensible heat storage: thermal oil.....	52
3.2.3 Sensible heat storage: molten salts.....	52
3.2.4 Sensible heat storage: steam.....	54
3.2.5 Latent heat storage.....	56
3.2.6 Thermochemical storage.....	60
3.3 Storage system in the power plant.....	62
3.3.1 Modular approach for concrete storage.....	62
3.3.2 Two tank indirect system.....	63
3.3.3 Two tank direct system.....	65
3.3.4 Single thermocline tank system.....	65
3.4 Tank design.....	67
3.4.1 Cylindrical tank.....	68
3.4.2 Conical tank.....	72

Chapter 4

Storage medium choice.....75

4.1 Criteria of comparison.....	75
4.2 Storage media proposed.....	76
4.2.1 Molten salts.....	76
4.2.2 Liquid sodium.....	77
4.2.3 Liquid lead.....	80
4.2.4 Ceramic materials.....	84
4.3 Comparison between the storage media proposed.....	87
4.3.1 Results of the comparison.....	91

Chapter 5

Design of the thermal energy storage.....93

5.1 Description of the software used.....	93
5.1.1 Process CAD (LegoPC).....	94
5.2 General parameters of the TES.....	95
5.2.1 TES volume.....	95
5.2.2 Charging process.....	97

5.3 Design of the storage parameters.....	99
5.3.1 Number of channels and their diameter.....	100
5.3.2 Storage length.....	105
5.3.3 Storage response to thermal transients.....	109
5.4 Storage thermal insulation.....	117
5.4.1 Storage thermal losses.....	117
Chapter 6	
Thermal energy storage integration into the plant.....	121
6.1 Plant configuration.....	121
6.1.1 Power plant operation at nominal power.....	121
6.1.2 Power plant operation without storage charging.....	122
6.1.3 Power plant operation with storage discharge.....	123
6.1.4 Power plant operation with bypass line.....	124
6.1.5 Choice of the solar power plant operation mode.....	125
6.2 Power plant performance improvements.....	126
6.2.1 Increase of solar share.....	127
6.2.2 Fuel saving.....	129
6.2.3 Carbon dioxide emissions reduction.....	131
6.3 Storage behavior during solar transients.....	133
6.3.1 Storage discharge after a complete charge.....	135
6.3.2 Storage discharge after three quarters of the charge.....	136
6.3.3 Storage discharge after half of the charge.....	138
6.3.4 Storage discharge after a quarter of the charge.....	139
Conclusions and future developments.....	141
List of acronyms.....	145
Bibliography and references.....	146

Index of Figures

Figure 1.1: Fuel shares of electricity generation.....	6
Figure 1.2: CO ₂ abatement for different types of scenario.....	7
Figure 1.3: Map of the most appropriate areas for solar thermal power plants... ..	8
Figure 1.4: Global annual photovoltaic production by region.....	10
Figure 1.5:Electrical power production concept using salt-gradient ponds.....	12
Figure 1.6: Schematic overview of solar tower principle.....	13
Figure 1.7: Different types of CSP systems: a)Parabolic through b)Fresnel reflector c)Parabolic dish d)Solar tower.....	18
Figure 1.8: Scheme of a parabolic through collector.....	20
Figure 1.9: Albengoa Solar's Solnova 1 (50 MWe).....	22
Figure 1.10: AREVA Solar's Kimberlina Plant in Bakersfield, California.....	24
Figure 1.11: Components of a parabolic dish generator.....	27
Figure 1.12: Comparison between a volumetric receiver (left) and a tubes receiver (right).....	29
Figure 1.13: Picture of a solar power tower.....	30
Figure 1.14: Aerial view of the PS10 and PS20 power tower near Seville.....	31
Figure 2.1: Scheme of the SOLGATE test system.....	27
Figure 2.2: External view of the SOLGATE test plant at CESA 1.....	28
Figure 2.3: picture of the AORA's solar flower tower.....	29
Figure 2.4: Aerial photo of the Themis solar tower.....	30
Figure 2.5: Scheme showing the principle of the thermodynamic cycle PEGASE installed at the top of the Themis tower.....	31
Figure 2.6: Hybrid solar-gas turbine flow diagram.....	32
Figure 2.7: Conventional Siemens SGT800 gas turbine.....	34
Figure 2.7: Conventional Siemens SGT800 gas turbine.....	34
Figure 2.8: Adsorption and heat transfer of tubular and volumetric receiver.....	36
Figure 2.9: Schematic view of the low temperature module.....	37
Figure 2.10: Scheme of the high temperature module.....	38
Figure 2.11: Solar irradiation during vernal equinox at latitude of 35°N.....	40
Figure 2.12: Layout comparison between north field and surrounding field.....	41
Figure 2.13: Concept of a solar driven combined cycle plant with SCOT technology.....	43
Figure 2.14: Variation of the power output in function of the pressure drop.....	46
Figure 3.1: The use of thermal energy storage in a CSP plant to shift electricity output from morning off-peak to evening on-peak demand.....	50

Figure 3.2: Specific heat capacity as a function of total tube length for different thermal conductivities (λ , W/mK) and distance of tubes (r_a , cm).....	51
Figure 3.3. Molten salt power tower system schematic at Solar Two.....	53
Figure 3.4: Principle of steam accumulator heat storage.....	55
Figure 3.5: Schematic system of PS10 plant.....	55
Figure 3.6: Theoretical temperature distribution in a PCM-TES for SEGS, one PCM (left), five PCMs (right).....	56
Figure 3.7: Number of tubes needed in PCM volume depending on heat conductivity of PCM for three different values of average volume specific power.....	57
Figure 3.8: Bundle of capsules filled with PCM before integration into pressure vessel.....	58
Figure 3.9: Effective thermal heat conductivity of PCM/graphite composite dependent on temperature for various compositions.....	59
Figure 3.10: Storage made of PCM and compressed graphite.....	59
Figure 3.11: Calculated results for time needed to charge storage system with various fin materials and fin thicknesses.....	60
Figure 3.12: Schematic of generalized thermochemical storage cycle for CSP technologies.....	61
Figure 3.13: Basic storage (left), modular charging concept (center), modular discharging concept (right).....	63
Figure 3.14: Schematic of parabolic trough power plant with indirect two tank, molten salt thermal storage.....	64
Figure 3.15: Power plant with two tank direct storage.....	65
Figure 3.16: Direct thermocline thermal energy storage schematic.....	67
Figure 3.17: Schematic of low temperature carbon steel storage tank.....	68
Figure 3.18: Schematic of insulated high temperature storage tank.....	69
Figure 3.19: Costs for direct two tank thermal energy storage.....	71
Figure 3.20: Schematic of a conical storage tank [SERI, 1985].....	72
Figure 4.1: From the top: Sodium thermal conductivity, heat capacity and density.....	78
Figure 4.2: From the top: lead thermal conductivity, heat capacity and density.....	81
Figure 4.3: From the top: LBE thermal conductivity, heat capacity and density.....	83
Figure 4.4: From the top: SiC thermal conductivity, heat capacity and density.....	85
Figure 4.5: Storage unit used at the Jülich solar plant.....	86
Figure 4.6: Example of a TES using magnesia as storage medium. In this figure helium is used instead of air.....	87
Figure 4.7: Thermal conductivity of the materials in function of the temperature.....	88
Figure 4.8: Thermal diffusivity of the materials in function of the temperature.....	89

Figure 4.9: Volumetric heat capacity of the materials in function of the temperature.....	90
Figure 4.10: Specific volume of the materials.....	91
Figure 5.1: LegoPC graphic interface.....	94
Figure 5.2: Translation of the component link into a non-linear equation system	95
Figure 5.3: Variation of the air flow recirculated in function of the time required for the charging process.....	98
Figure 5.4: Variation of the power required by the fan in function of the air flow rate.....	99
Figure 5.5: Scheme of the thermal storage and parameters describing the geometry.....	100
Figure 5.6: Air velocity in function of channels number and of channels diameter.....	101
Figure 5.7: Channels number in function of channels diameter. The darker the color, the lower is the air velocity.....	102
Figure 5.8: Storage pressure drop for four channel diameter.....	106
Figure 5.9: Storage length in function of the channels number and of their diameter.....	108
Figure 5.10: From the top: profile of the air temperature (in Kelvin) at the storage outlet during the discharging process for a storage with a 0.015 m, 0.02 m, 0.025 m, 0.03 m diameter channels.....	111
Figure 5.11: From the top: profile of the wall temperature (in Kelvin) at the storage outlet during the discharging process for a storage with a 0.015 m, 0.02 m, 0.025 m, 0.03 m diameter channels.....	113
Figure 5.12: Air temperature profile inside the storage at 1 hour and 2 hours after the beginning of the discharging process.....	116
Figure 6.1: Scheme of the solar power plant operating at nominal power.....	122
Figure 6.2: Scheme of the solar power plant without storage charge.....	123
Figure 6.3: Scheme of the solar power plant operation with storage discharge	124
Figure 6.4: Scheme of the solar power plant operation with bypass line activated.....	125
Figure 6.5: Control logic scheme that determines the proper mode of operation of the solar power plant.....	126
Figure 6.6: Average annual solar share for the power plant with and without TES.....	128
Figure 6.7: Specific fuel consumption in mid load and base load operations for the three reference plants.....	130
Figure 6.8: Specific CO ₂ emissions in mid load and base load operations for the three reference plants.....	132

Figure 6.9: Scheme of the storage configuration used on the LegoPC software for simulating the charging and discharging processes.....	134
Figure 6.10: Air temperature (measured in Kelvin) at the storage outlet during the discharging process, starting from a completely charged storage.....	136
Figure 6.11: Air temperature (measured in Kelvin) at the storage outlet during the discharging process, starting from a storage that has been charged for three quarters of the nominal charging time.....	137
Figure 6.12: Air temperature (measured in Kelvin) at the storage outlet during the discharging process, starting from a storage that has been charged for half of the nominal charging time.....	138
Figure 6.13: Air temperature (measured in Kelvin) at the storage outlet during the discharging process, starting from a storage that has been charged for half of the nominal charging time.....	139

Index of Tables

Table 1.1: Biggest photovoltaic power plants in the world.....	6
Table 1.2: Comparison between CSP technologies.....	19
Table 1.3: Global installed CSP plants.....	20
Table 1.4: Global CSP plants under construction.....	21
Table 1.5: Announced CSP plants in the U.S.....	23
Table 2.1: Technical specifications of the SGT-800 gas turbine.....	35
Table 3.1. Liquid Candidate Storage Media for SEGS Plants.....	52
Table 3.2. Price of nitrate salts.....	54
Table 3.3: PCM Candidate Storage Media for SEGS Plants.....	57
Table 3.4: Component costs for two tank molten salt storage system.....	70
Table 4.1: Properties of sodium, NaK and Potassium.....	79
Table 4.2: Characteristics of the proposed storage media.....	92
Table 5.1: Channels parameters in function of the air velocity and channels diameter.....	104
Table 5.2: Minimum storage length and pressure drop for different channels configurations.	109
Table 5.3: Parameters of the TES.....	117
Table 5.4: Storage thermal losses.....	119
Table 6.1: Composition of natural gas.....	131

Abstract

Despite the attention toward solar thermal power generation systems is grown up in the last decade, the hybrid open solar Brayton cycle remains a underrated but promising technology. In particular, only few small size projects have been made operative, but have demonstrated the feasibility of using a solar tower to heat the pressurized air flow of a gas turbine. However, all these projects have never been integrated with a thermal energy storage system.

Purpose of this master thesis work is the creation of a model for optimizing the design of the thermal energy storage. First of all, the reference power plant, where the storage should work, is determinate, in order to know the boundary conditions of operation.

After that, the storage medium is selected between some candidate materials, taking into account the maximum operating temperature and the specific volume, in order to contain the costs.

Finally the storage model is created and its parameters are optimized for obtaining a high heat transfer coefficient and low pressure drops. In particular, the charging and discharging processes are simulated for several combination of parameters and the most suitable are selected.

Lastly, the improvements due to the storage installation into the solar power plant are calculated, especially the increase of solar share, the fuel saving, the reduction of carbon dioxide emissions and the storage response to solar transients that happens after different charging times.

Keywords: Thermal energy storage; Solar thermal power plant; Solar Brayton cycle; Hybrid gas-solar turbine power plant.

Sommario

Nonostante l'attenzione verso il solare termodinamico per la generazione di energia elettrica sia andata crescendo nell'ultimo decennio, l'utilizzo di un ciclo Brayton ibrido solare-gas rimane un'opzione sottovalutata, ma molto promettente. A differenza di tutte le centrali solari esistenti, le quali utilizzano un ciclo Rankine a vapore acqueo per produrre energia elettrica, un ciclo ibrido Brayton ha la possibilità di lavorare con un'efficienza maggiore, quindi, a pari potenza prodotta, il campo specchi, che è il componente più costoso di una centrale solare, può essere ridimensionato. Inoltre, il calore disponibile all'uscita dalla turbina, presente sotto forma di gas di scarico caldi, può essere utilizzato per alimentare un ciclo a vapore a recupero sottostante e incrementare ulteriormente il rendimento totale, oppure può essere usato per alimentare processi di dissalazione o per far funzionare l'impianto in assetto cogenerativo. Dato che il fluido termovettore deve essere per forza aria compressa, la temperatura massima del ricevitore solare non è limitata, a differenza degli impianti solari che lavorano con sali nitrati od olio diatermico, ma lo scambio termico all'interno di esso è scadente a causa della bassa densità dell'aria, quindi sono richieste ampie superfici di scambio termico o l'utilizzo di costosi ricevitori volumetrici. Inoltre, dato che il consumo di acqua è praticamente nullo, questa tecnologia può essere installata anche in territori aridi e desertici, dove l'irradiazione solare annua è molto elevata, ma c'è scarsità di acqua. L'energia elettrica prodotta in queste zone può poi essere trasportata in altre dove i consumi sono elevati per mezzo di linee elettriche a corrente continua ad alta tensione. Infine i tempi di avviamento di un impianto turbogas sono molto brevi (nell'ordine di 20-30 minuti) e permettono di avviare l'impianto solo quando è presente la radiazione solare e di spegnerlo quando essa viene a mancare.

In questo tipo di impianti l'aria, all'uscita del compressore, è mandata in un ricevitore collocato in cima a una torre solare, dove centinaia di eliostati posizionati a terra riflettono e concentrano la radiazione solare, ed è riscaldata fino a una temperatura all'incirca di 800-900 °C. A questo punto l'aria è mandata in camera di combustione e, grazie all'iniezione di combustibile (ad esempio il gas naturale o il biogas), raggiunge una temperatura dell'ordine di 1300-1400 °C ed è espansa in turbina, producendo potenza elettrica. Il ciclo termodinamico è paragonabile a quello di un turbogas tradizionale, ad eccezione delle perdite di carico aggiuntive dovute dal ricevitore solare, e così è anche il rendimento di primo principio. La presenza della camera di combustione permette di mantenere la potenza elettrica generata costante, anche se la radiazione solare varia nel tempo o è totalmente assente (per esempio di notte). In questo modo la rete elettrica è più stabile e l'impianto può produrre energia elettrica anche di

notte o per lunghi periodi di assenza di sole a differenza della più tradizionale tecnologia fotovoltaica. Comunque, l'installazione di un sistema di accumulo termico è preferibile, in modo da mantenere costante la temperatura d'ingresso in camera di combustione e allungare il periodo di produzione oltre il tramonto senza aumentare il consumo di combustibile.

I primi prototipi di turbine a gas ibride risalgono all'inizio degli anni 2000, quando fu avviato il progetto SOLGATE alla Plataforma Solar di Almeria. A questo progetto, che dimostrò la realizzabilità della tecnologia, seguirono la costruzione in Israele dell'“AORA's solar flower tower”, che è il primo impianto costruito partendo da zero, l'avvio del progetto PEGASE in Francia, che è il primo prototipo capace di produrre più di 1 MW_{el}, e il futuro avviamento del progetto SOLUGAS, che sarà il più grosso impianto di questo tipo mai realizzato. In quest'ottica si inserisce la proposta per il progetto europeo HYCOSOL, il cui scopo consiste nello studio e nella dimostrazione di soluzioni tecniche per la produzione di energia elettrica da un impianto turbogas ibrido gas-solare da 50 MW_{el} collocato alla latitudine di 35 °N. In particolare questa tesi si occupa di creare un modello per lo studio del sistema di accumulo termico di questo impianto al variare dei principali parametri di progetto.

Il primo passo consiste nel determinare le caratteristiche dell'impianto in cui l'accumulo termico dovrà lavorare. In particolare devono essere determinati il tipo di turbina, il tipo di ricevitore solare in cui l'aria viene riscaldata, e il tipo e le dimensioni del campo specchi, della torre solare e dei tubi di collegamento. Successivamente vengono analizzate le attuali tecnologie per l'accumulo termico in impianti solari, come ad esempio l'impiego di olio diatermico o di sali nitrati fusi o di vapore acqueo, ma risultano essere inadatte per l'accumulo termico ad alte temperature, così è necessario trovare altri materiali adatti allo scopo.

Tra i materiali studiati i più importanti sono i metalli liquidi, come ad esempio il sodio, il piombo e la lega piombo-bismuto, e i materiali ceramici che permettono il contatto diretto con l'aria eliminando l'obbligo di usare costosi tubi fatti da leghe di nickel e la possibilità di utilizzare un sistema rigenerativo come gli ossidatori termici rigenerativi impiegati negli impianti industriali. La scelta del materiale più adatto si basa sul confronto tra le proprietà termodinamiche dei materiali candidati, come ad esempio la conduttività termica, la diffusività termica, la densità e il calore specifico, la massima temperatura che possono raggiungere e la loro pericolosità, ad esempio l'infiammabilità e la tossicità. Il sistema di accumulo viene caricato tramite una portata d'aria che all'uscita è reimpressa nella torre solare, dove viene riscaldata insieme alla portata d'aria che poi finirà nella camera di combustione, e poi mandata all'ingresso del sistema di accumulo.

Una volta scelto il tipo di materiale con cui è fatto l'accumulo termico si può creare il modello sul software LegoPC. Alcuni parametri del sistema di accumulo vengono calcolati prima per semplificarne lo studio. Tra di essi c'è il volume totale, che influenza l'energia termica massima che può essere accumulata, e la portata d'aria necessaria per caricare l'accumulo, che influenza la durata del processo di carica e la potenza del ventilatore necessaria per ricircolare l'aria nella torre solare. A questo punto si possono ottimizzare i parametri geometrici del sistema di accumulo, ma prima devono essere correlati tra loro attraverso un sistema di equazioni. I parametri fondamentali sono il numero di canali in cui passa l'aria e il loro diametro interno, che sono collegati con la portata massica dell'aria in ingresso e influenzano la velocità dell'aria e quindi le perdite di carico distribuite e il coefficiente di scambio convettivo. La lunghezza dei canali è un altro parametro importante perché influenza sia le perdite di carico totali sia la formazione di un termoclino all'interno del sistema di accumulo, infatti canali più lunghi implicano perdite di carico più grandi, ma anche un termoclino più ripido e quindi una temperatura dell'aria all'uscita durante la fase di scarica più elevata.

Dopo una scrematura primaria di questi parametri, il modello costruito simula l'andamento nel tempo della temperatura all'uscita dell'aria e del materiale ceramico sia in fase di carica sia in fase di scarica. A questo punto vengono scelti i valori del numero di canali, del loro diametro e della loro lunghezza che offrono un comportamento più adeguato.

Per concludere viene progettato il sistema di isolamento termico dell'accumulo e ne viene calcolata l'efficienza termica nel peggior caso possibile, ossia quando il sistema di accumulo è alla sua massima temperatura operativa e non viene utilizzato per 24 ore e la radiazione solare incidente è nulla.

Per ultimo viene mostrato come il sistema di accumulo di energia termica è inserito nella centrale solare e come possa funzionare a seconda della intensità della radiazione solare, in particolare nei casi di accumulo carico, fase di carica dell'accumulo, fase di scarica dell'accumulo e accumulo esaurito.

Inoltre vengono illustrati i benefici dovuti all'utilizzo di un accumulo termico, calcolando, per tre diversi impianti (una tradizionale turbina a gas, un impianto solare senza accumulo termico e un impianto solare dotato dell'accumulo progettato), il contributo dato dall'energia solare alla produzione di energia elettrica, noto anche come “solar share”, il consumo specifico di combustibile per produrre 1 kWh_{el} e le emissioni di anidride carbonica causate dalla produzione di 1 kWh_{el}. Questi valori sono calcolati sia nel caso l'impianto funzioni in carico base, ossia ininterrottamente per 24 ore, sia nel caso l'impianto lavori a medio carico, ossia venga avviato alle 6 di mattina e venga spento alle 22. Inoltre viene tenuto conto della irradiazione media solare a seconda del mese in cui l'impianto funziona e della variazione della temperatura dell'aria ambiente lungo l'anno, la quale influenza il rendimento del ciclo.

Infine viene simulato il funzionamento del sistema di accumulo in risposta a dei transitori solari che avvengono durante la sua fase di carica. In questi casi viene rilevata la temperatura dell'aria all'uscita dell'accumulo dopo che la fase di carica è stata interrotta ad un determinato istante.

Parole chiave: Sistema di accumulo termico; Solare termodinamico; Ciclo Brayton solare; Turbogeneratore ibrido gas-solare.

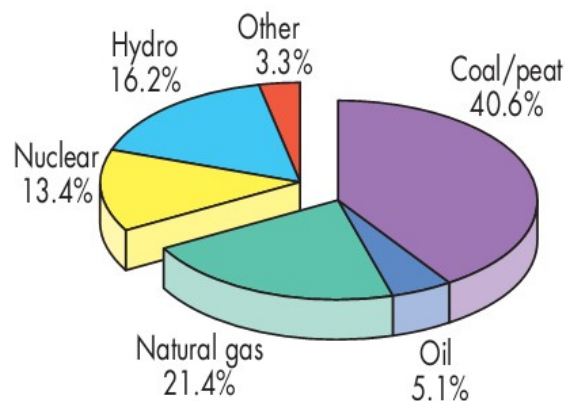
Chapter 1

Electricity production from the sun

This chapter introduces the various technologies for the production of electricity from solar power.

1.1 Electricity generation in the world

As seen in figure 1.1, the greatest contribution (80.5%) to electricity generation in the world is given by fossil fuels (like coal, natural gas and oil) and nuclear energy, which are non-renewable sources. The remaining 19.5% is given by renewable energy, mainly by hydroelectric power that has been used since the Industrial Revolution thanks to its flexibility and its low and stable power costs. Other renewable sources include wind power, which is the fastest growing energy sources in the world due to its cleanliness and abundance[1], geothermal power, biofuels and, with a little share, solar power.



20 055 TWh

Figure 1.1: Fuel shares of electricity generation[2].

The continuous increase in energy demand, in combination with the overexploitation of fossil fuels during the last century that is leading to the depletion of their reserves, results in an electricity price fluctuation.

Another important effect of the use of fossil fuels for electricity generation is the emission of CO₂ and other greenhouse gases (for example CH₄, N₂O, O₃) into the atmosphere. Despite the correlation between planet temperature and CO₂ concentration in atmosphere has not been demonstrated scientifically, there are too many evidences that point on this direction, so it's necessary to avoid its emission in order to prevent climate changes.

A solution to contain these problems consists in the diversification of the electricity generation mix, with an increase of the renewable energy share. In figure 1.2 is shown the expected CO₂ emission reduction for different types of scenario and different types of technology. An important share of the CO₂ emission reduction is represented by the use of renewable energies.

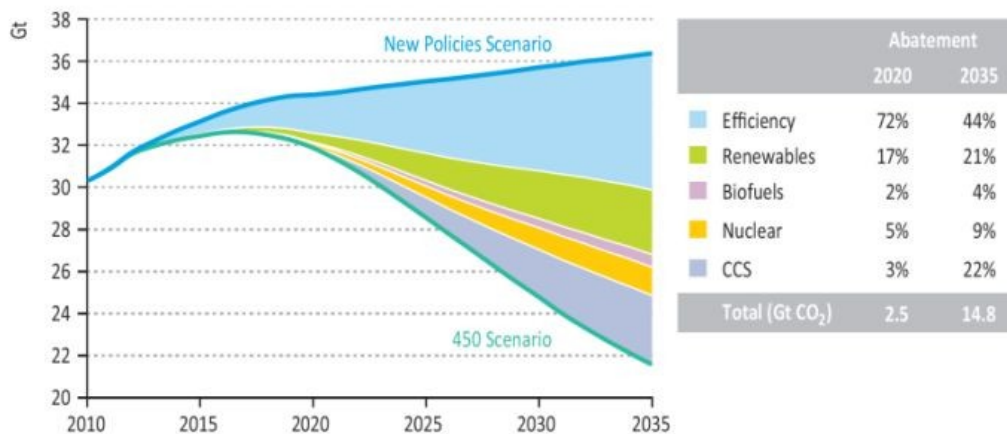


Figure 1.2: CO₂ abatement for different types of scenario[3].

Among all the renewable resources, the solar power seems to have a great potential due to the fact that this technology is at the beginning of its evolution and there is still room for cost-reduction and performance improvement. It also have several advantages compared with the other renewable resources:

- It can produce electricity during sunny hours, when the grid demand is higher.
- It can exploit desert lands and create work in relatively poor countries.
- It is available everywhere in the planet.

On the other hand it has also some disadvantages:

- Unlike other renewable resources, for example wind energy or tidal energy, it cannot produce electricity during the night.
- It has an high installation cost.
- Despite it is available everywhere in the planet, the main potential is in the sun belt area (from latitudes 35°N to 35°S, see figure 1.3), where the electricity consumption is low.

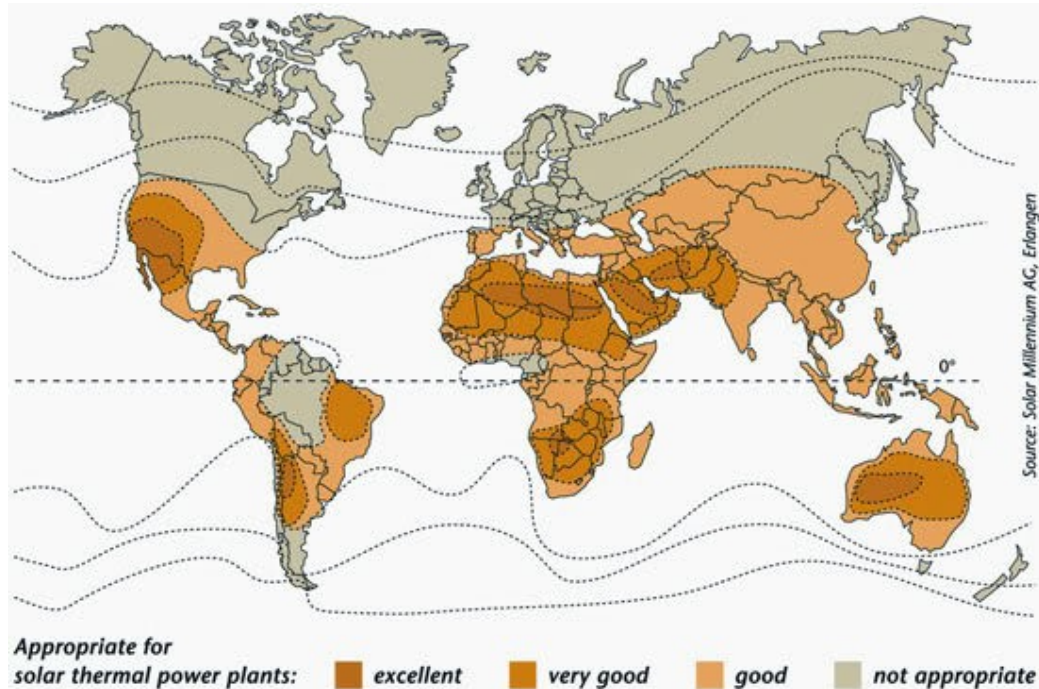


Figure 1.3: Map of the most appropriate areas for solar thermal power plants.

However, according to a 2011 projection by the International Energy Agency (IEA), solar power generators may produce most of the world's electricity within 50 years, dramatically reducing the emissions of greenhouse gases that harm the environment [4].

The technologies for converting solar energy into electricity can be divided in two categories: non concentrating solar power systems and concentrating solar power systems.

1.2 Non concentrating solar power systems

Non concentrating solar power systems can collect both direct and diffuse solar radiation, but they need a larger collecting surface in order to receive the same thermal power of a concentrating solar system.

1.2.1 Photovoltaic system

A photovoltaic system converts solar radiation directly into electricity without the need of a thermodynamic cycle, so the conversion efficiency is not limited by the Carnot cycle efficiency.

A solar cell is made of a thin wafer consisting of a an ultra-thin layer of phosphorus-doped (N-type) silicon on top of a thicker layer of boron-doped (P-type) silicon. When the photons, which compose the sunlight, hit the solar cell, some of them pass through the cell or are reflected, others are absorbed. In this last case the energy of the photon is transferred to an electron in an atom of the cell and, if the energy of the photon is higher than the energy gap of the semiconductor material, the electron escapes from its normal position, causing the formation of a hole. The excess electrons in the n-type material flow to the p-type, and the holes thereby vacated during this process flow to the n-type, creating an electric field at the junction surface. This field causes the electrons to jump from the semiconductor out toward the surface and make them available for the electrical circuit, meanwhile the holes move in the opposite direction, toward the positive surface, where they await incoming electrons.

Generally a solar cell has a low voltage output, so it's necessary to link several cells in series and in parallel to achieve the voltage and the electrical power required. An inverter must be installed to convert the direct current (DC) generated by the photovoltaic cell into alternate current (AC).

To contain the cost caused by the use of ultra-pure silicon, a thin film photovoltaic cell has been developed, so the diminution of the thickness of the cell implies a reduction of the quantity of silicon used. This technology consists in the chemical vapor deposition onto glass or a flexible substrate of a photoactive material, generally amorphous silicon, cadmium telluride or gallium arsenide.

However this second generation technology requires rare metals, like gallium or tellurium, and toxic metals, like arsenic or cadmium, and, moreover, their efficiency is lower than the silicon cells.

The European Photovoltaic Industry Association (EPIA) estimates that global cumulative installed photovoltaic capacity totaled nearly 67.4 GW. The approximately 27.7 GW of additional capacity installed in 2011 constitutes a 67% increase over the 16.6 GW installed in 2010, for a 69% increase in global cumulative installed PV capacity[5]. Figure 1.4 shows the annual production of photovoltaic cells by region.

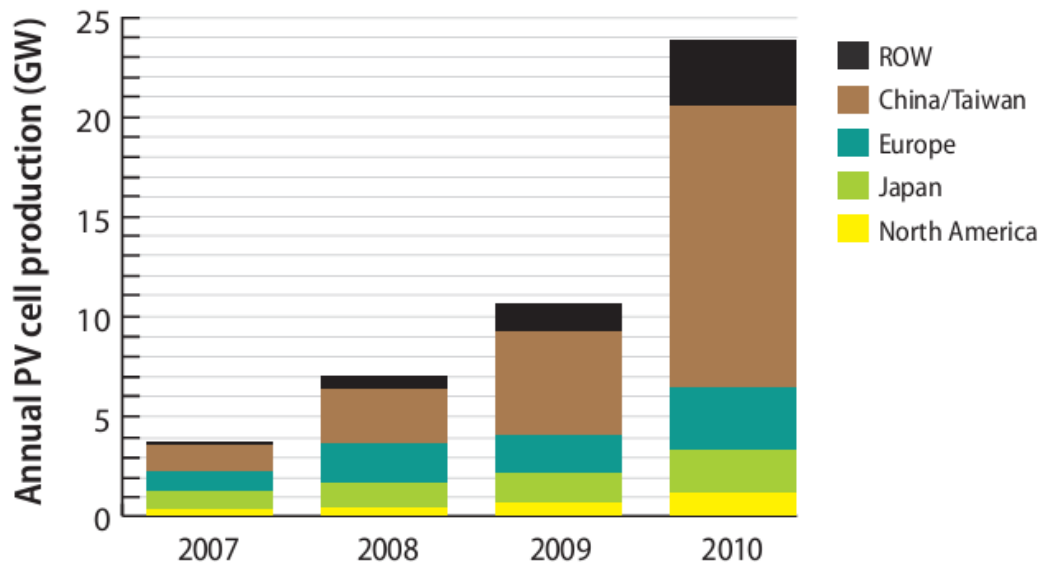


Figure 1.4: Global annual photovoltaic production by region[5].











The applications of photovoltaic cells can be divided in two groups:

- *Stand-alone solar electric systems*: these systems are typical of rural zones, water pumping and telecommunications and are designed to operate independent of the electric utility grid. It's necessary to install a battery backup to ensure the operation even at night.
- *Grid connected solar electric systems*: the excess power generated by these systems is injected into the grid. No battery backup is installed since the electricity can be bought from the grid, but it's necessary to install an inverter to convert the electricity produced by the photovoltaic cell in alternate current.

The efficiency of a photovoltaic cell decreases with the increase of its temperature, so a photovoltaic cell installed in an equatorial zone could produce less energy than one installed in a less insulated area.

Photovoltaic cells are principally used to supply electricity to small consumer and only few plants have been built. Table 1.1 shows the most important power plants in the world, bearing in mind that the Agua Caliente Solar Project (Arizona, 200 MW), the Golmund Solar Park (China, 200 MW) and the Perovo Solar Park (Ukraine, 100 MW) are under construction.

Table 1.1: Biggest photovoltaic power plants in the world.

	Country	Name	Capacity (MW)	Owner	Module type	Grid connection
1.		Sarnia	92*	Enbridge	CdTe	2010
2.		Montalto di Castro	84	Sunpower	c-Si	2011
3.		Finsterwalde I, II & III	83	Q-Cells	c-Si	2010
4.		Rovigo	70	First Reserve	c-Si	2010
5.		Olmedilla de Alarcón	60	Nobesol Levante	c-Si	2008
6.		Boulder City (Copper Mountain)	55*	Sempra Generation	CdTe	2010
7.		Strasskirchen	53	Q-Cells	c-Si	2009
8.		Lieberose	53	Juwi Solar	CdTe	2009
9.		Puertollano I	52	Renovalia Energy	c-Si	2008
10.		Moura (Amareleja)	46	Acciona Solar	c-Si	2008

1.2.2 Solar pond

A solar pond is a pool of saltwater that collects and stores solar thermal energy. In a typical freshwater pond, when the sun penetrates the water, the layers that are heated up decrease their density and rise to the top of the pond, maintaining the pond temperature constant.

Instead, in a saltwater pond, the layers that are heated increase their salt concentration as well as their temperature, so they stay in the bottom of the pond because their density is higher than the one of the cold layers.

The salinity gradient generates three zones in the solar pond:

- The surface zone, which has a low salt content and a temperature of about 30°C.
- The gradient zone, also called non-convective zone because it establishes a density gradient that prevents heat exchange by natural convection.
- The storage zone, where the solar radiation is absorbed and stored, which has a high salt content and a temperature above 80°C.

The temperature difference between the top and the bottom layers is very low (only 50-60°C), but can be used for desalination process, for heating buildings or for generating electricity with an organic Rankine cycle.

In this last case the hot water is used for evaporating a compressed organic working fluid that subsequently expands in the turbine. Figure 1.5 shows the scheme of a solar pond.

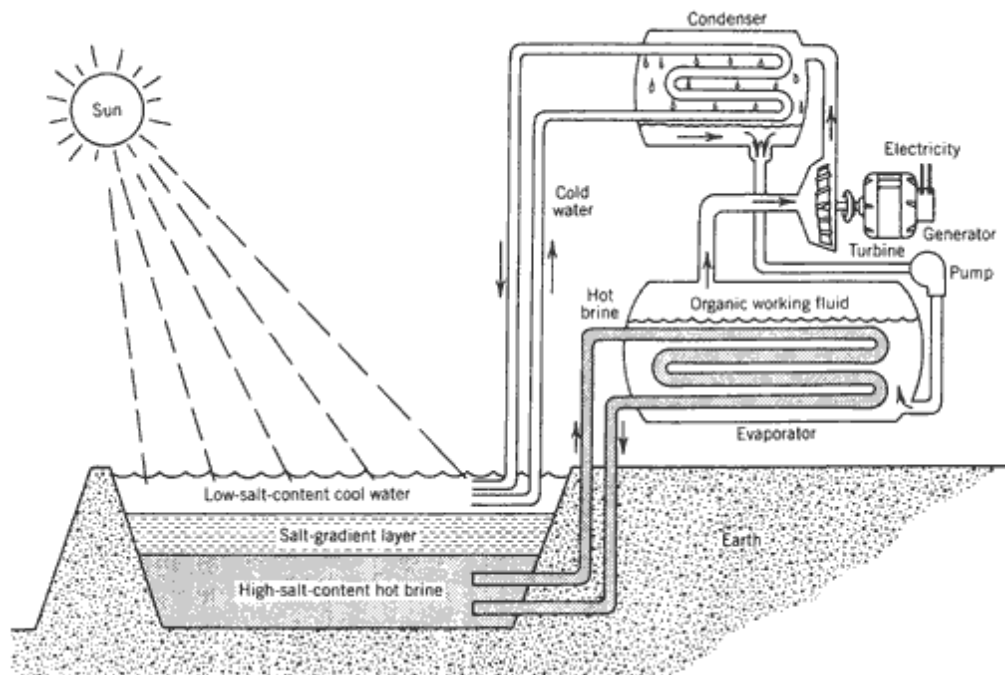


Figure 1.5:Electrical power production concept using salt-gradient ponds[6].

Advantages of the solar pond technology are the relatively low cost and the possibility of producing electricity during winter even if the pond is covered with a sheet of ice[7].

However solar ponds require a large amount of land and the cycle efficiency is very low (the maximum theoretical efficiency is below 20%). These disadvantages limit the diffusion of this technology.

The largest operating solar pond was the Beit HaArava pond built in Israel and operated up until 1988. It had an area of 210,000 m² and generated an electrical output of 5 MW.

1.2.3 Solar updraft tower

A solar updraft tower consists of a tall chimney surrounded by a transparent collector made of plastic or glass. The collector functions as a greenhouse, heating the air that tends to flow through the chimney. Thanks to the chimney effect, the wind force becomes strong enough to spin a wind turbine that generates electricity. The wind turbine can be placed at the top of the tower or with other horizontal axis turbines around the base of the tower.

The power and the efficiency of this system depends on the collector area (a larger area collects and warms a greater volume of air) and on the chimney

height (a taller tower increases the pressure difference thanks to the chimney effect). A schematic of a solar updraft tower is shown in figure 1.6.

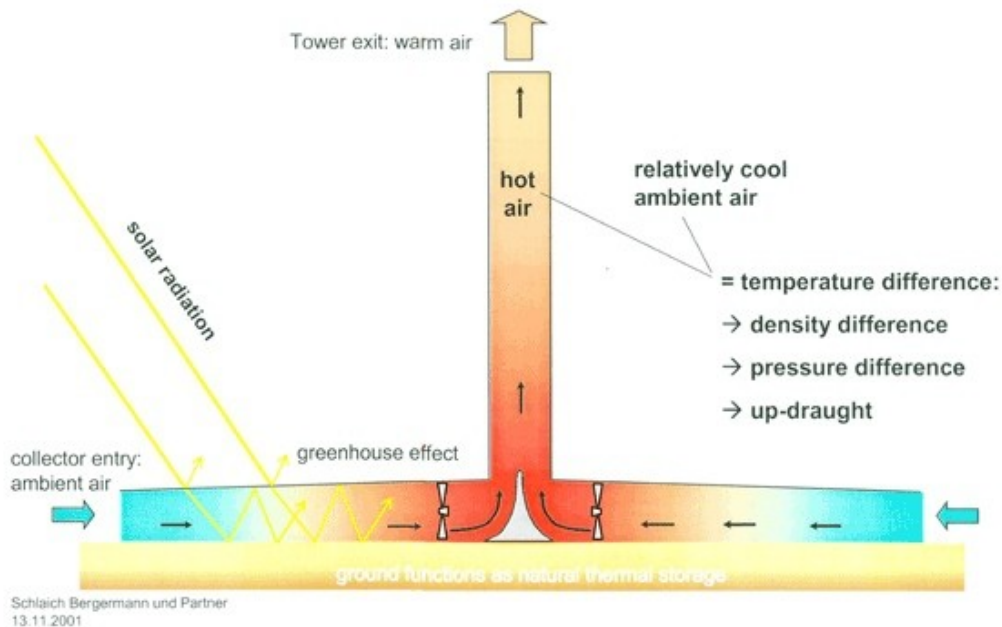


Figure 1.6: Schematic overview of solar tower principle.

The tower can work even at night with a reduced output. To increase it, it's necessary to install water tubes under the collector roof, which absorb part of the radiated energy during the day and release it into the collector at night[8].

Despite its low efficiency and large area request, solar updraft tower has a low operating cost. Photovoltaics and solar collectors may be placed under the collector in order to maximize the power production of the plant.

The major drawback of this technology is the great area occupied by the plant: for a 100 MW plant it's required a 1000 meters tower with a solar collector of 20 square kilometers.

Although several projects have been proposed during the years (for example the Ciudad Real Torre Solar (Spain, 40 MW), the Greentower (Namibia, 400 MW), the Arizona Tower (United States, 200 MW)), the only power plant realized was the Manzanares solar tower in 1982.

The chimney of this plant had a height of 195 meters and a diameter of 10 meters with a collection area of 45 square meters, generating a maximum power output of 50 kW.

The tower was dismissed in 1989 when, after eight years of operation, the tower blew over due to the rusting of the guy-wires and storm winds.

1.3 Concentrating solar power systems

Concentrating solar power systems (CSP) use a high mirrors or lenses to concentrate a large area of sunlight onto a small receiver area, where a fluid is heated before being expanded in a turbine. The ratio between the reflecting area and the receiving area is called concentration ratio.

The more the concentration ratio increases, the more the efficiency of the plant increases too, because, on equal receiver area, the fluid can reach a higher temperature.

These systems can only use direct sunlight, which is the radiation that is not deviated by atmosphere and reaches the earth's surface in parallel beams. For this reason, suitable sites should receive at least 2000 kWh of direct solar irradiation per m²[9], in particular suitable sites are located in the sun belt (figure 1.3).

There are four types of CSP plants: parabolic trough, Fresnel reflector (these two are linear concentrators because reflect the solar radiation onto a tube), parabolic dish and solar tower (these are punctual concentrators because reflect the solar radiation onto a punctual receiver). They can be seen in figure 1.7.

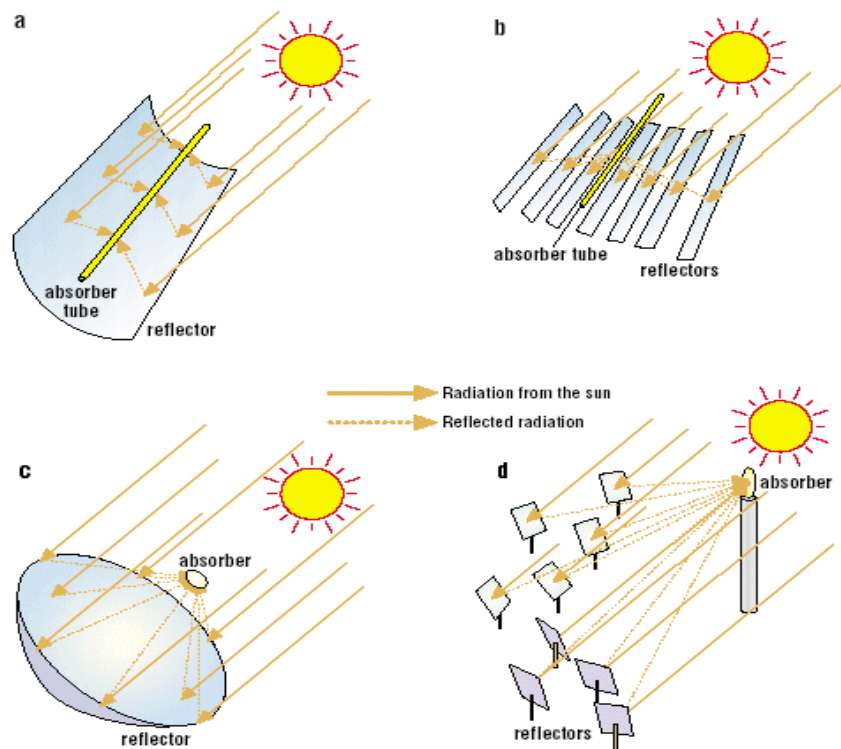


Figure 1.7: Different types of CSP systems: a)Parabolic through b)Fresnel reflector c)Parabolic dish d)Solar tower.

To increase the productivity of a concentrating solar power plant, it's necessary to install a sun-tracking system, in order to have the mirrors always oriented toward the sun. Although sun-tracking systems increase the daily production of a CSP plant, they are also very expensive and, generally, the more a sun-tracking system is precise, the higher is its cost.

1.3.1 Parabolic trough

In a parabolic trough plant the solar collector field is composed of rows of trough-shaped solar collector elements, usually mirrors, with an integral receiver tube, in which flows the heat transfer fluid. They are parabolic in one dimension only and form a long parabolic shaped trough of up to 150m in length[9]. The collectors are usually installed in rows, which are connected to an one axis solar tracking system in order to collect the maximum amount of sunlight during the day.

The absorber tubes are made of stainless steel pipes with a selective coating, like cobalt or chromium. The coating is designed to allow pipes to absorb high levels of solar radiation while emitting very little infra-red radiation. To reduce thermal losses, the pipes are insulated in an evacuated glass envelope. Figure 1.8 represents the scheme of a parabolic trough collector.

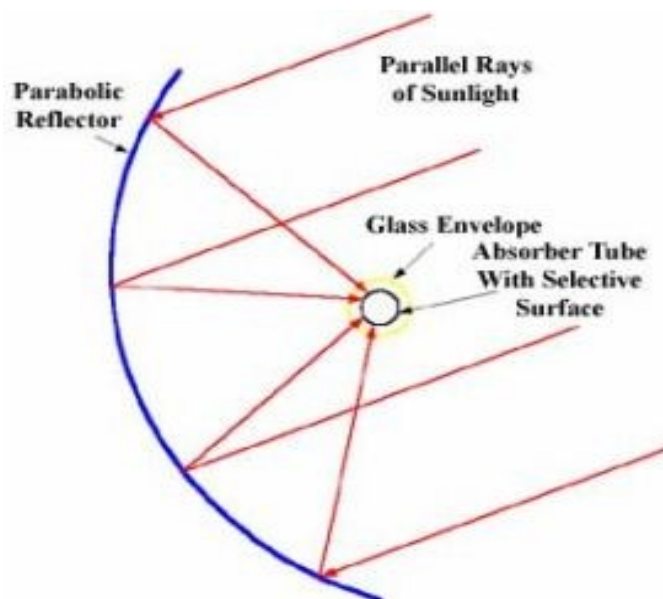


Figure 1.8: Scheme of a parabolic through collector.

At the solar field outlet, the hot heat transfer fluid is sent into a heat exchanger where water is preheated, evaporated and overheated. This superheated steam is used for making a turbine run, producing electricity.

The heat transfer fluid is generally synthetic thermal oil thanks to its low operating pressure and its low freezing temperature. However, for avoiding its cracking, the maximum temperature of the oil must be limited at 400 °C, a temperature that limits also the cycle efficiency.

To solve this problem, two different approaches have been adopted. The first consists in the use of water as heat transfer fluid. This system doesn't require a heat exchanger, since the heat transfer fluid and the working fluid are the same, with a resulting cost reduction. Moreover, the maximum temperature can be increased up to 500 °C. On the other hand the water requires a high operative pressure (about 100 bar), so the tube receiver wall must be thicker and heavier. A sophisticated control system is required for the phase change water, in order to keep the steam flow steady. This solution has been adopted by the Direct Solar Steam (DISS) project at the Plataforma Solar of Almeria.

The second solution consists in the use of molten salts, especially nitrate salts, as heat transfer fluid. These salts have a maximum temperature of 550 °C and their cost is lower than oil's, but have also some technological drawbacks. The most important is the high solidification temperature (230°C), so it's necessary to install electrical resistances on the external surface of the tubes in order to prevent the salts solidification during the night and at start-up. Furthermore, the high corrosivity of the salts requires to use more expensive pipes and components. This solution has been adopted by the Archimede solar plant near Syracuse (Italy).

Figure 1.9 shows an example of a parabolic trough power plant.



Figure 1.9: Albengoa Solar's Solnova 1 (50 MW_e).

The power plant can be equipped with a storage system, in order to work even

during solar transients and by night. Generally nitrate salts are used as storage fluid, even if synthetic oil is used as heat transfer fluid, because their cost is lower and they are not flammable like oil.

The parabolic trough technology is the most mature CSP technology in commerce, but is also the less efficient due to its low concentration ratio (under 100X).

Most of the CSP plants built in the world are parabolic trough systems, in particular the largest plants are the SEGS (USA, 354 MW), the Nevada Solar One (USA, 64 MW) and, in Europe, the Solnova Solar Power Station (Spain, 150 MW) and the Andasol Solar Power Station (Spain, 150 MW).

1.3.2 Linear Fresnel reflector

A Linear Fresnel Reflector is a line focus system similar to parabolic troughs in which solar radiation is concentrated on an elevated inverted linear absorber using an array of nearly flat mirrors. These mirrors are typically aligned in a north-south orientation and can rotate around their longitudinal axis to maintain the proper angle of incidence between the sun's rays and the mirrors during the day.

To minimize the amount of ground space required for installation, multiple receiver tubes can be installed within the vicinity of the mirrors. This solution is also known as Compact Linear Fresnel Reflector system (CLFR).

Figure 1.10 shows the AREVA Solar's Kimberlina Solar Thermal Energy Plant in Bakersfield, California, that uses the CLFR technology.



Figure 1.10: AREVA Solar's Kimberlina Plant in Bakersfield, California.

The main advantage of this technology is that the simple design of flexibly bent mirrors and the fixed receivers facilitate direct steam generation, thereby eliminating the need for heat transfer fluids and heat exchangers.

Comparing with the parabolic trough technology, this results in a cost reduction and a better exploitation of land. Moreover, this system is not susceptible to damage from strong winds.

Since the concentration ratio is in the range of 30-80X, the collector efficiency and the maximum temperature of the working fluid are lower than in a parabolic trough system. However this disadvantage is compensated by the installation cost reduction and the better land exploitation thanks to its linear design.

The real limitation of this technology is the absence of a multi-hour thermal storage for direct steam generating cycle, so it's necessary to add a fossil fuel burner for supplying thermal power when the sunlight is absent.

Despite the good potential of this technology only few plants have been realized. The first application of the CLFR technology for steam generation was in 2004, when a linear Fresnel collector field was built near the Lidell Power Station in Australia. In this plant the solar field is used for heating steam at 265 °C and 65 bar, which preheat the water used in the 2,000 MW coal-fired Lidell Power Station, avoiding the bleeding of steam from the turbine.

With a 5 MW of nominal power output, the Kimberlina Solar Thermal Energy plant in Bakersfield (California, for a picture see figure 1.10) is the biggest CLFR power plant built and is also the first stand-alone commercial plant using this technology. This plant produces steam at 270 °C and 40 bar, with a cycle efficiency of about 20%.

1.3.3 Parabolic dish

Parabolic dish technology uses a parabolic dish mirror (which can be comprised by one or several facets that approximate the geometry of a paraboloid) to concentrate solar radiation in a receiver positioned at the reflector's focal point.

Instead of installing a tube in which flows a heat transfer fluid like other CSP technologies, in this case the receiver consists of an independent generator, generally a Stirling engine or, in rare cases, a micro turbine.

Figure 1.11 illustrates the components of a parabolic dish generator.

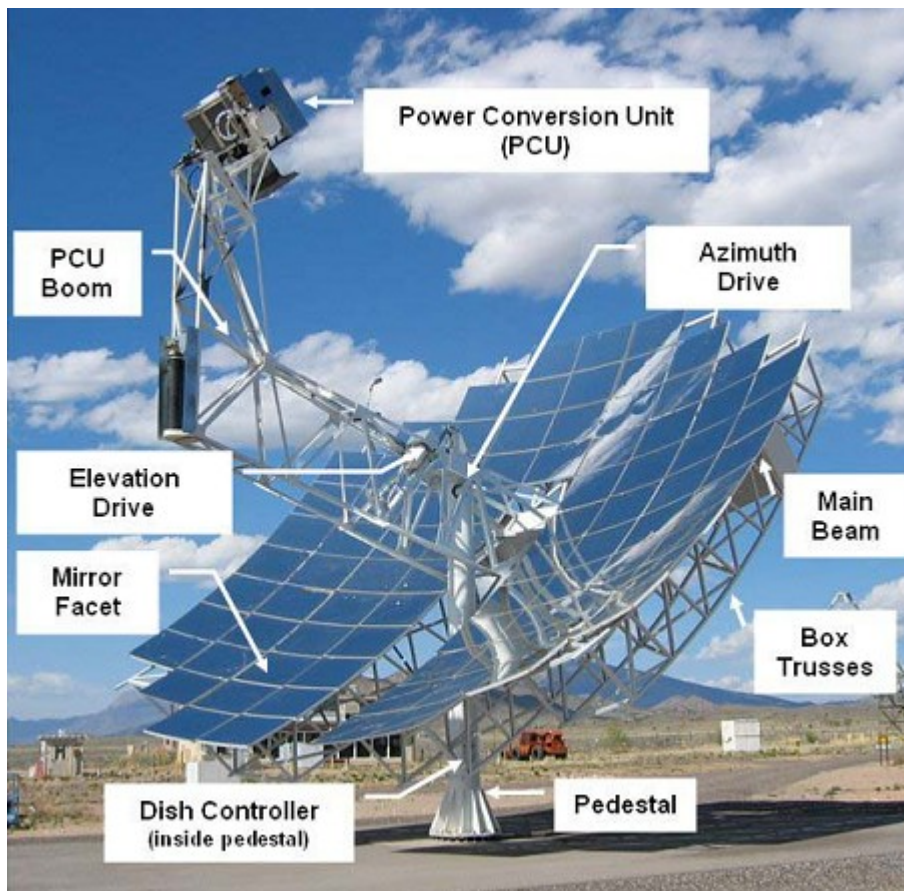


Figure 1.11: Components of a parabolic dish generator[5].

In the Stirling engine receiver, a working fluid, usually hydrogen or helium, is heated by the concentrated solar radiation at temperature up to 700 °C and leads the engine internals to produce a compress and expand cycle which can be used to produce electricity.

More in detail, the Stirling engine used in a parabolic dish system is an alpha type, which has two pistons in two independent cylinders, one cold and one hot, where the solar radiation is concentrated.

Parabolic dishes offer the highest concentration ratio (up to 2000X) and the highest solar-to-electric conversion performance of any CSP system, setting the world record for solar thermal conversion efficiency (31.4%).

Moreover, dish engine systems are cooled by closed-loop systems and lack a steam cycle, therefore endowing them with the lowest water usage per megawatt-hour compared to other CSP technologies[5].

A disadvantage of this system is that, to improve the daily efficiency, it's necessary to install a dual-axis track system, with the dish and receiver moving in tandem resulting in a high maintenance cost.

Moreover, parabolic dishes are limited in size (typically tens of kW or smaller) and each produces electricity independently, which means that hundreds or thousands of them would need to be co-located to create a large-scale plant.

A rigid frame is required in order to maintain the engine receiver in the focus point of the dish, resulting in a more expensive structure.

However some power plants have been realized, for example the Maricopa Solar Plant near Peoria, Arizona. This plant is composed of 60 Stirling dishes, each with a power output of 25 kW, resulting in a overall power output of 1.5 MW.

1.3.4 Solar power tower

Solar Tower technology uses a solar field composed of hundreds or thousands of flat (or slightly bended) mirrors called heliostats to reflect and point solar radiation to a receiver placed on the top of a tower.

Generally, the fluid flowing through the receiver is a molten salts mixture thanks to its high maximum temperature, its high heat capacity and the possibility of using a direct storage. However its problems are the same of the parabolic trough system: high solidification temperature and high corrosivity.

Liquid sodium could be an alternative, since its solidification temperature is about 98 °C and can reach temperatures above 550°C, but high flammability limits its utilization.

Some projects, for example the PS10 and PS20 solar power plants in Seville (Spain), have proven the feasibility of using water as heat transfer fluid. The receiver produces saturated steam at 250 °C and 40-45 bar that is expanded in a steam turbine generating electricity.

The use of superheated steam in the receiver increases the turbine inlet temperature and, consequently, the cycle efficiency, but is also more complex because it's difficult to predict the coefficient of heat transfer. The under construction Ivanpah Solar Electric Generating System will utilize this technology to produce 392 MW.

Another option is the use of air at ambient pressure, so there's not a temperature limitation, but it's required a larger receiver area due to the low heat transfer coefficient. The Jülich solar power plant uses air as heat transfer fluid and can produce steam at 480 °C and 26 bar. A variation of this solution consists in the use of compressed air as heat transfer fluid.

The receiver can be divided into two groups:

- *Tubes receiver*: the heat transfer fluid flows through several tubes that can dilate down. They can be arranged in a cavity shape (to reduce emission losses) or in a flat shape. This design is used for steam, molten salts or oil receivers.
- *Volumetric receiver*: it's made of porous silicon carbide, in which the external air flows and is heated. A steel frame supports the receiver and

allows its thermal dilatation. If a quartz window is placed in front of the receiver it can heat also compressed air.

Figure 1.12 shows a comparison between these two technologies.

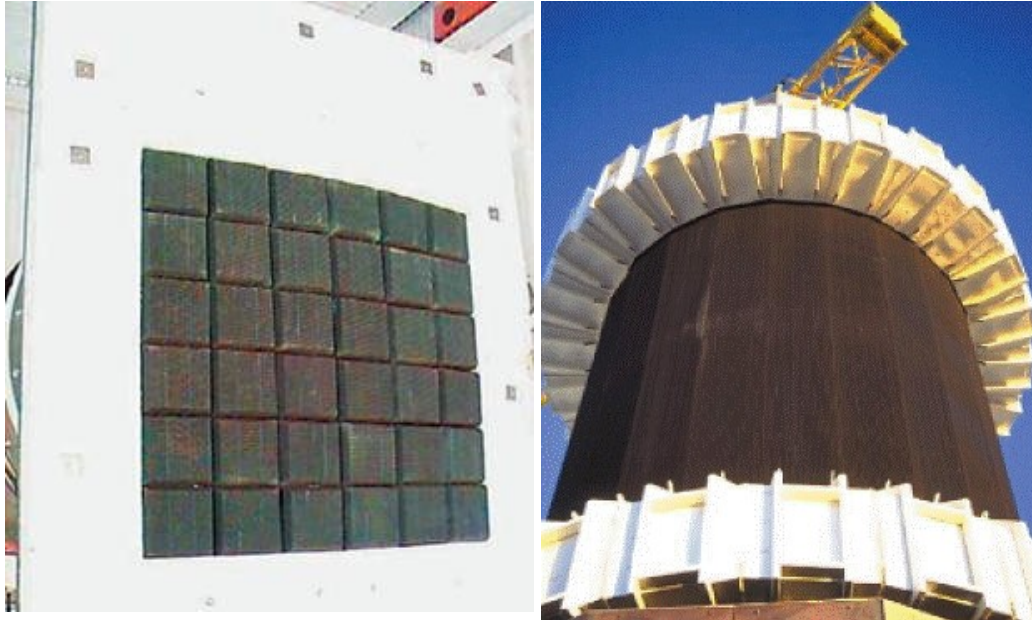


Figure 1.12: Comparison between a volumetric receiver (left) and a tubes receiver (right).

The tower, where is placed the receiver, is made of steel or concrete and must be 80-150 meters in height in order to reduces shadowing and blocking losses. To reduce the installation cost, a multi-tower configuration can be adopted. It consists of installing more than one tower for the same turbine and, eventually, for the same heliostat field. This enables an increase in the efficiency of each tower (up to 5%) by the reduced distance between heliostats and towers which mitigates light dissipation issues. Additionally, smaller towers have lesser construction requirements (high towers are exposed to higher wind forces) which can reduce costs by ~25%.

However, due to higher pressure drops and thermal losses of the piping system resulting from the sharing of a single power block, and an increased control complexity, its competitiveness at high-capacity plants is yet to be established[10].

Due to the increase of the maximum operating temperature, expensive materials with better thermal properties must be used to build the receiver, but the significant increase in efficiency outweighs its corresponding cost increase.

The heliostat field is the most expensive component of a solar power tower, with a share of about 50% of the global installation cost.

The high cost of the solar field is caused by the dedicated motors for azimuthal and altitudinal tracking that each heliostat requires. To reduce the cost of this aspect, larger heliostats can be used, so a minor number of them is required for reflecting the same solar energy.

Generally, the solar field area is three times bigger than the reflecting area, because it's necessary to have space between the heliostates for avoiding shadowing and blocking losses. However, looking at electricity output versus total size, a solar power tower uses less land than a hydroelectric dam (including the size of the lake behind the dam) or a coal plant (including the amount of land required for mining and excavation of the coal)[11].

The heliostates can be disposed around the tower or only on the north side, depending on the size of the tower.

A picture of a solar power tower can be seen in figure 1.13, where various components of the plant are indicated.

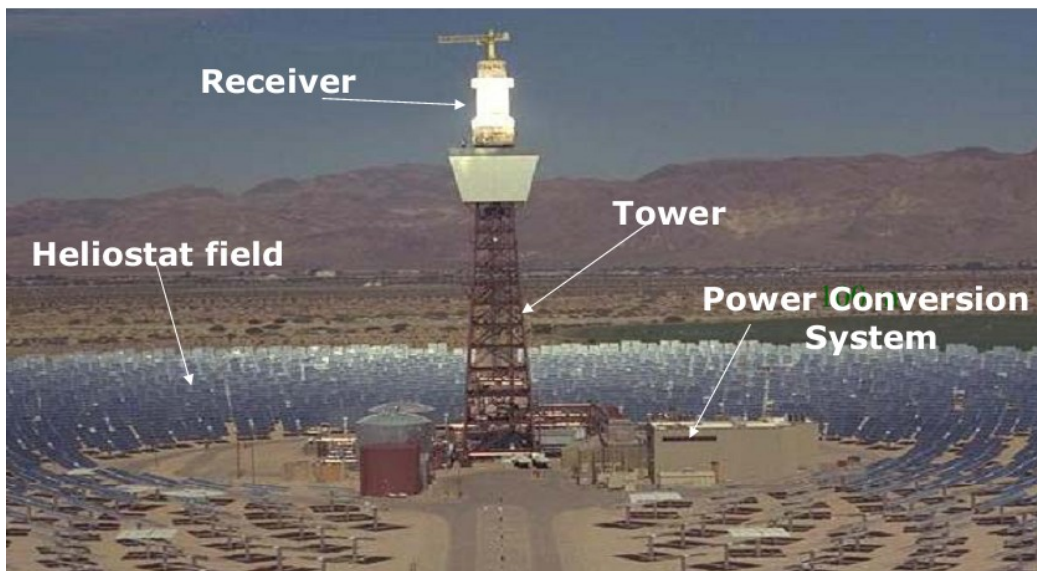


Figure 1.13: Picture of a solar power tower.

The first solar power tower built was the Solar One in 1982 near Barstow (California, 10 MW), which used thermal oil as heat transfer fluid and remained operative until 1986. In 1995 it was converted into Solar Two that used nitrate salts instead of thermal oil as heat transfer medium and the solar field was expanded in order to increase the power generation up to 20 MW. The Solar Two was demolished in 2009.

More recent tower plants are the PS10 and the PS20 located near Seville (Spain, with a power production of 11 MW and 20 MW respectively). These plants demonstrate that direct steam generation system is feasible, producing about 23400 and 48000 MWh per year respectively.

The Jülich Solar Tower (Germany, 1.5 MW) deserves a special mention not only because it is the first solar plant that uses air as heat transfer fluid, but also because it is located at latitude 50 °N, an area where solar irradiation is very low. Figure 1.14 shows a picture of the PS10 and PS20 power plants.



Figure 1.14: Aerial view of the PS10 and PS20 power tower near Seville.

1.4 Perspectives for CSP plants

Nowadays there is 1.32 GW of cumulative installed CSP capacity worldwide and 69 GW of cumulative installed photovoltaics capacity worldwide, thanks to a rapid growth of both technologies during the last years.

Since photovoltaic is more suitable for distributed electricity production, the CSP technology may be the future for solar power plants, thanks to the integration of a storage system that makes the power production more predictable.

Moreover, CSP plants can be built in desert zones and a high voltage direct current (HVDC) grid can be used to link them to large consumption centers. It's necessary to use a HVDC technology (despite the higher cable costs and the 3% to 5% conversion losses) because a high voltage alternate current (HVAC) lines are not viable for transporting electricity over distances above a few hundred kilometers[10].

For example, by using a mere 0.4% of the total surface of the Sahara desert, the

European demand for electricity could be entirely met, and the global demand by using only 2%[12].

Among all the CSP technologies, parabolic trough is the most mature and has been commercially proven worldwide, while the solar tower is the most promising, as is shown in table 1.2.

Table 1.2: Comparison between CSP technologies[13].

<i>Technology</i>	<i>Optical efficiency</i>	<i>Annual solar-to-electric efficiency</i>	<i>Land occupancy</i>	<i>Water cooling (L/MWh)</i>	<i>Storage possible</i>	<i>Possible backup/hybrid mode</i>	<i>Solar fuels</i>	<i>Outlook for improvements</i>
Parabolic troughs	**	15%	Large	3 000 or dry	Yes, but not yet with DSG	Yes	No	Limited
Linear Fresnel receivers	*	8-10%	Medium	3 000 or dry	Yes, but not yet with DSG	Yes	No	Significant
Towers (central receiver systems)	**	20-35% (concepts)	Medium	2 000 or dry	Depends on plant configuration	Yes	Yes	Very significant
Parabolic dishes	***	25-30%	Small	none	Depends on plant configuration	Yes, but in limited cases	Yes	Through mass production

1.4.1 CSP plants installed

At the end of 2011, there was 1318 MW of cumulative installed CSP capacity worldwide.

Spain is the world leader in CSP installations, with 450 MW of added capacity in the last year and 55.4% of cumulative installed capacity worldwide. During the same period, the United States added 78 MW of CSP capacity, for a total of 38.5% of cumulative installed CSP capacity worldwide. Iran (5.0% of market share), Israel (0.5%), Australia (0.2%), and Germany (0.1%) have all recently entered the CSP market[5].

Table 1.3 lists installed CSP plants worldwide.

Table 1.3: Global installed CSP plants[5].

Plant Name	Location	Developer	Technology	Year Installed	Capacity (MW)
Martin Next Generation Solar Energy Center (MNGSEC)	Florida	NextEra Energy Resources	Trough	2010	75
Mariopca Solar Project	Arizona	Tessera Solar	Dish/Engine	2010	2
Greeco Coal-Fired Hybrid Demonstration Plant	Colorado	Abengoa Solar	Trough	2010	1
Nimberlina Solar	California	AREVA	CLFR	2009	5
Sierra SunTower	California	eSolar	Tower	2009	5
Holaniku	Hawaii	Sopogy	Trough	2009	1
Nevada Solar One	Nevada	Acciona	Trough	2007	64
Saguaro	Arizona	APS	Trough	2006	1
Solar Electric Generating Stations (SEGS) (I-IX)	California	Luz	Trough	1985-1991	354
Manchasol-1	Ciudad Real	ACS-Grupo Cobra	Trough	2010	50
Palma del Rio II	Cordoba	Acciona	Trough	2010	50
La Dehesa	Badajoz	Renovables SAMCA	Trough	2010	50
Majadas I	Caceres	Acciona	Trough	2010	50
La Florida	Badajoz	Renovables SAMCA	Trough	2010	50
Solnova 1	Sevilla	Abengoa Solar	Trough	2010	50
Solnova 3	Sevilla	Abengoa Solar	Trough	2010	50
Solnova 4	Sevilla	Abengoa Solar	Trough	2010	50
Extresol-2	Badajoz	ACS-Grupo Cobra	Trough	2010	50
Extresol-1	Badajoz	ACS-Grupo Cobra	Trough	2009	50
Alvarado 1 (La Risca)	Badajoz	Acciona	Trough	2009	50
Puertollano (Ibersol Ciudad Real)	Puertollano	Iberdrola Renovables	Trough	2009	50
Andasol-2	Granada	ACS-Grupo Cobra	Trough	2009	50
Puerto Errado 1 (PE1)	Calzadama	Novatec Biosol	CLFR	2009	1
Planta Solar 20 (PS20)	Sevilla	Abengoa Solar	Tower	2009	20
Andasol-1	Aldaire	ACS-Grupo Cobra	Trough	2008	50
Planta Solar 10 (PS10)	Sevilla	Abengoa Solar	Tower	2006	10
Yazd ISCC Power Station	Yazd	TBA	Trough	2009	67
Solar Energy Development Center (SEDC)	Negev Desert	Bright Source	Tower	2008	6
Liddell	New South Wales	AREVA	CLFR		3
Julich Solar Tower	Kraftanlagen München	TBA	Tower	2009	2
THEMIS Solar Power Tower	Pyrénées-Orientales	TBA	Tower		1

The largest plant in the world is the Solar Electric Generating System (SEGS), that consists of nine parabolic trough plants in the Mojave Desert. It has a 354 MW of installed capacity, supplying electricity to 232,500 homes and covers an area of 6.5 km².

Another important plant is the Nevada Solar One that, with an installed capacity of 64 MW, is the second largest solar plant in the world. As well as the SEGS, the Solar One is a parabolic trough plant and its electricity production is estimated to be 134 GWh per year.

In Spain the biggest plant is the Andasol Solar Power Station, which is also the first European commercial parabolic trough solar thermal power plant. This plant has a gross electricity output of 50 MW, producing around 180 GWh per year. It has also the biggest storage system in the world, which can be used for

working full-load for 7.5 hours without the sun.

1.4.2 CSP plants under construction

The majority of solar plants under construction in the world are located in Spain, where is planned to install a total capacity of 582 MW.

Some countries have started the construction of their first solar plant, for example China, Egypt, Algeria and Morocco.

In particular, in December of 2009, the Clean Technology Fund approved financing of \$750 million, which will mobilize an additional \$4.85 billion from other sources, to accelerate deployment of CSP in the Middle East and North Africa (MENA) regions. These funds will be used, in part, to support the transmission infrastructure in the MENA region, including a 3,000 km transmission cable that will allow export of 100 GW of solar electricity from MENA to Europe[5].

Table 1.4 shows CSP plants currently under construction.

Table 1.4: Global CSP plants under construction[5].

Plant Name	Developer	Technology	Capacity (MW)
Andasol 3	Solar Millenium AG	Trough	50
Arcosol 50 (Valle 1)	Torres of Energy	Trough	50
Estresol-2	ACS-Grupo Cobra	Trough	50
Helioenergy 1	Abengoa Solar	Trough	50
Helioenergy 2	Abengoa Solar	Trough	50
Manchasol-1	ACS-Grupo Cobra	Trough	50
Palma del Rio I	Acciona	Trough	50
Palma del Rio II	Acciona	Trough	50
Termesol 50 (Valle 2)	Torres of Energy	Trough	50
Lebrija 1	Soludia Renovables	Trough	50
Puerto Errado 2 (PE2)	Novatec Biosol	CLFR	30
Gemasolar (Solar Tires)	Torres of Energy	Tower	17
Casa del Angel Termosolar	Renovilla	Dish/Engine	1
Friedemo II	Solar Power Group	CLFR	
Yulin Alternative Energy Park	Penglai Electric/eSolar	Penglai Electric/eSolar	92
Dezhou	Himin Solar	Himin Solar	3
Yanqing	Himin Solar	Himin Solar	1
Shams 1	Abengoa Solar	Trough	100
El Kuraymat	Solar Millenium AG	Trough	20
ISCC Argelia	Abener Energia	Trough	20
ISCC Morocco	Abener Energia	Trough	20
Cincoyury Solar Power Station	Ergon Energy	Tower	10
Ivanpah PG&E 2	BrightSource	Tower	133
Ivanpah SCE	BrightSource	Tower	133
Ivanpah PG&E 1	BrightSource	Tower	126
Mojave Solar Park	Siemens Energy	Trough	553
Crescent Dunes Solar Energy Project	SolarReserve	Tower	100

One of the most interesting plant in construction is the Ivanpah Solar Power Facility, which is built by Bright Source in the Mojave Desert.

After its completion, it will become the biggest CSP plant in the world, thanks to a capacity of 392 MW. With an estimated cost of 2.2 billion of dollars, the plant will occupy an area of about 16 km² with 170,000 heliostat mirrors focusing solar energy on boilers located on three centralized solar power towers. The boilers will produce superheated steam in order to increase the plant efficiency and to demonstrate the feasibility of a direct superheated steam generation system.

Since the plant is built in an arid area, an air cooling system must be installed to condensate the steam at the turbine outlet instead of a conventional wet cooling system, resulting in a 90% reduction in water usage.

Another interesting plant is the Yulin Alternative Energy Park that will be the first hybrid biomass and CSP plant.

1.4.3 Announced CSP plants

From 2010 to 2020, the global roll out of CSP initiated before 2010 is expected to accelerate, thanks to the ongoing industry efforts and the adoption of suitable incentives for CSP in sunny countries.

The European Solar Thermal Electricity Association estimates that the global installed capacity will reach 148 GW by 2020, with an average capacity factor of 32% (2,800 hours per year), thereby providing 414 TWh annually (1.3% of the global electricity production expected by 2020)[13].

It's expected that the future solar plants will have larger solar fields and storage systems in order to work at least 10 hours without sunlight. The capacity of the power plant will also be bigger, passing from the actual range of 50-200 MW to about 1,000 MW.

The market of CSP will expand to new zones, in particular to North Africa, China and India, where the electricity consumption is expected to grow rapidly.

A decrement of the levelized cost of electricity from 0.27 €/kWh to 0.1 €/kWh (thanks to economies of scale) will promote the diffusion of the CSP technology.

In table 1.5 are shown several announced projects for the construction of CSP plants in the United States.

Table 1.5: Announced CSP plants in the U.S.[5].

Plant Name	Developer	Technology	Capacity (MW)
BrightSource SCE (Solar Partners XVI-XXI)	BrightSource	Tower	1,200
Calico Solar Project II (Solar One)	Tessera Solar	Dish/Engine	575
Bythe (Phase I)	STA (Solar Millenium & Ferrostaal)	Trough	500
Bythe (Phase II)	STA (Solar Millenium & Ferrostaal)	Trough	500
Fort Irwin	Acciona	Trough	500
Palen Solar Power Project	STA (Solar Millenium & Ferrostaal)	Trough	484
Amargosa Farm Road	STA (Solar Millenium & Ferrostaal)	Trough	484
Imperial Valley Solar II (Solar Two)	Tessera Solar	Dish/Engine	409
Sonoran Solar Energy Project (Ika Jojoba)	NextEra Energy Resources	Trough	375
Hualapai Valley Solar Project	Mohave Sun Power	Trough	340
Imperial Valley Solar I (Solar Two)	Tessera Solar	Dish/Engine	300
Calico Solar Project I (Solar One)	Tessera Solar	Dish/Engine	275
Abengoa Mojave Solar (AMS) Project	Abengoa Solar	Trough	250
Beacin Sikar Energy Project	NextEra Energy Resources	Trough	250
Solana Generating Station	Abengoa Solar	Trough	250
Harper Lake Solar Plant	Harper Lake LLC	Trough	250
Ridgecrest Solar Power Project	STA (Solar Millenium & Ferrostaal)	Trough	242
BrightSource PG&E 5	BrightSource	Tower	200
BrightSource PG&E 6	BrightSource	Tower	200
BrightSource PG&E 7	BrightSource	Tower	200
Coyote Springs 1 (PG&E 3)	BrightSource	Tower	200
Coyote Springs 2 (PG&E 4)	BrightSource	Tower	200
Saguache	SolarReserve	Tower	200
Rice Solar Energy (RSEP)	SolarReserve	Tower	150
San Luis Valley	Tessera Solar	Dish/Engine	145
Gaskell Sun Tower (Phase II)	NRG Energy	Tower	140
Genesis Solar Energy Project-1	NextEra Energy Resources	Trough	125
Genesis Solar Energy Project-2	NextEra Energy Resources	Trough	125
Gaskell Sun Tower (Phase I)	NRG Energy	Tower	105

Chapter 2

Design of the reference plant

Before analyzing in detail the storage design, it's necessary to establish the reference plant layout where the storage should work.

In reference to similar existing projects, this chapter shows what kind of technology is suitable for our purposes and determines the working points of our cycle.

2.1 Description of the hybrid solar-gas technology

In a hybrid solar-gas turbine power plant (HSGTTP) the air at the compressor outlet is sent to a solar receiver where is heated by the concentrated solar radiation coming from the solar field. If the temperature of the air at the outlet of the solar receiver is high enough the air can be expanded in the turbine generating electrical power, otherwise it enters the combustion chamber that closes the temperature gap between the receiver outlet temperature and the turbine inlet temperature (generally 1300-1400°C). This means that the efficiency of the cycle, neglecting the pressure drop caused by the solar receiver, is the same of a conventional gas turbine.

The control of the injection of the fuel into the combustion chamber allows to adapt the power output in order to meet the grid demand, even during rapid solar transients. As such, the output of the plant becomes highly predictable, removing the need for synchronous reserve to compensate for sudden and unexpected variations in output.

Although the turbine is designed to work with natural gas, alternative fuels (for example sustainably derived biogas or syngas) can be used for realizing a zero CO₂ emission power plant¹.

If the gas turbine power plant is integrated with a Rankine bottoming cycle that is heated by the hot air at the turbine outlet, the efficiency of the solar-to-electricity conversion is increased. In this way, if the power capacity installed is the same, the expensive solar field, as well as the land footprint, is downsized and the fuel consumption reduced. The levelized cost of electricity is minimized too and, exploiting the economies of scale with the construction and operation of multiple distributed plants, a cost below 10 c€/kWh is expected[14].

¹ The carbon emissions caused by the fuel combustion are captured during the production of the biogas.

2.1.1 Comparison with a solar Rankine cycle

Despite the Rankine cycle is the most common way to produce electricity in a solar power plant, the use of an air cycle instead of a steam cycle offers some advantages.

First of all the fluid that circulates in the receivers and the working fluid are the same, while the steam cycle requires a heat transfer fluid (generally thermal oil or nitrate salts) with a limitation on the maximum temperature at the receiver outlet² and an efficiency loss during the heat exchange phase.

Another advantage of the Joule-Brayton cycle is the higher efficiency thanks to the installation of a recuperative bottoming steam cycle that uses the otherwise wasted heat at the turbine outlet to produce electrical energy.

The yearly average efficiency is also higher since the combustion chamber keeps the temperature at the turbine inlet constant, so the power plant can work at nominal charge even at times of insufficient solar radiation or during the night. The energy output can be adjusted in order to meet fluctuating electricity demand and there's no need for the construction of additional spinning reserve that accompanies the connection of conventional renewable energy sources (RES) to the grid[15].

The start-up and load ramping times are shorter than in a steam cycle, with a start-up time estimated between 20-30 minutes[16].

Compared with steam cycles that have large water consumption for cycle cooling and water makeup, gas turbine systems don't have large water consumption and can be installed in arid and desert locations that benefit from strong radiation and large areas of land (required for the construction of the solar field), but suffer from scarcity of water resources.

On the other hand, if a Joule-Brayton cycle is adopted, the heat transfer fluid that flows through the receiver must be air, which is a poor heat transfer medium due to its low heat conductivity and low density (even if it's pressurized). The high temperature required in the solar receiver forces to abandon the traditional tube receiver configuration in favor of a more expensive and less reliable volumetric technology. These volumetric receivers are made of porous material in which the air flows, but, under high heat flux, the airflow through the porous material isn't equally distributed and this leads to local overheating of the absorber material that causes mechanical failures such as melting or cracks.

2.2 Operating hybrid solar-gas power plants

Despite the hybrid solar-gas technology is very attractive, only a few projects have been made operative and all these have a power output below 5 MW_{el}.

² Maximum temperature for nitrate salts is 565°C and for thermal oil is 400°C

2.2.1 SOLGATE project

The SOLGATE³ project was realized for the demonstration of the feasibility of a solar-hybrid cycle. The test system consisted of a gas turbine based on a helicopter engine, which was modified to enable the solar heating of the pressurized air through three receivers (scheme of the test system can be seen in figure 2.1)

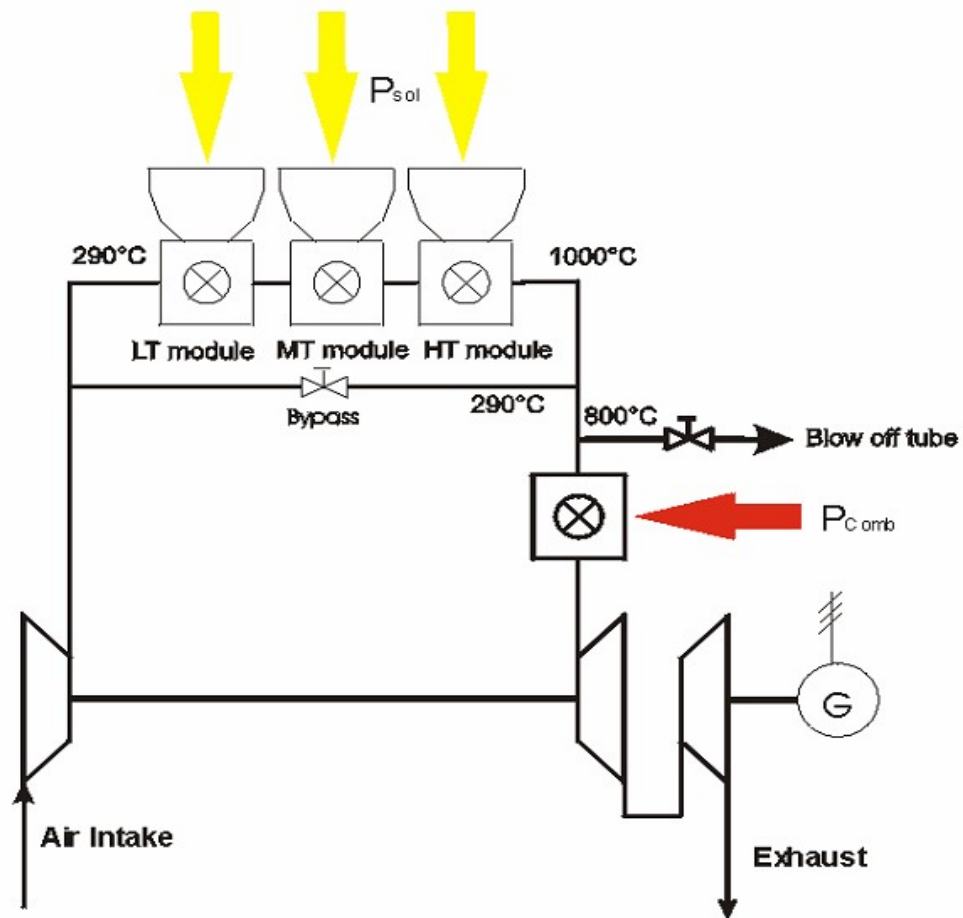


Figure 2.1: Scheme of the SOLGATE test system[17].

With a receiver outlet temperature designed to be 1000°C, it was necessary to add fuel in the combustion chamber in order to reach the minimum turbine inlet temperature of 1150°C and achieving the design power output of 250 kWe. Despite a lower turbine inlet temperature increases the solar share of the power plant, it limits the overall efficiency of the cycle.

³ SOLGATE means SOLAR hybrid GAS Turbine Electric power system

The test plant was installed in the solar tower of the Plataforma Solar de Almeria (PSA) and began operations at the end of November 2002 for a total of 134⁴ hours with the gas turbine in function, partially satisfying the primary objectives.

About the solar receivers, their window temperatures were lower than expected thanks to the air cooling system that lowered the window temperature by about 150 °C. The aimed outlet air temperature of 1000°C was nearly achieved, with a maximum measured temperature of 959 °C[17], but, due to the low operating time of the test, long term degradation of the receivers cannot be excluded.

In general, the technical feasibility of solar-hybrid gas turbine power plants was successfully demonstrated, but further researches and developments are required to develop the system to a marketable status, with a target specific investment cost of 1440 €/kWh and a levelized cost of electricity of 0.057 €/kWh with a 16% of solar share and a 24 hours operation per day[17].

An outlook of the test plant at CESA 1 can be seen in figure 2.2.



Figure 2.2: External view of the SOLGATE test plant at CESA 1[17].

2.2.2 AORA's solar flower tower

Located in the desert near Kibbutz Samar (Israel), the AORA's solar flower

⁴ 96 hours of them were performed with solar radiation[17].

tower⁵ is the first and only solar-hybrid gas turbine that is not installed on a preexisting solar tower, but that was built with it.

The construction was completed in 2009 and the power plant consists of a 30 meters high solar tower, where was placed the 100 kW gas turbine that receives pressurized air heated by 30 heliostats, situated on a half an acre of desert land, that deflect the sun rays toward a 6 meter-high receiver[18].

The receiver uses the 170 kW coming from the sun rays reflected by the heliostats to heat the air up to 1000°C, a temperature that allows the entrance into the turbine without the addition of fuel. However, the air is always routed through the combustion chamber on the way to the turbine so, if the temperature falls below a certain level⁶, the fuel can be fed automatically in order to provide heat and ensure the constant provision of electricity. The AORA's solar flower tower can be seen in figure 2.3.



Figure 2.3: picture of the AORA's solar flower tower.

Thanks to the fuel injection, the gas turbine can work without fluctuation in power level during partial solar radiation and even during the night. This means that the gas turbine can work at full load 24 hours a day, with a 100% solar production during the most sunny hours[19].

In order to contain the installation costs, the solar tower is made of recyclable materials, mainly pre-fabricated curved steel sheets, which can be easily

⁵ It's called flower tower because it looks like a golden yellow tulip.

⁶ This level is set at 950°C[19].

assembled and erected in just two days[18]. The heliostat frames also use structural steel, while the mirrors, that are solar quality mirrors, with 94% reflectivity and aluminum backing, and the receivers, for which the solar window is composed of high purity quartz, are more expensive[18].

2.2.3 THEMIS solar power plant

Started in 2009, the PEGASE⁷ project aims at harnessing the solar radiation in order to generate 1.4 MWe from a hybrid solar-gas cycle, a nominal size six times bigger than SOLGATE.

The plant is installed on the solar power tower Themis, a 105 meters high tower, located in the region of Cerdanya, an area very suitable for the concentrated solar power because it has almost 2400 hours of sunshine a year with low wind and a high solar radiation thanks to its altitude. A photo of the Themis solar power tower is shown in figure 2.4.



Figure 2.4: Aerial photo of the Themis solar tower.

The 101 heliostates of the solar field, each with a 53.9 m² surface, reflect the solar radiation to the receiver, where pressurized air is heated from 350°C to 750°C. In order to reach 1000°C, that is the minimum turbine inlet temperature, it's necessary to inject fuel into the combustion chamber. A scheme of the system, that marks also the thermal and electrical power exchanged, is shown in figure 2.5.

⁷ Production of Electricity with Gas Turbine and Solar Energy.

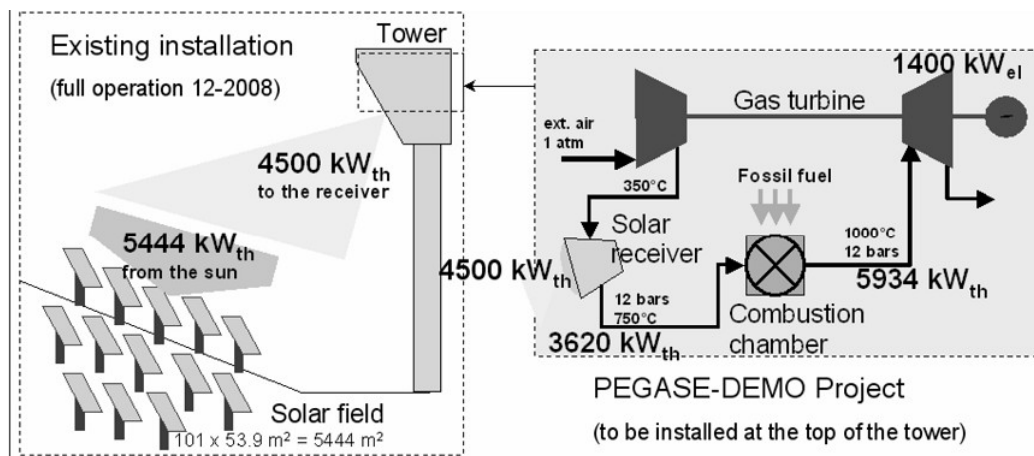


Figure 2.5: Scheme showing the principle of the thermodynamic cycle PEGASE installed at the top of the Themis tower[20].

Results of the plant will be available after the conclusion of the test, that is predicted at 2013. It's expected that, in the future, the unit power of the commercial power plants with hybrid technology solar-fossil gas turbine will be 10 to 25 MWe with combined cycles, about ten times the size of the PEGASE project[20].

2.2.4 SOLUGAS project

With an electrical power output of 4.6 MW, the SOLUGAS⁸ project aims to be the biggest hybrid solar-gas power plant worldwide. It consists of a commercial gas turbine Mercury 50 TM modified for making the air pass through the solar receiver.

Differently from the traditional volumetric receivers, the SOLUGAS uses an innovative tubular design that can heat the pressurized air from 330°C up to 800°C in a more reliable way.

More specifically, the solar receiver consists of a cavity with 170 parallel tubes 6 meters long, in which the air passes through with a pressure drop of less than 250 mbar, arranged in a circular shape with a diameter of 5 meters. During the first phase of the test part of the air will bypass the receiver in order to maintain the combustion chamber inlet temperature below 650°C.

The SOLUGAS project was started in 2008, but the construction of the plant will finish only in 2012 and will remain operative for two years.

⁸ SOLUGAS means SOLar Up-scale GAS turbine system.

2.3 The HYCOSOL proposal

The overall objective of the HYCOSOL⁹ project is to provide and demonstrate technical solutions which will allow the efficient use of concentrated solar energy through the use of hybrid solar gas turbine power plants (HSGTTPs). Hybridization of solar power with other energy sources (for instance biogas or syngas) ensures the availability of solar thermal power plants (STPPs) to meet fluctuating electricity demand. Dispatchable STPPs with hybridization and storage can form the backbone of the low-carbon electricity grid[15].

Another objective of the project is the search of the optimum ratio between gas turbine inlet temperature (in order to ensure high solar-electric conversion efficiencies and reduce costs, the turbine inlet temperature must be similar to current gas turbines) and the receiver outlet temperature (to obtain high solar shares and reduce the fuel consumption). The typical values of temperature are in the range of 1200-1400°C for the turbine inlet and 850-950°C for the receiver outlet.

Another way to increase the solar share of the power production and extend solar operation beyond sunshine duration consists in the deployment of a thermal energy storage system placed in parallel to the solar receiver. Like is shown in figure 2.6.

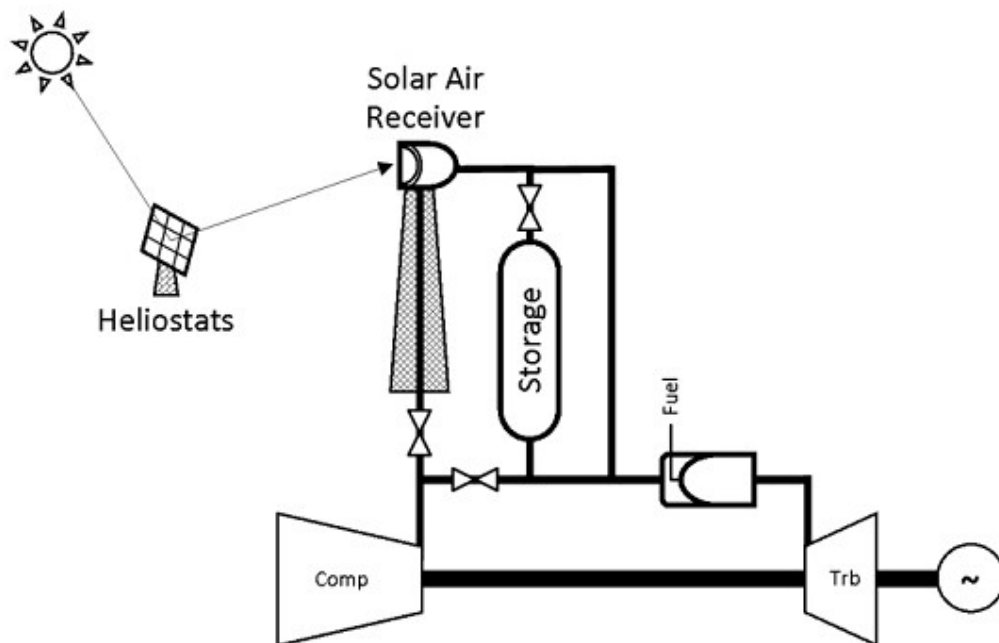


Figure 2.6: Hybrid solar-gas turbine flow diagram[15].

9 HYCOSOL means HYbrid gas turbines for the efficient use of COncentrated SOLar energy.

The hot air at the turbine outlet¹⁰ can be used to heat a bottoming cycle in order to produce additional energy from an otherwise wasted heat source and increase the overall solar-to-electricity conversion efficiency. Since one of the advantages of the plant is the suitability of installation in an arid location, it's necessary to use dry cooling systems in the bottoming cycles for maintaining a low water consumption.

To diversify the energy services offered, the exhaust heat can be used also for driving thermal desalination processes, for cogeneration or supply clean fresh water to desert regions.

2.4 Power plant components

Basing on the previous experiences, it's now possible to describe the components of our power plant and the working points of the cycle.

2.4.1 Gas turbine

The gas turbine chosen for the project is a Siemens SGT800. It has a 47 MWe power generation with an electrical efficiency of 37% and a turbine inlet temperature of 1300°C. The turbine can be seen in figure 2.7.

At the axial compressor inlet, an air flow of 130.2 kg/s is drawn from atmosphere and pressurized up to 20 bar. Part of this air (12.7 kg/s) is sent to cool the first two stages of the turbine, while the remaining (117.5 kg/s) is heated by the solar receiver and the combustion chamber.

Despite the exhaust temperature is about 544°C, hot enough to drive a steam cycle and increase the overall efficiency, it was decided to start the plant operations at the sunrise and stop them after the depletion of the thermal storage and not to install a bottoming cycle, which requires long start-up times.

In this way the power plant produces electricity only when the grid demand is high, and also the price of electricity, furthermore the solar share is increased because electricity is produced only with solar contribution, as the thermal storage has a short duration and during the night it's necessary to burn natural gas in order to maintain the plant working.

¹⁰ Generally the turbine outlet temperature is in the range of 500-600°C.



Figure 2.7: Conventional Siemens SGT800 gas turbine[21].

The combustion chamber must provide a stable and reliable operation as the inlet temperature changes¹¹, while maintaining the desired turbine inlet temperature to achieve high efficiencies. Two development paths will be followed, lean premixed combustion (LPC) and one innovative combustion system consisting in a flameless oxidation (FLOX)[15], to keep NO_x and CO emissions low.

To be more precise, during solar operation, the air entering the combustion chamber is much hotter than the standard compressor air, so the volumetric flow is significantly higher than that in a regular turbine. To allow for the same mass flow and low pressure drop, the connecting air pipes from the receiver to the combustor and the combustor air inlets have a much larger diameter than the original combustor inlets[22].

Moreover the hot air affects the materials and components strength and durability in the cold zone of the combustion chamber, so it's required the use of nickel based super alloy for the casing construction.

Also the fuel system must be modified, including a fuel metering valve with the capacity to return most of the fuel to the fuel pump when the solar share is high, a fuel shut-off valve and a nitrogen purging system to keep the injector clean.

Another problem of the hybridization of a gas turbine is the addition of dead volume between the the compressor and the combustion chamber caused by the installation of the solar receiver and the connecting pipes, which affects the starting schedule and the engine acceleration rate. This problem can be solved by adapting a set of control coefficients in a series of systematic tests[22].

¹¹ The inlet temperature can vary from 300°C at the start-up to 850°C when the solar receiver work at nominal condition.

Since the gas turbine is quite cumbersome¹², it's impossible to install it on the top of the tower, so it must be placed at ground level. Technical specifics of the machine are given in table 2.1.

Table 2.1: Technical specifications of the SGT-800 gas turbine[21].

Parameter	Value
Power generation	47.0 MW(e)
Electrical efficiency	37.5%
Turbine speed	6608 rpm
Compressor pressure ratio	19.9:1
Exhaust gas flow	131.5 kg/s
Exhaust temperature	544 °C
Number of compressor stages	15 (3 with variable guide vanes)
Number of turbine stages	3 (the first two are cooled)

2.4.2 Solar receiver

The objective of the solar receiver is to efficiently transfer the solar radiation onto the working medium (in this case pressurized air) in order to obtain temperatures in the range from 800°C to 1000°C. These high temperatures make a tubular approach unusable, since the temperature on the outer tube surface is limited by the temperature resistance of the material employed and, to avoid its destruction, the concentrated thermal flux must be kept low, so it's necessary to install large receiver surface.

Instead, in a volumetric receiver the concentrated solar radiation is captured by an absorber material that heats the crossing air, which increases its temperature when reaches the inner absorber volume (and the temperature difference between solid and fluid vanishes). In this case the maximum receiver's temperature is close to the air's, so the solar radiation can be more concentrated. A comparison between the two approaches can be seen in figure 2.8.

¹² The gas turbine is 20 meters in length, 6.6 in height and 7.1 in width[21].

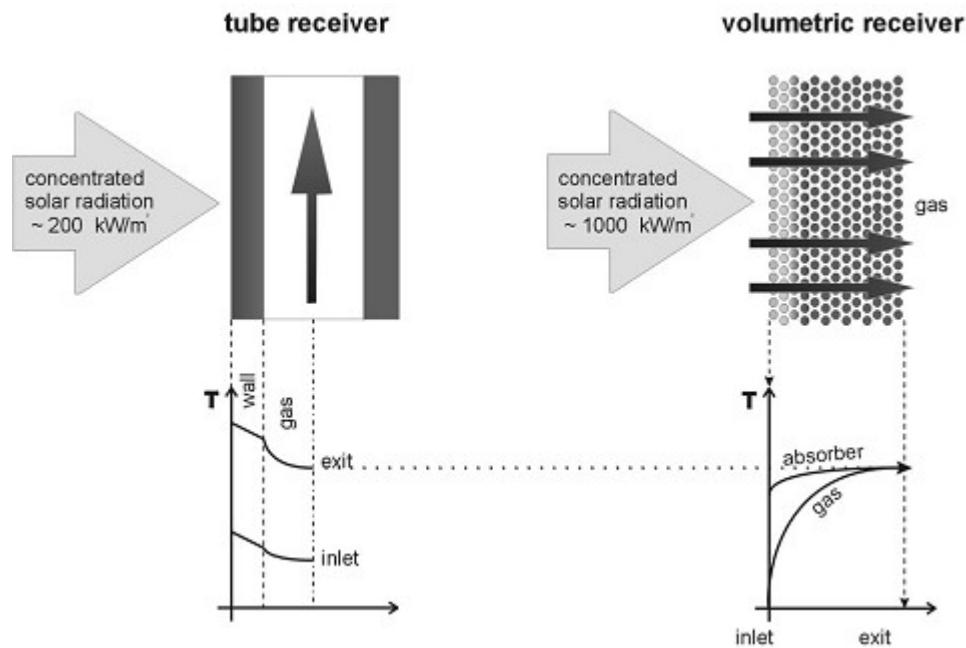


Figure 2.8: Adsorption and heat transfer of tubular and volumetric receiver[23].

The temperature of the outer surface should be as low as possible, since the thermal radiation losses are proportional to this temperature. In the volumetric receiver the front of the absorber volume is in contact with cold air, so it can be kept relatively cool; instead, in a tube receiver, the maximum temperature lies in the outer tube surface and is significantly higher, leading to higher radiation losses[24].

Therefore it's clear that a volumetric receiver is preferable to a tube receiver, but is also more expensive. In order to combine the advantages of the two approaches, it's necessary to separate the receiver into two sections: a low temperature section, that uses a tubular approach to contain the costs, and a high temperature, that can reach high temperatures.

This solution, called REFOS receiver, has been tested successfully in the SOLGATE project at the Plataforma Solar de Almeria, and is the same that is adopted in our plant.

In the REFOS receiver several modules are connected in parallel or in series to raise the temperature gradually. In front of each module is placed a secondary concentrator with a hexagonal entrance aperture, in order to achieve higher concentration ratios. The modules are arranged in a honeycomb-like arrangement in the focal spot, with a cluster of low temperature receivers installed on the outer perimeter, where irradiation may be more scattered and less intense, then medium and high temperature receivers are located

progressively closer to the center of the focal point where the irradiation is most intense[25].

The hexagonal entry aperture of the secondary concentrator is inscribed in a circle of 1.2 m diameter and its length is 1 m, with an acceptance angle of the sun's ray of 21°. The trapezoidal aluminum plates of the concentrator are cooled with water.

A tubular receiver can be used in the first stage of the serial receiver connection instead of a volumetric receiver in order to maintain a low manufacturing cost without sacrificing high thermal efficiency and low pressure drop.

The concept of the low temperature module consists in a multi-tube coil attached to a secondary receiver. The coil geometry is necessary to improve the heat transfer coefficient and axial cross section of the absorber is approximately elliptical, in order to obtain a homogeneous solar flux density distribution over the tubes, avoiding local peak temperature. The bent tubes are very flexible so the mechanical stresses from thermal expansion of the tube material are reduced and are coated with a high temperature resisting black paint to reach a high solar absorption coefficient.

The layout of the low temperature receiver consists of 16 tubes connected in parallel, each with a length of 2.3 m and a diameter of 28 mm, with a frontal aperture area of 1.24 m². With an incident solar radiation of 200 kW/m², an air flow of 1.357 kg/s can receive a temperature increase of 250 °C, while the maximum tube temperature is 950°C at a module outlet temperature of 550°C. The pressure drop associated at this module is about 100 mbar, that is 2/3 of the total pressure drop of the receiver[17].

A schematic view of the low temperature module can be seen in figure 2.9.

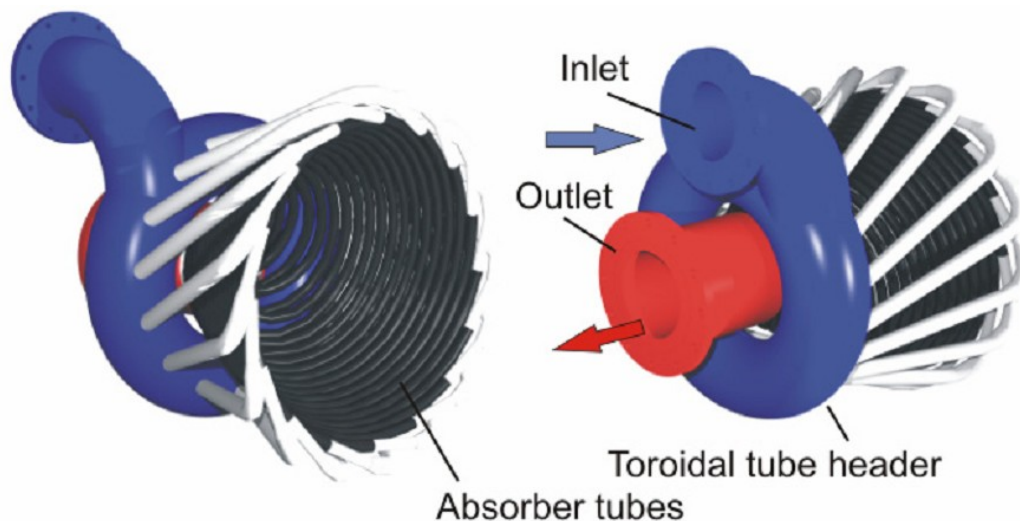


Figure 2.9: Schematic view of the low temperature module[17].

The high temperature receiver module consists of a ceramic foam absorber of SiC with a porosity of 20 ppi installed on a fiber reinforced alumina based structure. To contain the costs, a rib geometry is selected, resulting in a relatively low amount of expensive ceramic structures. The final mounting structure consists of twelve rib segment held together by two clamping rings, also manufactured from the same fiber-reinforced ceramic material. At the feet of the ribs, a T-like shape is formed to allow clamping to the metallic outer casing (which is at lower temperature)[17].

The pressurized air is kept into the receiver by a quartz window that has a semi-elliptical profile with a 620 mm diameter at the open end and a 420 mm depth. Its 8 mm thickness allows pressure up to 19.5 bar. An active cooling system, based on 18 nozzles that blow cold air toward the quartz window, is installed to prevent the break of the window caused by overheating. The installation of the cooling system doesn't affect the power balance of the plant since the energy consumption of the blower is negligible.

Figure 2.10 shows a scheme of the volumetric receiver used as high temperature module.

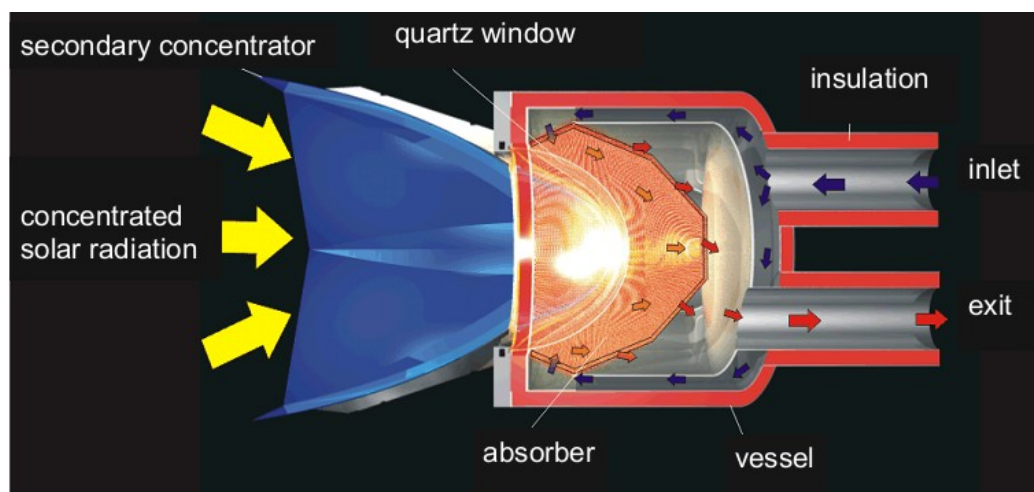


Figure 2.10: Scheme of the high temperature module[17].

The module has a nominal thermal power of 400 kW, a temperature increase of 250 °C for an air flow of 1.357 kg/s and an average efficiency of about 80%¹³. A bypass over the receiver is installed to allow the reduction of the receiver mass flow and increase the receiver outlet temperature, while maintaining the combustor inlet temperature constant.

With a temperature at the outlet of the receiver assumed at 850 °C and a compressor outlet temperature of 450°C, the thermal power, which the receiver

¹³ The efficiency can be higher if the geometry of the secondary concentrator is optimized.

must supply to the 117.5 kg/s of air flowing through, is calculated with formula (2.1):

$$\dot{Q} = \dot{m} \cdot \bar{c}_p \cdot (T_{in,r} - T_{out,r}) \quad (2.1)$$

and is equal to 52.922 MW_{th}.

This means that 84 low temperature modules and 84 high temperature modules are required (formula 2.2), for a total frontal area of 208,32 m² (each receiver has a nominal thermal power of 400 kW and a frontal area of 1.24 m²).

$$N_{modules} = \frac{\dot{Q}}{\dot{Q}_{module}} \quad (2.2)$$

The receiver is installed over the four side of the tower instead of only one side, in order to contain the tower's dimensions.

2.4.3 Solar field and solar power tower

The design of the solar field shouldn't be overlooked because it's the most expensive component of a solar power plant, but, before starting, it's necessary to choose the location of the plant.

Since the HSGTPPs are ideal for working in areas with low water supply, a latitude of 35° north, which is included in the Mediterranean and American sunbelt, has been chosen. In order to obtain a high solar share over the year, the power plant is designed to work in nominal conditions not at the noon on summer solstice, when the solar irradiation is the highest of the year, but at the noon of the vernal equinox. In this case the peak solar radiation, that determines the size of the solar field, is equal to 800 W/m². The solar irradiation varies during the day as is shown in figure 2.11.

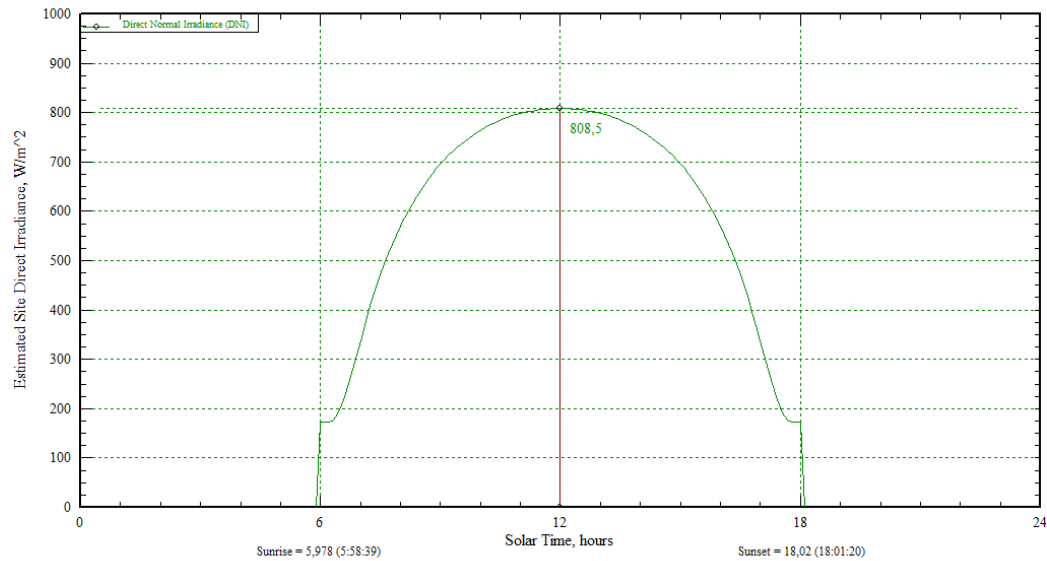


Figure 2.11: Solar irradiation during vernal equinox at latitude of 35°N.

Now it's possible to determine the configuration of the solar field. Two options are available:

- *Surrounding field*: typical of high latitudes where the sun stays high in the sky for most of the day. The heliostates are arranged in a circular shape surrounding the tower.
- *North field*: typical of low latitudes. The heliostates are placed only on the north side¹⁴ of the tower.

In a north field, in comparison with the surrounding field, the heliostats are more far away from the tower so the intercept factor is reduced and the atmospheric attenuation losses are increased, while, on the other hand, the cosine factor is better.

In conclusion, the parameter that determines the choice between the surrounding field and the north field is the size of the power plant: generally for smaller plants (less than 50 MW_e) the north field configuration is preferable, otherwise, for bigger plants (more than 50 MW_e) the surrounding field is the best choice[26]. Figure 2.12 shows a schematic comparison between the two configurations.

¹⁴ If the power plant is installed in the southern hemisphere the solar field is built on the south side.

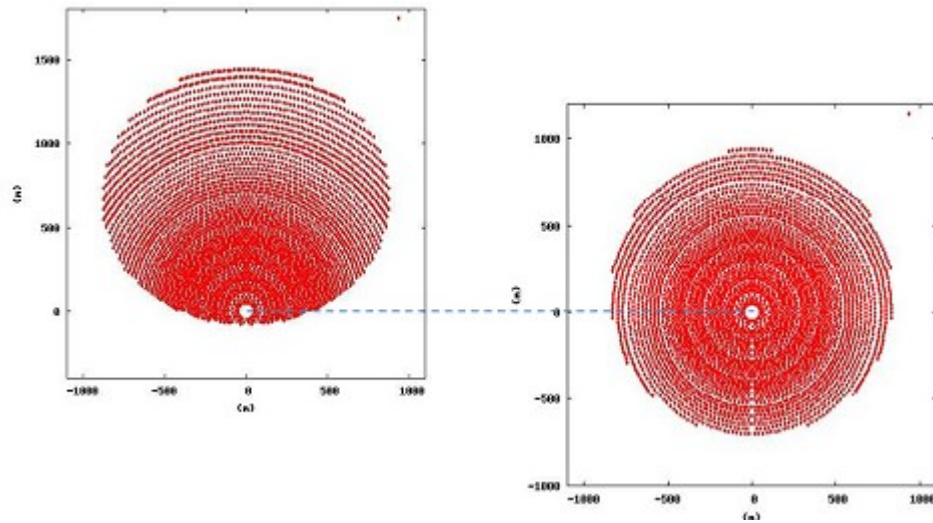


Figure 2.12: Layout comparison between north field and surrounding field[26].

The area occupied by the solar field can be calculated with formula 2.3:

$$A_{sf} = \frac{\dot{Q}}{\eta_{sf} \cdot I_N} \quad (2.3)$$

Where:

- \dot{Q} is the thermal power required by the receivers (52.922 MW_{th}).
- I_N is the nominal solar irradiation (at the noon of the vernal equinox is equal to 800 W/m²).
- η_{sf} is the annual efficiency of the solar field.

The solar field annual efficiency depend on several factor such as mirror reflectivity and cleanliness, atmospheric losses due to dust and other pollutants, tracking precision of the heliostats, field geometry and location in relation to the tower, blocking and shadowing effects by other heliostats and the tower and spillage effect¹⁵. It varies from 50% up to a theoretical limit of 70%[27], so an intermediate value of 60% has been chosen, with which the solar field area is equal to 110250 m².

The solar field is composed of several mirrors, which reflect the sun ray to the solar receiver at the top of the tower, called heliostats. More in particular a heliostat is composed of a reflecting surface, usually a plane or a slightly

¹⁵ The spillage effect consists in a fraction of the reflected solar radiation that misses the solar receiver

concave mirror, a support structure and a two axis¹⁶ control system. Once calculated the area occupied by the solar field it's possible to value the number of the heliostats required with formula 2.4:

$$N_h = \frac{A_{sf}}{A_h} \quad (2.4)$$

Where:

- N_h is the number of heliostats required
- A_{sf} is the area occupied by the solar field previously calculated and is equal to 110250 m²
- A_h is the reflecting surface area of a single heliostat

Despite the size of the reflecting surface area of a single heliostat doesn't affect the area occupied by the solar field, the selection of a smaller or a bigger heliostat depends on the relative cost per m² and on the receiver size[26]. More in details, bigger heliostats benefits of improved economies of scale and, in addition, fixed costs per heliostat (such as controls, installation and operation&maintenance) can be spread over more area to reduce the relative cost per m². On the other hand, smaller heliostats have more precise solar tracker and require a relatively smaller receiver and this fact could also have a positive impact on the cost and on the thermal losses of this essential component of the plant[28].

For a single heliostat surface area of 141 m² the total number of heliostats required is equal to 782.

Since the gas turbine must be placed at the ground level, the air must be sent to the top of a tower where it is heated by the reflected solar radiation. This procedure adds pressure losses to the cycle, caused by friction and corners, that lower the overall efficiency.

A solution to this problem consists in locating the solar receiver at ground level and installing a hyperboloid reflector at the top of the tower where the radiation is concentrated. This solution is know as Solar Concentration Off Tower (SCOT), but is also called Reflective Tower or Beam-Down. A schematic of this concept can be seen in figure 2.13.

¹⁶ Generally azimuth and elevation axes are used.

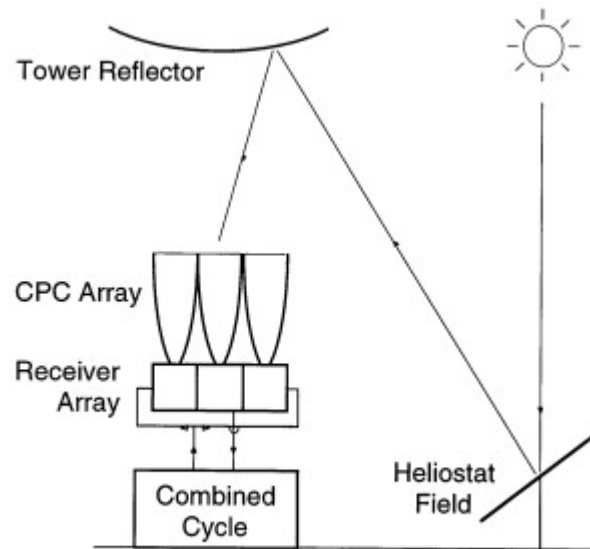


Figure 2.13: Concept of a solar driven combined cycle plant with SCOT technology[29].

The principal advantages of this technology are:

- *Better collection optics*: the arrangement produces low concentration at its lower focus, but, however, it also produces a narrow view angle and a large effective focal length (due to magnification by the hyperboloidal mirror). This reduces optical aberrations, and allows a higher overall maximum concentration by non-imaging terminal concentrators installed at the lower focus. The effect is especially significant for large fields, where the field radius is typically three times the tower height.
- *Stable flux distribution*: the heliostat field has a single aim point, producing a single “spot” at the lower focal region. This spot is divided among several CPC secondary concentrators, each accepting radiation from the entire field, and therefore the fraction of power allocated to each CPC varies little with time. Thermal balancing and heliostat field control issues are therefore greatly reduced, unlike tower-mounted CPC’s.
- *Ground level plant*: the major hardware (CPC, receiver, storage, power block, etc.) is located near ground level. This eliminates a massive and expensive tower, long piping and the need for frequent personnel access to the tower top. The tower is light and inexpensive, supporting only a passive reflector component[29].

However, the SCOT system has some technological difficulties, such as the

mechanical integrity of the central reflector against the wind force, and a wider focus due to the dilution of the beam concentration at the receiver aperture, so this concept is discarded in favor of the more popular and reliable solar tower technology.

An approximate value of the tower height can be calculated with the empirical formula 2.5[27]:

$$H_t = 29.1 + 0.5113 \cdot \dot{Q} - 0.00887 \cdot \dot{Q}^{1.5} + 32801.719 \cdot \dot{Q}^{-2} \quad (2.5)$$

Where:

- \dot{Q} is the thermal power required by the receivers expressed in thermal megawatts (52.922 MW_{th})
- H_t is the tower height and is calculated in meters

A value of 80 meters is chosen¹⁷ for the tower height.

Since the power block of the gas turbine is placed at ground level and the solar receiver is on top of the tower, it's necessary to link the two sections with pipes.

The dimensions and the number of tubes must be optimized in order to maintain low the pressure drop and the heat dispersion toward the outer ambient. This can be achieved with the choice of a large diameter and a high quantity of tubes, so the velocity of the air flow is reduced (formula 2.6), like so the pressure drop (formula 2.8) and the heat transfer coefficient.

On the other hand, a small diameter and a low quantity of tubes imply a lower volume of tubes that entails a cost reduction.

$$\dot{m} = v \cdot \rho \cdot \frac{\pi \cdot D^2}{4} \cdot N_t \quad (2.6)$$

Where:

- \dot{m} is the total air flow at the compressor outlet (117.5 kg/s).
- v is the air flow velocity.
- ρ is the air density.
- D is the internal diameter of a single tube.
- N_t is the total number of tubes.

The air density is calculated with the ideal gas law (formula 2.7) and varies with the temperature.

¹⁷ The calculated tower height is equal to 65 meters, but it is increased to take account of the area occupied by the receiver's modules.

$$\rho = \frac{P}{R^* \cdot T} \quad (2.7)$$

Where:

- p is the air pressure (21.17 bar)
- R^* is the specific gas constant (287.04 J/kgK for air)
- T is the air temperature (450°C at the compressor outlet, 850°C at the receiver outlet)

Since the air density at the compressor outlet is higher than the air density at the receiver outlet, it's better to choose two different diameter for the ascent phase and the descent phase in order to obtain the same air velocity and the same pressure drop.

However, for simplicity of design and to contain the costs, it's chosen to use four tubes for the ascent phase and four tubes for the descent phase (one tube for each side of the tower) with a diameter of 0.84 meters in order to contain the pressure drop calculated with formula 2.8.

$$\Delta p = f \cdot \frac{1}{2} \frac{L}{D} \cdot \rho \cdot v^2 \quad (2.8)$$

Where:

- f is the friction factor (depends on the tube roughness and on the Reynolds number, in this case it is assumed equal to 0.05)
- L is the length of the tube (from the ground level, where lays the compressor, to the receiver placed at the top of the tower)
- D is the tube diameter (0.84 meters)
- ρ is the air density (10.2 kg/m³ at the compressor outlet, 6.57 kg/m³ at the receiver outlet)
- v is the air velocity (assumed equal to 5 m/s)
- Δp is the pressure drop over the tube

When the gas turbine works in nominal conditions with the air heated by the solar receiver, the pressure losses caused by friction are equal to 0.006 bar for the ascent tubes and 0.01 bar for the descent tubes.

A value for the pressure drop associated at the solar receiver can be taken from the SOLGATE project, which has measured a pressure drop of 0.18 bar, since its receiver technology is the same of this plant. However, it's expected a lower pressure drop in our plant because the air is compressed at 21.17 bar instead of 5 bar like in the SOLGATE project, so the air density is higher and the velocity, from which the pressure losses depend on a quadratic term, is lower.

Pressure losses causes a reduction of the power output because the turbine expands air from a lower pressure, generating less power, while the compressor adsorb always the same power.

The reduction of the power output can be calculated with formula 2.9.

$$W_t = \dot{m} \cdot \bar{c}_p \cdot \eta_t \cdot T_{it} \cdot \left(1 - \left(\frac{P_{atm}}{p_c - \Delta p} \right)^{\frac{\gamma-1}{\gamma}} \right) \quad (2.9)$$

Where:

- W_t is the power produced by the turbine.
- m is the air flow through the turbine (130.2 kg/s)
- c_p is the air average specific heat (1.126 kJ/kgK)
- η_t is the turbine efficiency (0.83)
- T_{it} is the turbine inlet temperature (1300°C)
- p_{atm} is the atmospheric pressure (1.01325 bar)
- p_c is the compressor outlet pressure (21.17 bar)
- Δp is the pressure drop between the compressor outlet and the turbine inlet
- γ is the air heat capacity ratio (1.4)

The variation of the power produced in function of the pressure drop can be seen in figure 2.14.

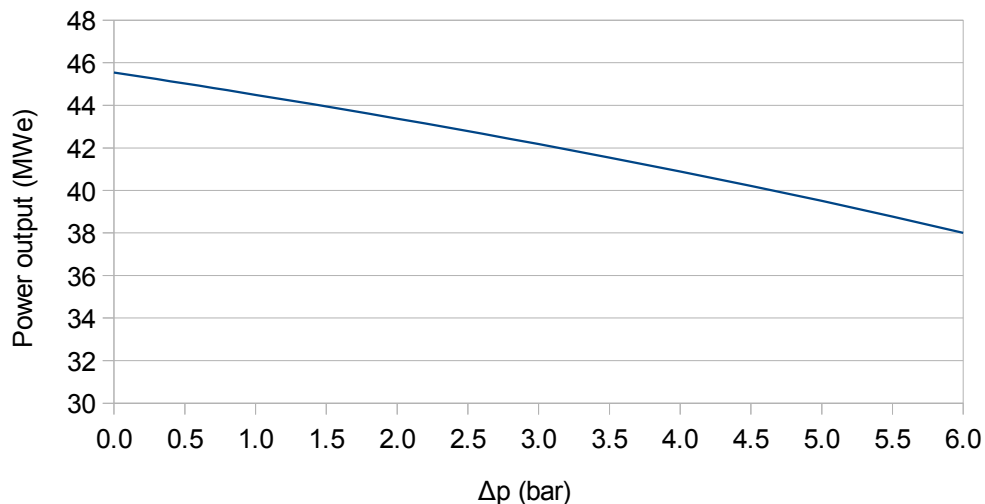


Figure 2.14: Variation of the power output in function of the pressure drop.

2.4.4 Thermal energy storage

In order to extend plant operation beyond sunlight hours without decreasing the solar share of the power production, a thermal energy storage (TES) system must be deployed. Such system would then harness additional solar energy during the day and release it at night to continue solar operation[15]. Moreover it can be used to maintain a stable power output during rapid solar transients.

The heat storage device is placed in parallel to the solar receiver, so part of the air at the receiver outlet is sent to heat the storage and is recirculated into the solar tower. This means that, to maintain the design nominal power output, it's necessary to install a bigger solar field in order to supply more thermal power to the receiver so the air outlet temperature is equal to 850 °C even when a greater quantity of air passes through the receiver's modules.

Since the storage reaches temperatures of about 850 °C, a regenerator-type heat storage is considered a particularly promising technology option. However, this component of the power plant will be treated in more detail in the next chapters.

Chapter 3

Thermal storage overview

This chapter analyzes the technologies that are currently used to store thermal energy in concentrated solar power plant.

3.1 Introduction

The electrical output of a solar power plant is closely related to the direct normal irradiation (DNI), which may change during the day due to the cloudiness of the sky and to the increase of the angle of incidence between the sun and the solar collector. When solar energy isn't available, it's necessary to burn natural gas to provide continuous operation of the plant unless solar energy has been stored previously.

To do that it's necessary to build a solar field bigger than a system without storage, so the surplus energy collected during the most sunny hours can be stored in a hot tank through a heat transfer fluid (HTF) that circulates through the solar collectors.

The installation of a thermal energy storage in a solar power plant allows production of electricity on demand unlike other renewable energies, such as wind, tidal or photovoltaic (storing electricity is much more expensive). This feature can be used to smooth out transients in the solar input, avoiding the turbine to work at partial load and with continuous transient, in this way electricity is produced with higher efficiency.

Storing thermal energy is helpful to reduce CO₂ emissions, in fact if the heat isn't supplied by solar energy previously stored it should be necessary to burn natural gas (that is converted into electricity with a lower efficiency than in a combined cycle) to make the turbine work. The solar share¹⁸ can raise up to 74% in base load consequently[30].

Another advantage of the thermal energy storage is the possibility to shift the electricity generation to meet a request profile that does not necessarily correspond to the insolation profile (see figure 3.1), in order to increase the revenues from power sale by storing off-peak solar energy during the morning hours and releasing it late in the afternoon, when the electricity's price is higher.

¹⁸ The ratio of the total annual solar heat and the total annual used heat of the power plant.

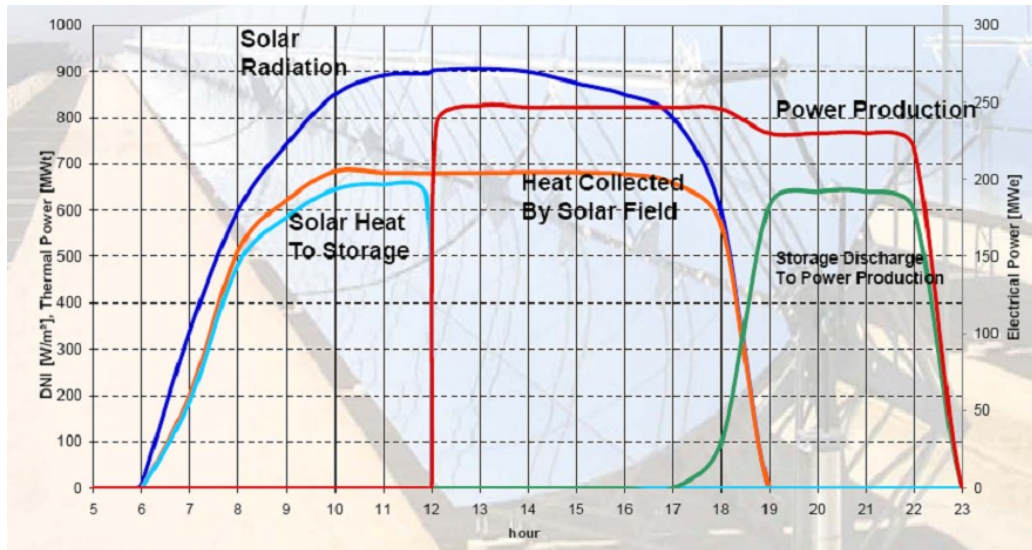


Figure 3.1: The use of thermal energy storage in a CSP plant to shift electricity output from morning off-peak to evening on-peak demand[31].

On the other hand the installation of a thermal energy storage represents a high investment cost, which is reflected to the levelized cost of electricity (LCOE), making the electricity produced by solar thermal power plant less competitive compared to other renewable energies. Therefore it's necessary to develop an economical and reliable way to store thermal energy.

3.2 Heat storage media

Various media storage can be grouped into three different categories by storage mechanism: sensible heat, latent heat and thermochemical energy. In sensible heat storage the thermal energy is stored with a change of the internal energy (temperature increasing), as it's shown in formula (3.1):

$$Q = m \cdot \bar{c}_p \cdot (T_h - T_c) \quad (3.1)$$

In latent heat storage the thermal energy is stored as latent heat of phase change (generally solid-liquid transition) and there's no temperature variation. In thermochemical energy storage an endothermic reaction is activated by the solar heat, which can be recovered completely when the backward reaction starts. The reaction must be completely reversible and, in some case, catalysts are necessary to control the reaction.

3.2.1 Sensible heat storage: concrete

Concrete storage is an attractive option thanks to the low cost of concrete and to the high temperatures that can be achieved in the storage (up to 400°C). The storage is made by a concrete block that contains a tube register heat exchanger to transfer the thermal energy to or from the HTF. Since an important part of the storage's expense is due to the tube register, various concepts have been investigated to reduce the overall cost.

The first option consists of a tubeless design, in which the prestressed concrete storage is directly in contact with the HTF. The cost is reduced, because the steel necessary for the tubes is eliminated, but the level of impermeability of the concrete isn't high enough to avoid leaks of the HTF. Another issue is the expensive and technically difficult junction of the pipe-storage interface.

A solution to clear the problem of the HTF's leaks is the encapsulation of the concrete with special tank steel¹⁹. The permeability's problem is solved, but the final cost is higher than the normal tube register storage.

Another method used to improve the storage is to increase thermal conductivity of the concrete so the tubes can be shorten and more distanced (see figure 3.2). The addition of axial fins to the tubes is considered[32] the best way to increase the thermal conductivity of the storage.

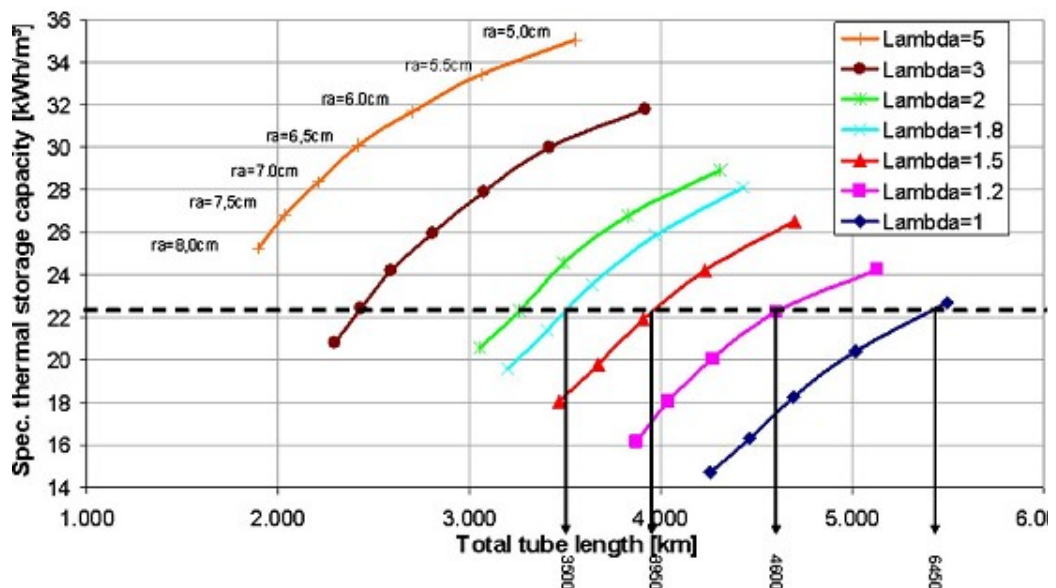


Figure 3.2: Specific heat capacity as a function of total tube length for different thermal conductivities (λ , W/mK) and distance of tubes (r_a , cm) [32].

¹⁹ For example ST 35.8 or 15Mo3 [32]

3.2.2 Sensible heat storage: thermal oil

The oil that circulates in the solar collector as HTF can be stored in appropriate tanks, so the use of a secondary storage medium and the building of a heat exchanger is avoided. The most common oils used in solar power plant are listed in table 3.1 and it's clear that the principal limitation to the adoption of oil as storage medium is the limited maximum temperature. Furthermore the synthetic oil, which is made of aromatic compounds, is classified as flammable, while silicone oil, which is considered a non-hazardous material[33], is too expensive. For those reasons the power plant Solar One²⁰ in California demonstrated the feasibility of the project, but the thermal storage system was inadequate for operating the turbine at peak efficiency because the storage system operated only between 220–305°C, whereas the receiver outlet (and design turbine inlet) temperature was 510°C[34]. Moreover, the introduction of water (used as HTF) into the oil storage tank led to a rupture of the storage tank resulting in a fire in 1986[35].

Table 3.1. Liquid Candidate Storage Media for SEGS Plants[36].

Storage Medium	Temperature		Average density (kg/m ³)	Average heat conductivity (W/mK)	Average heat capacity (kJ/kgK)	Volume specific heat capacity (kWh _t /m ³)	Media costs per kg (\$/kg)	Media costs per kWh _t (\$/kWh _t)
	Cold (°C)	Hot (°C)						
Mineral oil	200	300	770	0.12	2.6	55	0.30	4.2
Synthetic oil	250	350	900	0.11	2.3	57	3.00	43.0
Silicone oil	300	400	900	0.10	2.1	52	5.00	80.0
Nitrite salts	250	450	1,825	0.57	1.5	152	1.00	12.0
Nitrate salts	265	565	1,870	0.52	1.6	250	0.70	5.2
Carbonate salts	450	850	2,100	2.0	1.8	430	2.40	11.0
Liquid sodium	270	530	850	71.0	1.3	80	2.00	21.0

However, the low heat conductivity and the narrow range of operating temperatures make the realization of a single tank thermocline easier.

3.2.3 Sensible heat storage: molten salts

The most economical storage media that can be used in a solar power plant are the molten salts, in particular the nitrate salts which are composed of a mixture of 40% by weight KNO₃ and 60% by weight NaNO₃. Apart from the low medium cost per kg, the nitrate salts melt at 220 °C and are thermally stable to about 600°C[37] so, in comparison with storage oils, they can operate with a wider temperature range and need a minor mass to achieve the same heat stored. The sodium hydroxide, which has a melting point of 320 °C and could be used for temperatures up to 800 °C, must be rejected because it's highly corrosive and

²⁰ In this plant the HTF was water/steam and the storage was made by a single tank thermocline system filled with rock and oil.

there is difficulty in containing it at high temperature.

The experience in the Solar Two Project has proven the feasibility of a molten salts storage. The power plant²¹ used a mixture of 40% KNO_3 and 60% NaNO_3 as HTF and storage medium to produce 10 MW net electricity (12 MW gross electricity). With a hot tank temperature of 565 °C and a cold tank temperature of 280 °C the design thermal capacity was appraised at 105 MWh_{th} , but the actual thermal storage capacity based on the mass of salt (1.5 million kilograms in all the system) in the tanks, accounting for (subtracting) the 3 foot heels in each tank was 114 MWh_{th} [38]. This means that the storage, with the gross conversion efficiency measured 33%, could supply the turbine at full output for 3 hours. A schematic of the system is shown in figure 3.3.

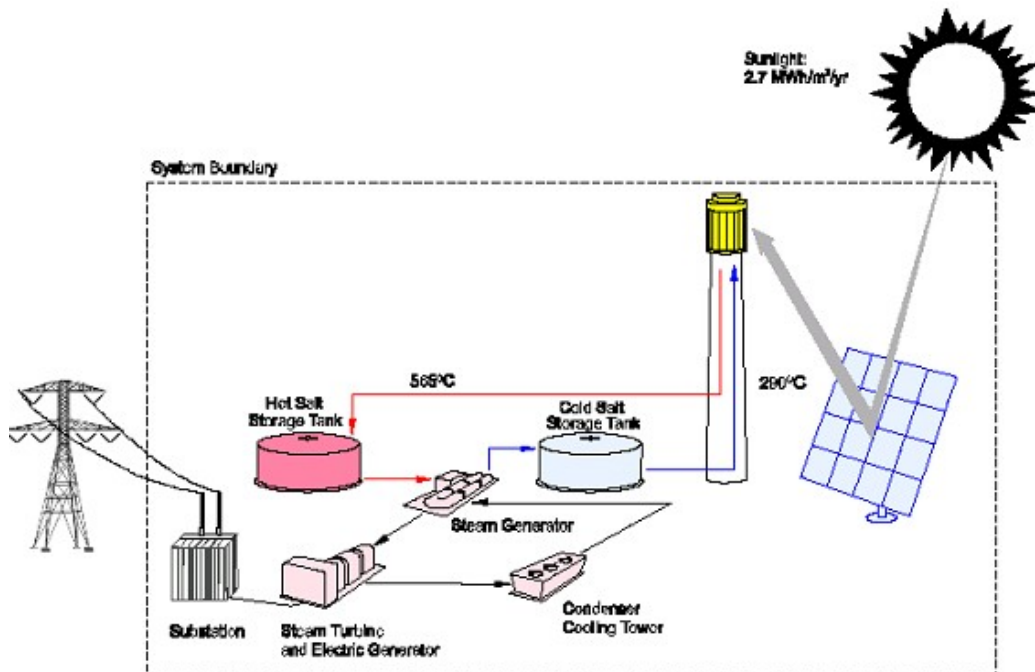


Figure 3.3. Molten salt power tower system schematic at Solar Two[37].

Because of the high freezing temperature of the salts, the evaporator tube bundle experienced several freeze thaw cycles[37]. The minimum temperature of the HTF loop can't be too low and it's necessary to heat the salts during plant shutdowns or at night for avoiding their solidification in the pipes. A solution to this problem is to wrap the piping with heat trace, a resistance wire that maintain heat on the pipes, to prevent freezing on the salts[39]. Another solution consists in using HITEC salts, composed of a mixture of 40% NaNO_2 , 7% of NaNO_3 and 53% KNO_3 , which have a melting point of 142 °C, but also a maximum

²¹ The Solar Two has been decommissioned in 1999.

temperature of 425 °C, above that decomposition and oxidation of the salts begin to take place[40]. A more attractive way to lower the melting point of the salts is the addition of calcium nitrate (CaNO_3)₂ in the mixture; a mixture of 48% of (CaNO_3)₂, 45% of KNO_3 and 7% of NaNO_3 has a melting temperature of 120 °C, but the calcium nitrate is more expensive than the other salts, as can be seen in table 3.2.

Table 3.2. Price of nitrate salts[39].

CaNO_3	KNO_3	NaNO_3
\$1300/ton	\$560/ton	\$360/ton

The only TES system that currently operates with multiple hours of storage is the sensible, two tank, molten salt system. This system is chosen because the components associated with molten salt handling (pumps, valves, tanks, and heat exchangers) have demonstrated reliable operation at commercial scale[41].

3.2.4 Sensible heat storage: steam

In solar power plant with direct steam generation (DSG) the steam can be used as storage medium, so the building of a heat exchanger and the use of a secondary fluid for storage can be avoided. In this case the storage is charged by condensing high temperature steam and thus raising the temperature of the water volume contained. During discharge, the pressure within the hot water vessel is decreased. Part of the water evaporates and can be withdrawn as saturated steam. The thermal capacity of the storage is proportional to the heat capacity of the contained water and to the temperature difference allowable for the steam process between charging and discharging. Despite the water cost is very low, investment of the pressurized steam vessel is rather high and the overall cost can be appraised at about 180 \$/kWh[42] and is used only as a buffer storage. Moreover temperatures above 373 °C (critical point of water) cannot be achieved. Figure 3.4 represent the draft of a steam storage.

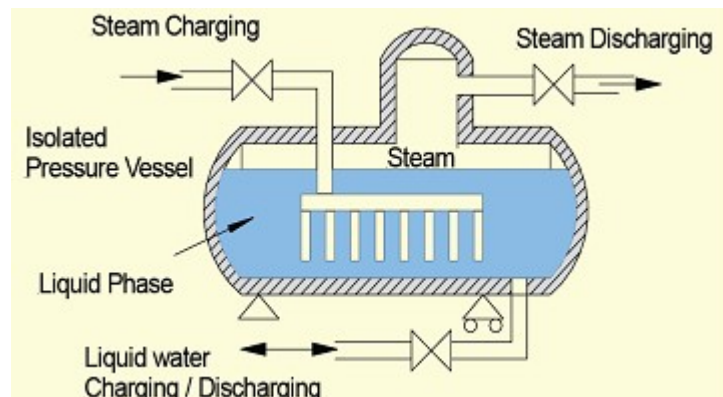


Figure 3.4: Principle of steam accumulator heat storage[42].

The PS10²² plant is provided with a steam storage system. The storage is composed by 4 tanks that are loaded by steam at 250 °C and 40 bar produced by the solar collector when the plant is working at full load operation. These tanks are sequentially operated in relation to their charge status and provide a thermal capacity of 20 MWh, equivalent to an effective operational capacity of 50 minutes at 50% turbine workload. The restricted duration of the storage is due to the choice of Solúcar²³ to work with frequent stops of the steam turbine in order to reduce the cost for the solar field (solar multiple value of 1,3) and for the storage[43]. Figure 3.5 shows the schematic system of PS10 plant.

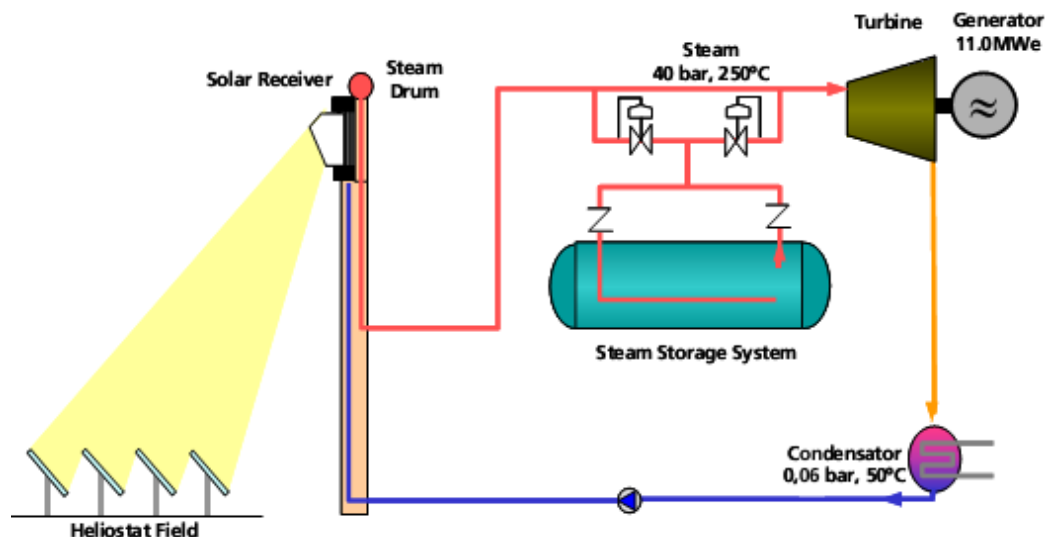


Figure 3.5: Schematic system of PS10 plant[43].

²² The PS10 is a 10 MW solar thermal power plant near Seville.

²³ Solúcar is the coordinator of the project.

3.2.5 Latent heat storage

Thermal energy can be stored isothermally as the latent heat of phase change (for example as heat of fusion in a solid-liquid transition) and the storage substances with this characteristic are called phase change materials (PCMs).

The isothermal storage is especially suitable for powering a Rankine cycle since most of the heat is exchanged in the evaporation phase, but if PCMs with different melting point are connected in a “cascade” design then they can be used even in a Joule-Brayton cycle. Since the PCM temperature must be always lower than the temperature of the HTF during charging and always higher during discharging, using different PCMs can optimize the storage reducing the temperature difference between the two processes. This idea has been developed by H. Michels and E. Hahne[44], who tested a storage with five different materials for solar electric generating systems. Results can be seen in figure 3.6.

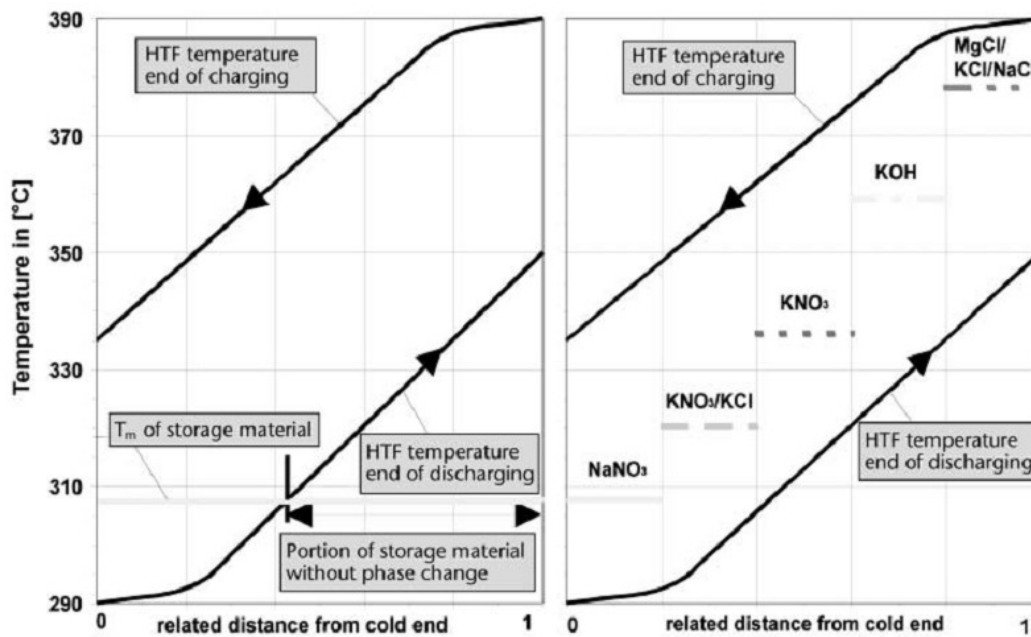


Figure 3.6: Theoretical temperature distribution in a PCM-TES for SEGs, one PCM (left), five PCMs (right)[44].

When selecting the appropriate PCM for a certain operation, the main criterion of choice is the melting temperature of the PCM, which must stay in the temperature range of the HTF. Another important criterion is thermal conductivity of the PCM, in fact the higher is thermal conductivity, the greater is the volume specific power density and this means lower quantity of PCM and, consequently, more affordable storage.

Materials such as lead, tin and lithium nitrate (LiNO_3) have good thermal

conductivity, but they are also too expensive so they must be excluded. Instead the nitrate salts balance a not excellent thermal conductivity (typical values are in the range of 0.5-2 W/mK) with a low cost. The most common salts are shown in Table 3.3.

Table 3.3: PCM Candidate Storage Media for SEGS Plants[36].

Storage Medium	Temperature		Average density (kg/m ³)	Average heat conductivity (W/mK)	Average heat capacity (kJ/kgK)	Volume specific heat capacity (kWh _t /m ³)	Media costs per kg (\$/kg)	Media costs per kWh _t (\$/kWh _t)
	Cold (°C)	Hot (°C)						
NaNO ₃	308		2,257	0.5	200	125	0.20	3.6
KNO ₃	333		2,110	0.5	267	156	0.30	4.1
KOH	380		2,044	0.5	150	85	1.00	24.0
Salt-ceramics (NaCo ₃ -BaCO ₃ /MgO)	500-850		2,600	5.0	420	300	2.00	17.0
NaCl	802		2,160	5.0	520	280	0.15	1.2
Na ₂ CO ₃	854		2,533	2.0	276	194	0.20	2.6
K ₂ CO ₃	897		2,290	2.0	236	150	0.60	9.1

The major problem of molten salts is the restricted thermal conductivity, in fact if it can be increased (for example from 1 W/mK to 10 W/mK) the number of tubes, in which flows the HTF, can be significantly reduced as shown in figure 3.7.

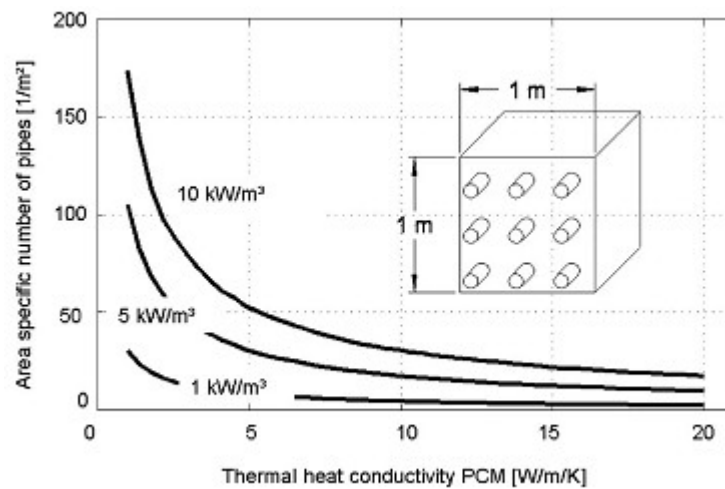


Figure 3.7: Number of tubes needed in PCM volume depending on heat conductivity of PCM for three different values of average volume specific power[45].

There are three different approaches in order to increase thermal conductivity. The first idea lies in macroencapsulation of storage material. In more detail the PCM is put in sealed capsules with an inert gas²⁴ and are piled into a pressure vessel that is filled with a heat transfer medium (water or steam). Typical dimensions of these capsules are 5-20 mm in diameter and 500 mm in length (for laboratory scale experiments, as seen in figure 3.8), a minimum wall thickness of 1mm is required²⁵ to prevent corrosion by nitrate salts and provide at least 10 years of life. An experiment[45], in which an eutectic mixture of KNO_3 - NaNO_3 is used as PCM, showed the feasibility of the macroencapsulation concept, but has also highlighted some economical disadvantages that exclude this solution:

- The amount of hull material needed for pressure-tight capsules is significant; if steel is used, the mass of steel is almost equivalent to the mass of PCM.
- The volume fraction of PCM in the pressure vessel is less than 40%.
- The filling and sealing procedure with molten PCM is complex, must be particularly avoided the contamination of the steam by PCM due to leakage of capsules.



Figure 3.8: Bundle of capsules filled with PCM before integration into pressure vessel[45].

The second way to enhance thermal conductivity consists in combining nitrate salts with a more conductive material like expanded graphite, that is chosen for its chemical stability. Since an infiltration of the graphite is not possible by the

²⁴ During phase change the volume of the PCM increases by about 10%[45]

²⁵ For this reason flexible capsules without inert gas are excluded

salt, the mixture is produced by cold compression of PCM and expanded graphite powder. For containing cost²⁶ it's necessary to limit the mass fraction of the graphite, although the increase of thermal conductivity is strictly tied to (see figure 3.9).

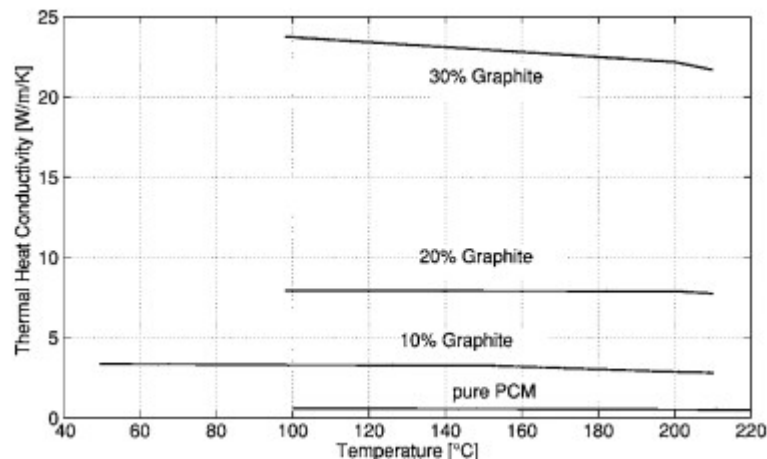


Figure 3.9: Effective thermal heat conductivity of PCM/graphite composite dependent on temperature for various compositions[47].

During one experiment[47] some leakage of salts was observed, which could be produced by the requirement of a void volume for salt expansion, outgassing caused by impurities and moisture in the technical salts and the poor testability of alkali metal nitrate salts on graphite and their good wettability on metal surfaces (creeping tendency)[45]. A portion of the composite storage can be seen in Figure 3.10.



Figure 3.10: Storage made of PCM and compressed graphite[45].

²⁶ The mass specific cost of expanded graphite is approximately 20 times higher than PCM's[46]

The last option for increasing thermal conductivity lies in the extension of the heat transfer surface. To do that finlike structures, integrated into the storage material, are necessary. These structures²⁷ are made of expanded graphite foils instead of steel fins since, at the same heat transfer capability, graphite foils require less thickness, have a better corrosion resistivity and are significantly cheaper. Experimental results can be seen in figure 3.11. However, for temperature higher than 250 °C, the expanded graphite becomes unstable with nitrate salts and metallic fins have to be used.

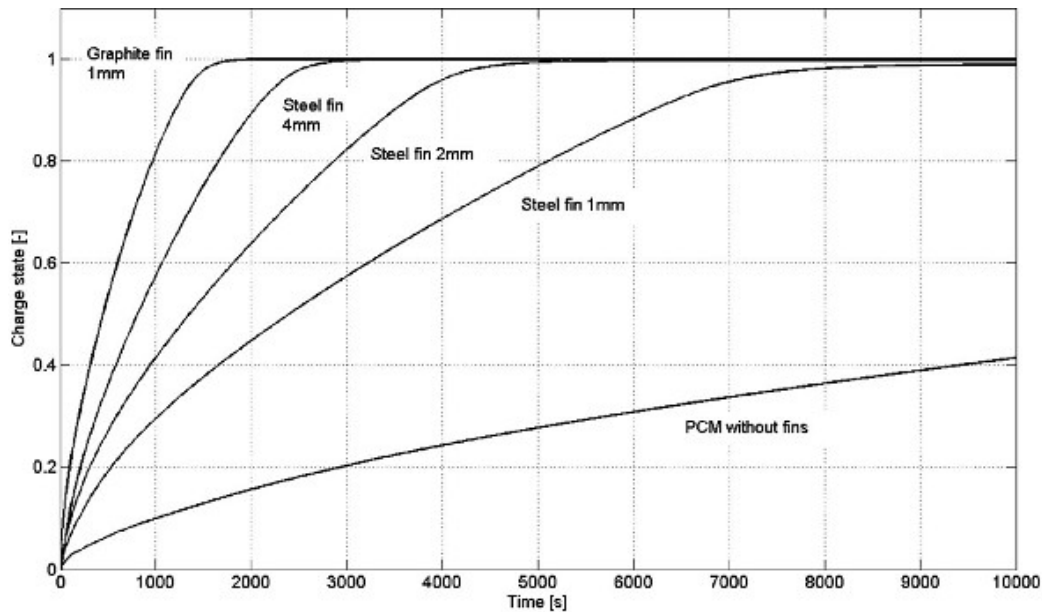


Figure 3.11: Calculated results for time needed to charge storage system with various fin materials and fin thicknesses[45].

This concept is considered the best solution to realize PCM-storage using nitrate salts[45], due to its proven feasibility and to the absence of any degradation of the heat exchanger or the storage material on the tests performed.

3.2.6 Thermochemical storage

In thermochemical storage systems, thermal energy is absorbed by a forward reaction ($A \rightarrow B$). The reaction product (B) preheats the reactant (A) and is stored at ambient temperature. To recover thermal energy, the reverse reaction generates product A and is used to preheat the reactant B for this reaction[48] (see figure 3.12). An attractive feature of this process is the potential for storing high grade heat at ambient temperature.

²⁷ This approach is also called “sandwich concept”.

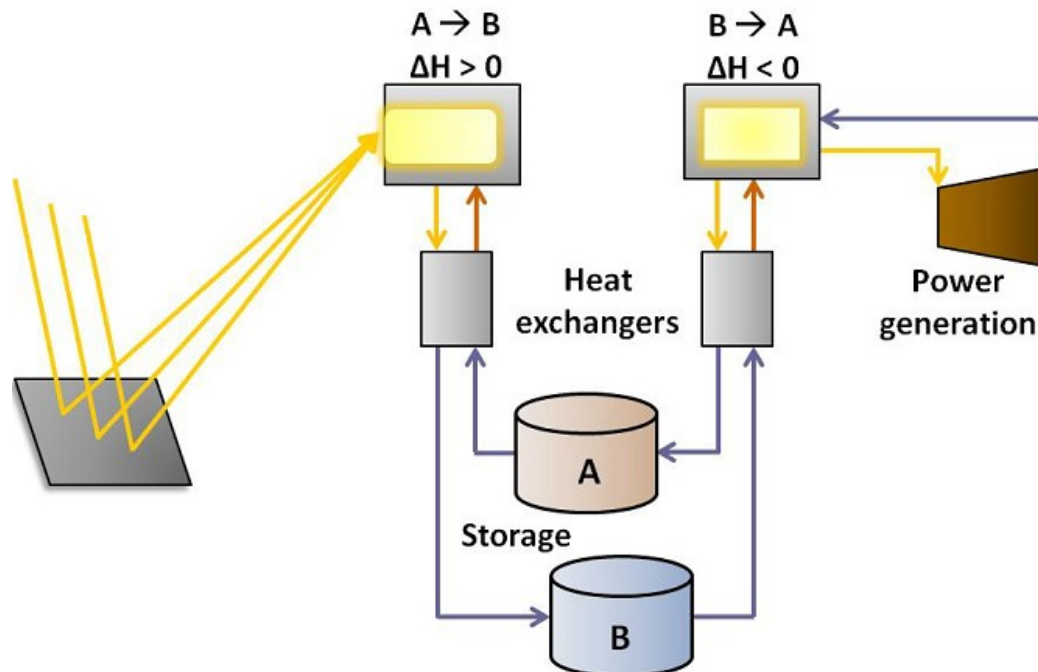


Figure 3.12: Schematic of generalized thermochemical storage cycle for CSP technologies[48].

The dissociation of ammonia into hydrogen and nitrogen (see formula (3.2)) is endothermic by 70 kJ/mol and proceeds catalytically at temperatures above 700K and at high pressures (50-100bar). This reaction has been used as thermal storage in a techno-economic feasibility study for a 10MW solar power plant design, which indicates a LCOE of 0,16 US\$1999 per kWh[49].



The energy efficiency of this storage may be very high, but, if the heat is released at low temperature, the exergy efficiency becomes too low. To minimize exergy losses it's necessary to operate the reversal reaction at the highest possible temperature and to reduce the exchange steps.

Another important problem of this kind of storage is the rapid degradation of the storage material, caused by poisoning and sintering of the catalysts that slow down the reaction kinetics.

3.3 Storage system in the power plant

There are different ways to insert the thermal storage in the power plant. For solid storage a modular approach can achieve a higher efficiency than the basic storage, while the liquid media can be stored in a two tank configuration (directly or indirectly) or in a single thermocline tank.

3.3.1 Modular approach for concrete storage

In a solar power plant with concrete storage the storage unit is placed parallel to the solar field and, during the charging phase, the thermal oil from the collectors is fed into the storage system at temperatures of about 390 °C. Temperatures of the oil above 400 °C must be avoided²⁸, so the temperature at the inlet of the collectors, that is also the temperature at the exit of the storage unit, is limited to 315 °C. To increase the average storage temperature and, consequently, the storage capacity, it's necessary to raise the exit temperature with a modular charging design.

In this concept the solar field and the storage unit are divided in shorter sections, so the temperature difference between the inlet and the outlet of the section is reduced and the allowed exit temperature, for the same inlet temperature, is increased[32].

This idea can be applied even to the discharging phase. The storage is divided in shorter sections, so the temperature differences between the thermal oil and the working fluid (generally steam) are reduced and the efficiency of the system is increased thanks to the reduction of the exergetic losses due to thermal exchange. Figure 3.13 illustrates the modular concept.

Another way to optimize the discharging phase consists in the sequential discharging, where not all storage sections are operated parallel. For example, in a Rankine cycle the storage section initially used for superheating can be used for evaporation and for preheating when its temperature goes down. In this way the average variation of the storage temperature is maximized, resulting in an increase of the storage capacity.

²⁸ The oil is thermally stable till 400 °C.

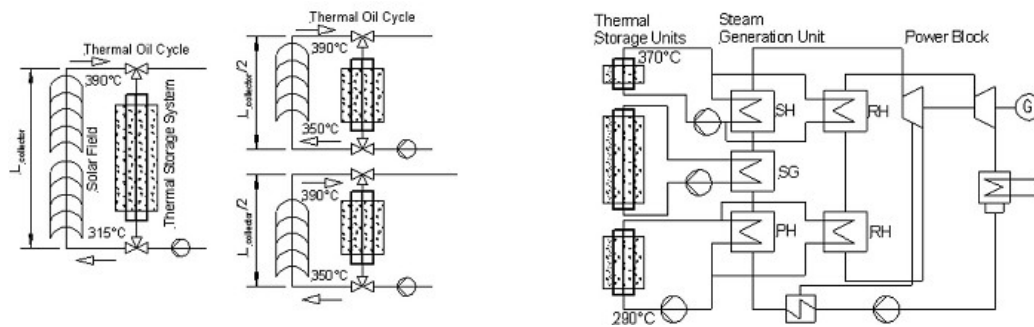


Figure 3.13: Basic storage (left), modular charging concept (center), modular discharging concept (right)[50].

The WANDA²⁹ project has proven that the installation of a storage with modular charging and modular discharging can increase the electrical energy production from 130 MWh, provided by the basic configuration, to 280 MWh. This means an increase of about 115% that can allow a reduction of more than a factor 2 in storage size and investment cost[32].

However modular charging and discharging require the installation of additional pumps, piping components, valves and an expansion vessel. The investment cost increases, but the specific cost of the thermal energy storage passes from 30.4 €/kWh for the basic concept to 14.1 €/kWh for the modular concept, while the LCOE passes from 0.2 €/kWh to 0.195 €/kWh, a reduction of around 2%[50].

Compared with the molten salt storage used in the Andasol power plant, the concrete storage has a decrease of the environmental impact by 7% for 1 kWh of electricity delivered to the grid. More in detail, the emissions of CO₂ and methane for the concrete storage are increased, mostly due to the production of the steel for the tubes, but the production of nitrate salts requires nitric acid, which causes the emission of N₂O, so, globally, the concrete storage has a lower environmental impact than the nitrate salts storage[50].

3.3.2 Two tank indirect system

This configuration is used when the HTF and the storage medium are different, for example when thermal oil is utilized as HTF and molten salts as storage medium.

The installation of a heat exchanger is required to transfer the thermal energy from the HTF to the storage medium, so the storage temperature doesn't coincide with the receiver outlet temperature of the HTF and the maximum temperature of the thermodynamic cycle is lower when the storage is in function. The heat exchanger feed is controlled by two valves that adjust the

²⁹ This project investigated the feasibility of a concrete storage instead of a nitrate salt storage in the Andasol power plant (50 MW).

quantity of HTF that flows through: in normal conditions the valves are partially open and part of the hot HTF goes to heat the working fluid and part to heat the storage; when the insolation is lowered the valves are completely open, so the cold HTF passes through the heat exchanger and increases its temperature. If molten salts are used as storage medium and oil as HTF, the temperature of the hot tank is limited to 380 °C, despite it can reach even more than 550 °C, and the temperature of the cold tank is about 290 °C in order to avoid the solidification of the molten salts. Figure 3.14 illustrates this concept.

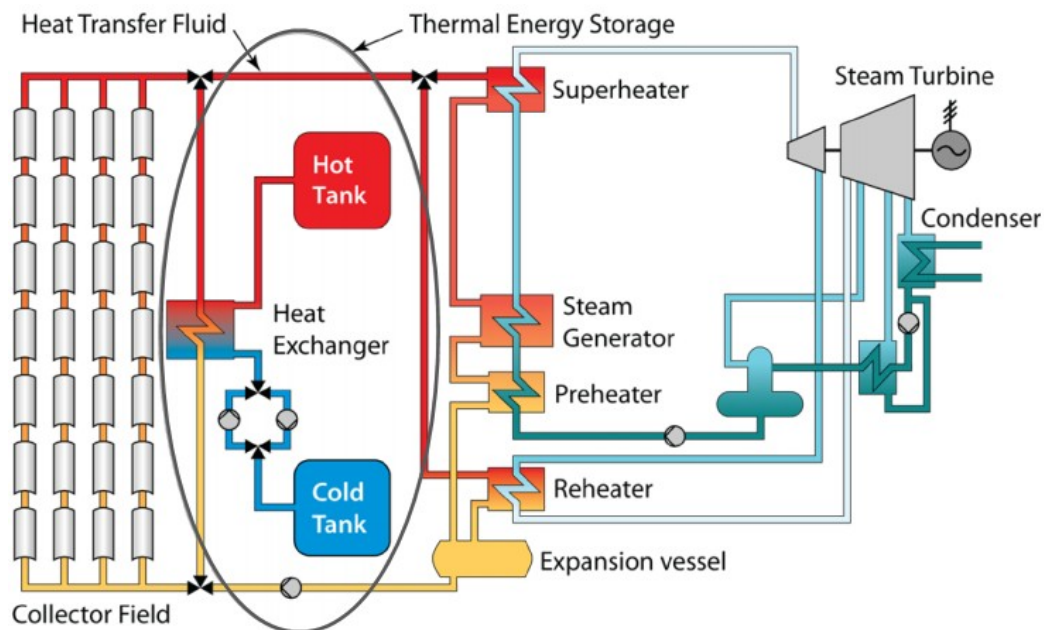


Figure 3.14: Schematic of parabolic trough power plant with indirect two tank, molten salt thermal storage[41].

A safety test³⁰ demonstrated that in case of a oil's leak in the heat exchanger there's no risk of explosion, but a fire could result, due to the high flammability of the oil vapors in contact with the air. If the oil leaks into the molten salts there can be no flame, since the headspace of the salt tanks is filled with an inert gas and no oxygen is present[39].

This storage system is installed in the Andasol 1, a 50MW power plant near Granada, where 28,500 tons of nitrate salts are stored in a hot tank at 390 °C and in a cold tank at 290 °C. This storage supplies a thermal reservoir of 1,010 MWh, enough to run the turbine for 7.5 hours at peak load[51].

³⁰ The salts used in this test are a mixture of 48%CaNO₃, 7%NaNO₃ and 45%KNO₃ and the oils are Therminol and Caloria.

3.3.3 Two tank direct system

A direct storage system is possible only if the HTF and the storage medium are the same. In this case the HTF is pumped from the cold tank through the solar field and, at the exit, is stored directly in the hot tank. When the insolation is lowered the HTF is withdrawn from the hot tank and sent to feed the power cycle. Figure 3.15 illustrates this concept.

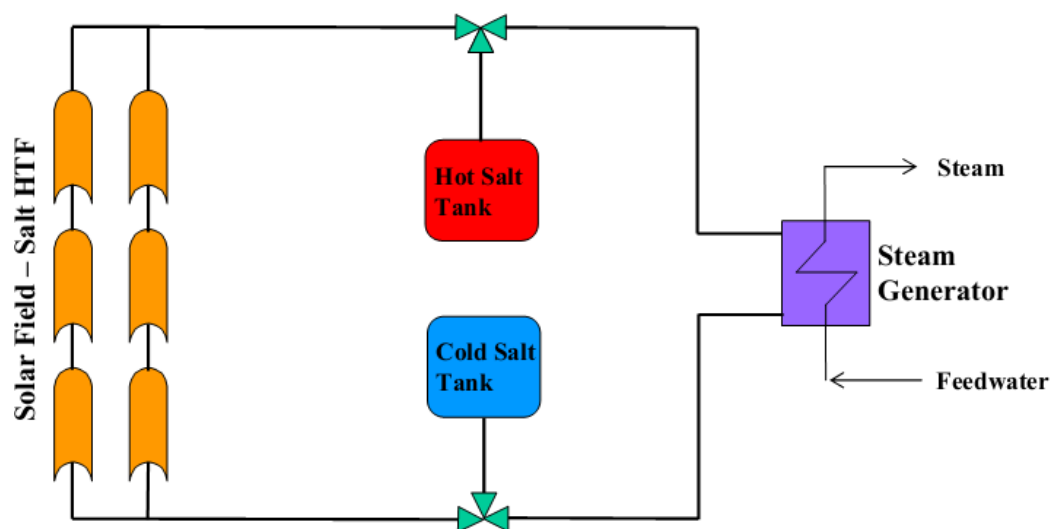


Figure 3.15: Power plant with two tank direct storage[52].

In comparison with the indirect storage, the direct storage doesn't require the installation of a heat exchanger and the conversion efficiency is higher because the maximum temperature of the storage isn't limited by the HTF. However, if molten salts are used as HTF, during the night there's a high risk of solidification of the salts in the solar field.

An example of this system is being built in Andalusia within the Solar Tres³¹ power plant. This storage is composed of a hot tank at 565 °C and a cold tank at 290 °C. These tanks are filled with 6,250 tons of nitrate salts and can supply 600 MWh_{th}, equal to 15 hours of work at full load for the 17 MW_e turbine. Moreover this storage will enable the plant to operate 24 h/day during summer and have an annual solar capacity factor of approximately 64% up to 71%, including 15% production from fossil backup[53].

3.3.4 Single thermocline tank system

In a single tank storage the hot and the cold HTF can be separated by a thin but

³¹ The project has been commissioned to Torresol Energy in May 2011.

distinct layer called thermocline, where the fluid temperature changes more rapidly than in the layers above or below. Since the density of a fluid is in inverse proportion to the temperature, the cold fluid stays on the bottom of the tank and the hot fluid on the top. To maintain the thermal stratification it's necessary to fill and empty the tank with a controlled charging and discharging procedure³² and appropriate methods or devices to avoid mixing[33]. Unlike the two tank system, the fluid level in the thermocline tank remains fairly constant, but the layer containing the thermal gradient between the high and low temperature zones moves up and down[54]. A schematic of this concept can be seen in figure 3.16.

Because the thermocline is favored by height, taller tanks with smaller diameters are preferred over shorter tanks with larger diameters. If only one tall tank is built, it may have the lowest overall surface-to-volume ratio, minimizing the overall requirements for insulation, heat trace, associated controls, and thermal losses (thus, maximizing efficiency and plant performance), but, on the other hand, a single tank may be so large that construction, start-up, operation, and maintenance may be very difficult to implement[52].

Filling the tank with a second solid storage material can be useful to improve the temperature's stratification. The most common filler materials are the quartzite rock and the silica sand due to their low cost, high heat capacity, wide availability and good resistance to high temperature and to salts corrosion (if salts are used as storage medium). Silica sand is added to the storage in order to fill the space between the quartzite rock and reduce the void fraction. The void fraction of a tank filled with silica sand and quartzite rock can be calculated with formula (3.3), but the results are reliable only if the diameter of the tank is 50 times the diameter of the largest rock[39].

$$(Void_{quartzite}) \cdot (Void_{sand}) = (Void_{combined}) \quad (3.3)$$

Another advantage of the employment of the filler materials is the cost reduction of the storage, since these materials replace the storage medium in the tank and are generally cheaper³³. Moreover, if the filler material is self supporting, such as a ceramic matrix material, the structural requirements of the containment vessel can be reduced and its associated cost may be less[41].

Both thermal oil and molten salts can be used in a single thermocline tank storage system, but the thermal oil is favored, because of its relatively low heat conductivity and its narrow temperature's difference between the hot and the cold layers.

The building of only one tank and the utilization of filler materials instead of

32 The fluid turbulence should be minimized so the growth of the thermocline is reduced.

33 In 1986 the price of quartzite rocks was about 70 \$/ton, while the price of thermal oil CALORIA was about 530 \$/ton[39].

storage medium entails a cost reduction of about 35%. For example, a molten salts storage can pass from a cost of 31 \$/kWh for a two tank system to a cost of 20 \$/kWh for a thermocline single tank[55].

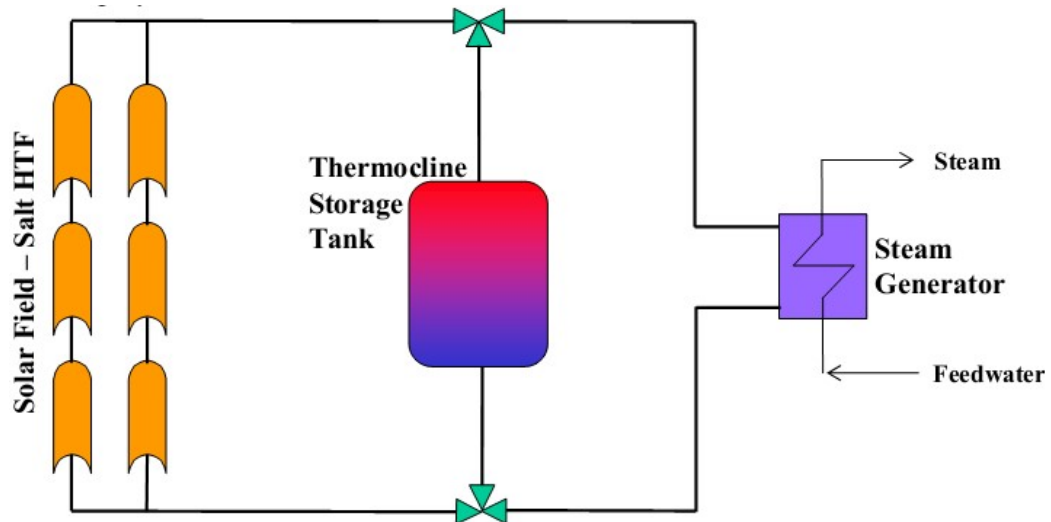


Figure 3.16: Direct thermocline thermal energy storage schematic[52].

The 10 MW Solar One power plant was built with an indirect thermocline single tank storage system. The tank was filled with 6,800tons of quartzite rocks and silica sand as filler materials (in a 2:1 weight ratio of rock to sand and a void fraction of 22%) and with 910 m³ of Exxon's CALORIA HT 43 as storage medium. During the charging cycle, oil entered the tank at 305 °C, and, during the discharging cycle, oil entered at 220 °C; the thermal energy stored was about 112 MWh[39][56]. The power plant became operational in 1982 and was dismissed in 1986.

3.4 Tank design

The storage system is the second³⁴ most expensive component of a solar power plant, so it's important to contain its construction cost and, at the same time, assure a high thermal efficiency. The tank must be designed to contain all the storage medium present in the plant in case of maintenance of the piping system. Almost any storage tank is built in a cylindrical shape, but ENEA, on the basis of an idea of SERI, has developed a conical storage tank concept[57], forecasting a cost reduction. Spherical tanks were considered early in some plant designs, but have been rejected because they were too expensive[54].

³⁴ The first most expensive component is the solar field[57].

3.4.1 Cylindrical tank

The storage can consist of a two tank system (one tank for the hot fluid and one tank for the cold fluid) or of a single thermocline tank system (in this case the tank is designed as the hot tank for the two tank system).

If the tank is designed to contain fluids at temperatures below 400 °C, for example thermal oil or molten salts in the cold tank, carbon steel is used as construction material for the tank's shell[54]. Figure 3.17 illustrates this concept. On the other hand, if the fluid's temperature is above 400 °C, for example in the hot tank of a molten salts storage, stainless steel with external insulation should be used instead of carbon steel.

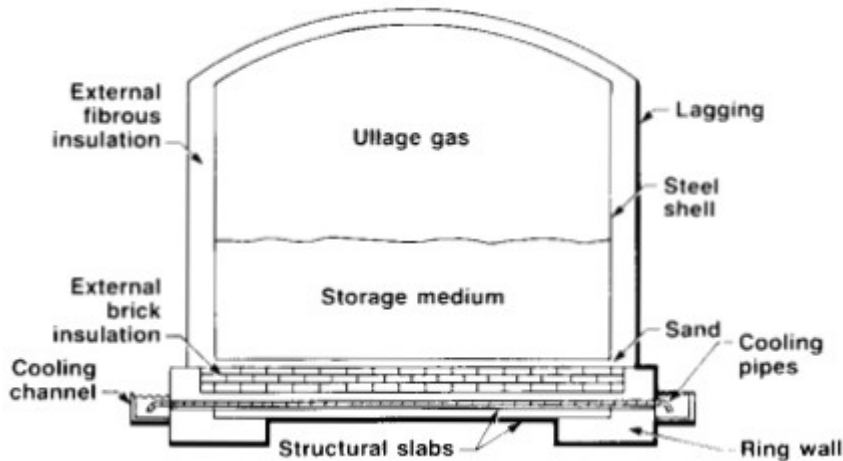


Figure 3.17: Schematic of low temperature carbon steel storage tank[54].

Another approach for a high temperature tank consists of a carbon steel shell with internal insulation and a thin liner³⁵ to avoid the contact between the internal insulation and the hot storage medium (see figure 3.18). The liner is of a waffled construction to transmit the pressure loads through the internal insulation to the tank shell and contain thermal expansion.

For molten salt storage it's possible to use an alternative internally insulated tank configuration, that consists of an annular layer of salt as the internal insulation material. In this design, the Incoloy 800 liner would have openings near the bottom of the tank which allow the molten salt to fill the annulus. Because the salt's relatively low thermal conductivity, a thermal gradient is created between the liner and the carbon steel tank wall[54].

³⁵ The most used is Incoloy 800[54].

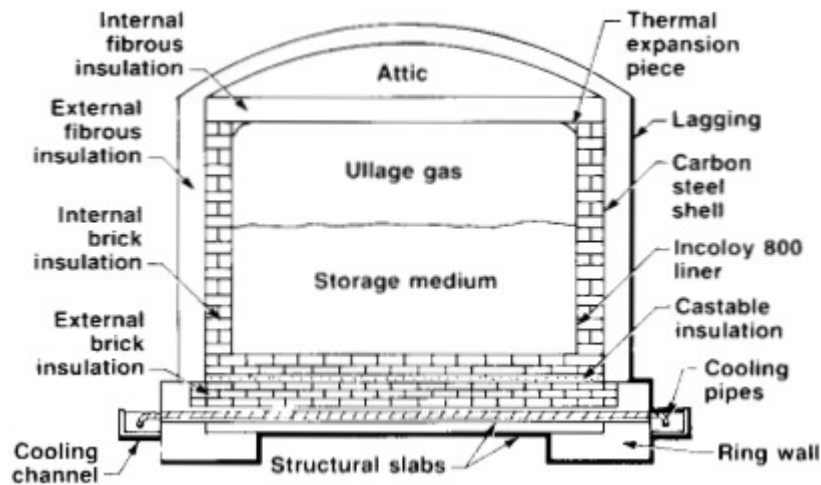


Figure 3.18: Schematic of insulated high temperature storage tank[54].

The storage tank walls are continually stressed by the high temperature of the storage medium, causing slow creep³⁶ of the containment materials and, possibly rupture. At the same time, raising and lowering the level of the contained fluid during system operation subject the tank to cyclic stresses, both thermal and applied, resulting in a combination of creep and fatigue stresses. Furthermore, at the joint of the bottom and the side walls these stresses are significantly higher than those predicted for simple hoop stress. This problem appears to be more severe for stainless steel tanks than for carbon steel tanks because of the lower allowable stresses that result from higher operating temperature. These stresses can spoil the liner integrity, causing leaks of the storage medium, that, not only necessitate replacement of the escaped fluid, but also damage insulation and jeopardize the tank foundation[54].

Both the cold and the hot tank are typically supported by a foundation, composed of (from the ground) a concrete slab, a thermal foundation, foamglass insulation, insulating firebricks, thin liner and sand[57]; an additional concrete ring wall is built to sustain the weight of the tank and of the roof. Cooling pipes are installed to prevent thermal degradation of the concrete and to maintain the underlying soil bearing strength.

Two other methods for storage tank support are top hung and tank leg support. These support alternatives accommodate tank thermal expansion while minimizing concrete strength degradation and maintaining the underlying soil bearing strength. The top hung support consists of suspending the storage tank from beams attached to a main support structure. Instead, the tank leg support consists of supporting the storage tank on one fixed leg located in the center of

³⁶ The creep is due primarily to grain boundary sliding.

the tank and several outer legs which allow tank thermal expansion by means of sliding surfaces or wheels[54].

An ullage gas control system is used in order to minimize the buildup of contaminants in the storage medium and to prevent damaging differential pressures from developing between the inside of the storage and the atmosphere. For thermal oil storage, the ullage gas control system continually removes hydrocarbon gases from the storage tank, while, for molten salt storage and liquid sodium storage, it removes the carbon dioxide and water vapor³⁷ from the tank cover gas[54]. Typical cover gasses used in a storage tank are argon, for liquid sodium systems, and air, for molten salt systems.

An electric heater system is placed in the tank in order to heat the storage medium when the solar receiver is not in operation and to avoid its solidification.

The costs for a two tank molten salt direct storage system are shown in table 3.4, which follows these assumptions[58]:

- High temperature= 565 °C, low temperature=293 °C, $\Delta T= 272$ °C.
- High temperature tank material= 321 stainless steel, low temperature tank material= carbon steel.
- Salt cost=1.23 \$/kg.
- Electrical and instrumentation costs= 7% of total tank costs.
- Piping, valves and fitting costs= 3% of total tank costs.
- Sales tax= 4%.
- Contingency= 7%.
- Hot and cold tank salt pump costs are not included.

Table 3.4: Component costs for two tank molten salt storage system[58].

Component	Materials (\$/kWh _{th})	Installation (\$/kWh _{th})	Total Cost (\$/kWh _{th})
High-temperature tank—stainless steel	5.20	1.84	7.04
Low-temperatures tank—carbon steel	1.30	1.84	3.14
Tank supports, foundations, and site work	1.10	1.55	2.65
Storage medium	11.74	0.36	12.10
Electrical and instrumentation	0.47	0.43	0.90
Piping, valves, and fittings	0.20	0.18	0.39
Totals	20.01	6.22	26.22

For an indirect storage, the 2009 Worley-Parson study[59] estimated the storage

³⁷ The presence of water vapor and carbon dioxide causes the formation of hydroxides and carbonates as salt decomposition products and oxidation of sodium[54].

cost at about 80 \$/kWh_{th}, but it includes also the costs of hot and cold tank salts pumps, of the heat exchanger and the maximum operating temperature is placed at 400 °C³⁸.

A reduction of the storage cost can be achieved changing the maximum operating temperature, the c_p of the storage medium or the tank material. Carbon steel can be used as the high temperature tank material up to 450 °C (1X cost factor), while from 450 °C to 650 °C the material is 321 stainless steel (4X cost factor) and, above 650 °C, a nickel based alloy is required (16X cost factor). The C_p for the NaNO₃/KNO₃ binary mixture is 1.5 kJ/kgK (1X cost factor), while the 1.5X and 2.5X factors are 2.25 kJ/kgK and 3.75 kJ/kgK respectively[58]. The storage cost goal of 15 \$/kWh_{th} can be met in the temperature range of 500 °C to 650 °C using a storage medium that has a c_p of 3.75 kJ/kgK and the storage steel as the storage tank material. The results can be seen in figure 3.19.

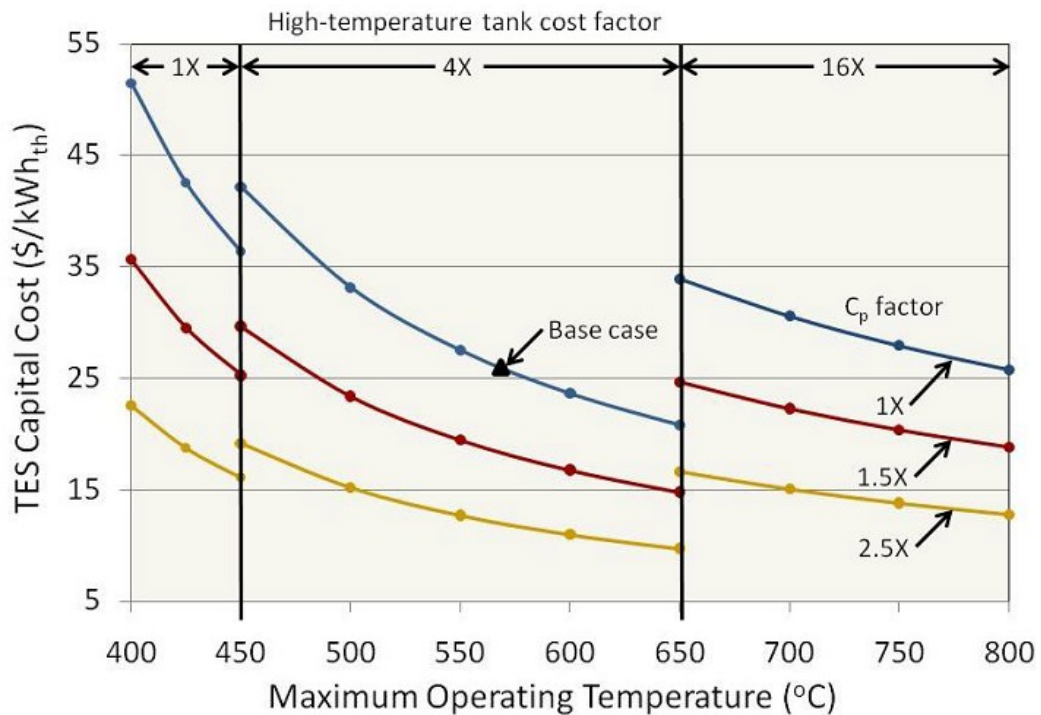


Figure 3.19: Costs for direct two tank thermal energy storage[58].

The maintenance requirements for the thermal storage system depend on the chosen storage medium. Molten salts and liquid sodium require special attention to monitor chemical degradation, the buildup of impurities and fluid solidification, while thermal oil, because of its thermal decomposition at high temperatures, needs continuous make-up and blow-down to maintain an

38 For a direct storage system at 400 °C the cost is estimated at 52 \$/kWh_{th}[58].

acceptable fluid composition.

3.4.2 Conical tank

The conical tank concept was first suggested in 1985 by American researchers of SERI³⁹ for high temperature applications, but was never tested. ENEA has resumed this concept and has adapted it with some improvements to middle temperature applications, as thermal storage in solar power plant.

One of the most expensive components of the storage tank is the waffled liner. Using sloped walls, thermal expansion of the liner can take place along the walls without losing contact with them, so that standard liner can be used instead of the more expensive waffled liner.

Conical tanks (see figure 3.20) can be built even on soft ground, since the tank's weight is only one-third of a cylindrical tank with the same surface. Moreover, the foundation can be made of high performance concrete (HPC), that can withstand temperatures above 95 °C, which is the limit temperature of ordinary concrete, and allows the utilization of a passive cooling system.

On the other hand the tank's roof, which cost represents about 45% of the total tank cost, is larger than one of a cylindrical tank, so a three tank storage system could be necessary to avoid structural problems. The final cost is about 10% higher than in a two tank storage system, because of the installation of additional pumps and the extension of the piping system[57].

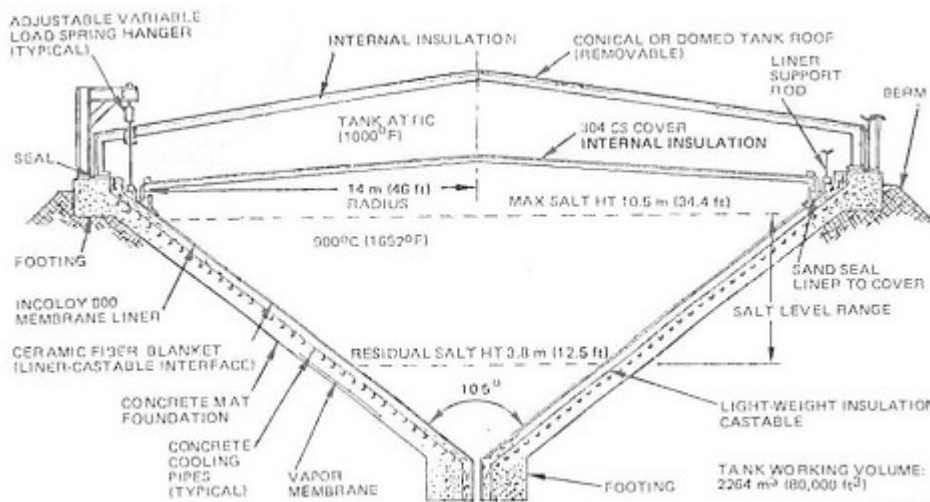


Figure 3.20: Schematic of a conical storage tank [SERI, 1985].

The total cost of the storage, including planning and maintenance costs, is estimated at 21.5 \$/kWh_{th} for the two tank system and 23.9 \$/kWh_{th} for the three

³⁹ SERI is an acronym for Solar Energy Research Institute.

tank system. These costs are comparable with the cylindrical tank storage system cost[58].

The primary objectives for developing an efficient storage tank are:

- Maintaining a high thermal efficiency: the Solar Two plant achieved an annual thermal efficiency of 98%[36].
- Reducing the total cost of the storage: a goal cost can be placed between 15 and 20 \$/kWhth[58].
- Avoiding the degradation of the tank materials in order to extend the service life of the system.

Chapter 4

Storage medium choice

The objective of this chapter is to present different types of material of which the thermal energy storage could be made of. After having explained the advantages and the limits of each materials, a comparison between them will determine which is the most suitable.

4.1 Criteria of comparison

The fundamental parameter of choice is the maximum operating temperature that a storage medium can reach.

Since the air temperature at the compressor outlet is equal to 450 °C, every materials with a maximum operating temperature below must be discarded, so synthetic thermal oil and water/steam won't be considered in the confrontation. In particular, materials that can reach 850 °C⁴⁰ and over will be favored.

In order to contain the dimensions of the storage, the product of heat capacity and density (called volumetric heat capacity) is considered.

In more detail, a material with a higher heat capacity requires lower mass to store the same energy. Moreover, a higher density is preferable, so the storage volume can be lower.

Another parameter of choice is the thermal conductivity. A higher thermal conductivity allows a better thermal conduction, so the storage can reach faster its maximum operating temperature and can transfer heat to air quicker during the discharge phase. Methods for increasing the thermal conductivity, such as fins, are not considered.

For the measure of thermal inertia of the storage is used the thermal diffusivity. It is the ratio between thermal conductivity and the volumetric heat capacity and expresses the ratio between the heat transferred and the heat accumulated into the material (formula 4.1).

$$\alpha = \frac{k}{\rho \cdot c_p} \quad (4.1)$$

Where:

- α is the thermal diffusivity (m²/s)
- k is the thermal conductivity (W/mK)

40 It's the temperature at the solar receiver outlet.

- ρ is the density (kg/m^3)
- c_p is the heat capacity at constant pressure (kJ/kgK)

Materials with a high thermal diffusivity are preferred, since a material with a high thermal diffusivity conducts heat quickly relative to the heat stored inside its mass. This means that the storage adapts better to a rapid load transient.

For liquid media the solidification temperature will be considered, since a material with a high solidification temperature could become solid during long periods of inactivity (for example during the winter season) and, if this happens, it requires a long time to liquefy all the storage.

A space on the thermal storage must remain empty to allow the thermal dilatation of the storage material. In case of using a liquid media this space must be fulfilled with an inert gas to prevent reaction with air. To reduce the dimensions of this empty space, materials with low coefficient of thermal expansion are preferred.

Other characteristics of the storage materials, such as toxicity, flammability etc., could exclude a material from the confrontation.

The total cost of the storage could be a decisive parameter of choice⁴¹, but it isn't considered in this analysis due to lack of data.

4.2 Storage media proposed

4.2.1 Molten salts

The use of nitrate salts as storage media has already been discussed in Chapter 3. They are composed of a mixture of 40% by weight KNO_3 and 60% by weight NaNO_3 .

Their principal advantage is the high heat capacity and the high density, resulting in a high volumetric capacity.

The feasibility of a nitrate salts storage has been proven by several solar power plants using it, moreover their low price makes them a good choice for future plants.

However, their low heat conductivity (under 1 W/mK) penalizes them in a heat exchanging storage, as the one in our plant, and, most important, they cannot reach temperatures above 565°C , that is a temperature too below the one of the air at the solar receiver outlet (850°C).

For these reasons the option of using nitrate salts must be discarded.

The sodium hydroxide, which has a melting point of 320°C and can reach temperatures up to 800°C , could be an interesting option, but it's highly corrosive and there is difficulty in containing it at high temperature, so it must

⁴¹ For example: a poorly performing storage can be preferred to a better, but also more expensive, one.

be discarded too.

Other molten salts, that can be used as storage medium, are the nitrite salts and the carbonate salts.

The nitrite salts, which are composed of NaNO_2 and KNO_2 , have the same advantages and limits of the nitrate salts. On the other hand, the carbonate salts, which are composed of Na_2CO_3 and K_2CO_3 , can reach higher temperatures but have also a higher solidification temperature (about 800 °C). Since the air at the storage inlet is at 850 °C, this means that part of the energy is transferred during phase changing, making the heat exchange coefficients more unpredictable. Moreover, the thermal conductivity of the carbonate salts is very low (2 W/mK), so it's required a long time to heat them up to their melting temperature when they are in solid state.

Lastly, since the storage is designed as a tubular heat exchanger, it's necessary to use specific materials for avoiding the corrosion by molten salts.

In conclusion, it's possible to state that molten salts aren't compatible with a high temperature storage.

4.2.2 Liquid sodium

Liquid sodium is commonly used as a primary coolant in Liquid Metal Fast Breeder Reactors (LMFBR). Thanks to its great thermal conductivity, it is an excellent heat transfer fluid and can be used as storage medium.

More in detail its thermal properties vary in function of temperature as is shown in formulae⁴² (4.2), (4.3) and (4.4)[60].

$$k = 124.67 - 0.11381 \cdot T + 5.5226 \cdot 10^{-5} \cdot T^2 - 1.1842 \cdot 10^{-8} \cdot T^3 \quad (4.2)$$

$$c_p = 1.6582 - 8.479 \cdot 10^{-4} \cdot T + 4.4541 \cdot 10^{-7} \cdot T^2 - 2992.6 \cdot T^{-2} \quad (4.3)$$

$$\rho = 219 + 275.32 \cdot \left(1 - \frac{T}{2505}\right) + 511.58 \cdot \left(1 - \frac{T}{2505}\right)^{0.5} \quad (4.4)$$

Where:

- k is the thermal conductivity (W/mK)
- c_p is the heat capacity at constant pressure (kJ/kgK)
- ρ is the density (kg/m³)
- T is the temperature expressed in Kelvin

Results can be seen in figure 4.1

⁴² These equations are valid when temperature varies between 371 K and 1773 K.

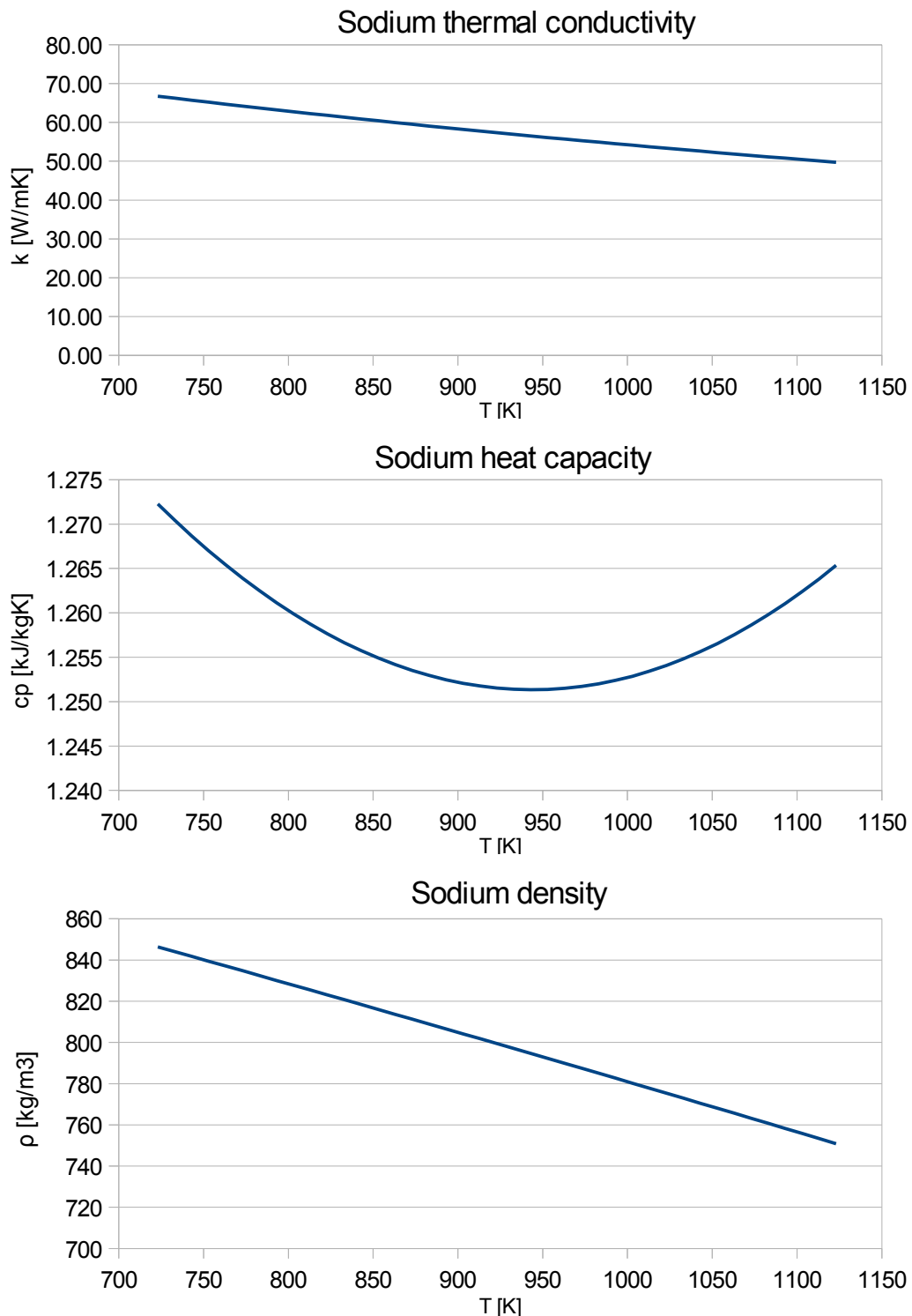


Figure 4.1: From the top: Sodium thermal conductivity, heat capacity and density.

Other points in favor of the liquid sodium are the high maximum working temperature (881.4 °C at atmospheric pressure[60]), which is above 850 °C, and the low melting temperature (97.82 °C).

However, sodium is also highly flammable and this limits its application. In fact, the IEA-SSPS High Flux Experiment conducted in the 80's at the Plataforma Solar de Almeria used liquid sodium as a heat transfer fluid, which caught fire and burned down in August 1985. This experiment put a hold to the development of using liquid sodium in solar power plants.

An alternative to sodium is the sodium-potassium alloy (NaK), in particular the NaK46 alloy, which is an eutectic composition made of 46% of potassium and the NaK77.8, which is composed of 77.8% of potassium. Table 4.1 shows the value of thermal properties of NaK.

Table 4.1: Properties of sodium, NaK and Potassium[61].

	Unit	Sodium	NaK	Potassium
Melting point	°C	97.82	-12.6	63.2
Boiling point or maximum operating temperature	°C	881.4	785	756.5
Density	<i>kg/m³</i>	820	749	715
Specific heat capacity	<i>kJ/kg.K</i>	1.256	0.937	0.782
Viscosity	<i>Pa.s</i>	0.000149	0.000176	0.000167
Thermal conductivity	<i>W/(m.K)</i>	119.3	26.2	30.7

In comparison to sodium, the NaK has a lower melting temperature (-12.8 °C for the NaK77.8 and 20 °C for the NaK46). This means that NaK is always liquid during the year, so the plant reliability is increased and the maintenance procedures and the safety protocol are simplified, resulting in a reduction of the operational cost.

The maximum operating temperature of NaK is 785 °C, that is lower than sodium one, but is also lower than the air temperature at the storage inlet during the charging phase. However, if the NaK is pressurized, temperatures over 1000 °C are possible.

The thermal conductivity of the NaK is four times lower than the liquid sodium one, but it is high enough for having a good heat exchange coefficient.

Since no decomposition of the NaK is expected and it doesn't require a trace heating, the NaK can be used even as a HTF that flows through the solar receiver, which dimensions are reduced thanks to the good heat transfer

properties of the NaK.

In conclusion, both liquid sodium and NaK are suitable for working as storage medium, but NaK is discarded due to its chemical incompatibility with air, which requires a complex monitoring system, and to its lower thermal conductivity.

4.2.3 Liquid lead

Another liquid metal proposed as storage medium is molten lead. Like the liquid sodium, even liquid lead has been studied for application as coolant for fast reactors as early as in the 1950s. Its thermal properties vary in function of temperature as is shown in formulae⁴³ (4.5), (4.6) and (4.7)[62].

$$k = 9.2 + 0.11 \cdot T \quad (4.5)$$

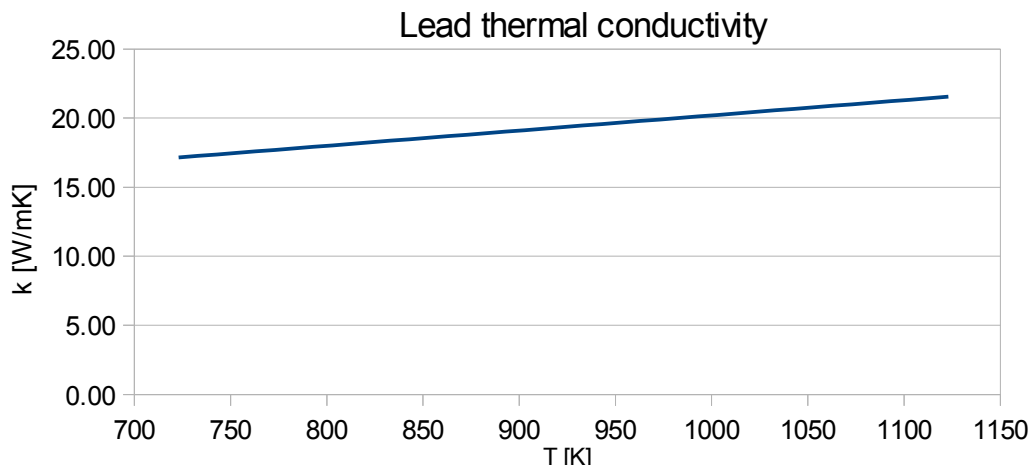
$$c_p = 175.1 + 0.04961 \cdot T + 1.985 \cdot 10^{-5} \cdot T^2 - 2.099 \cdot T^3 - 1.524 \cdot 10^6 \cdot \frac{1}{T^2} \quad (4.6)$$

$$\rho = 11367 - 1.1944 \cdot T \quad (4.7)$$

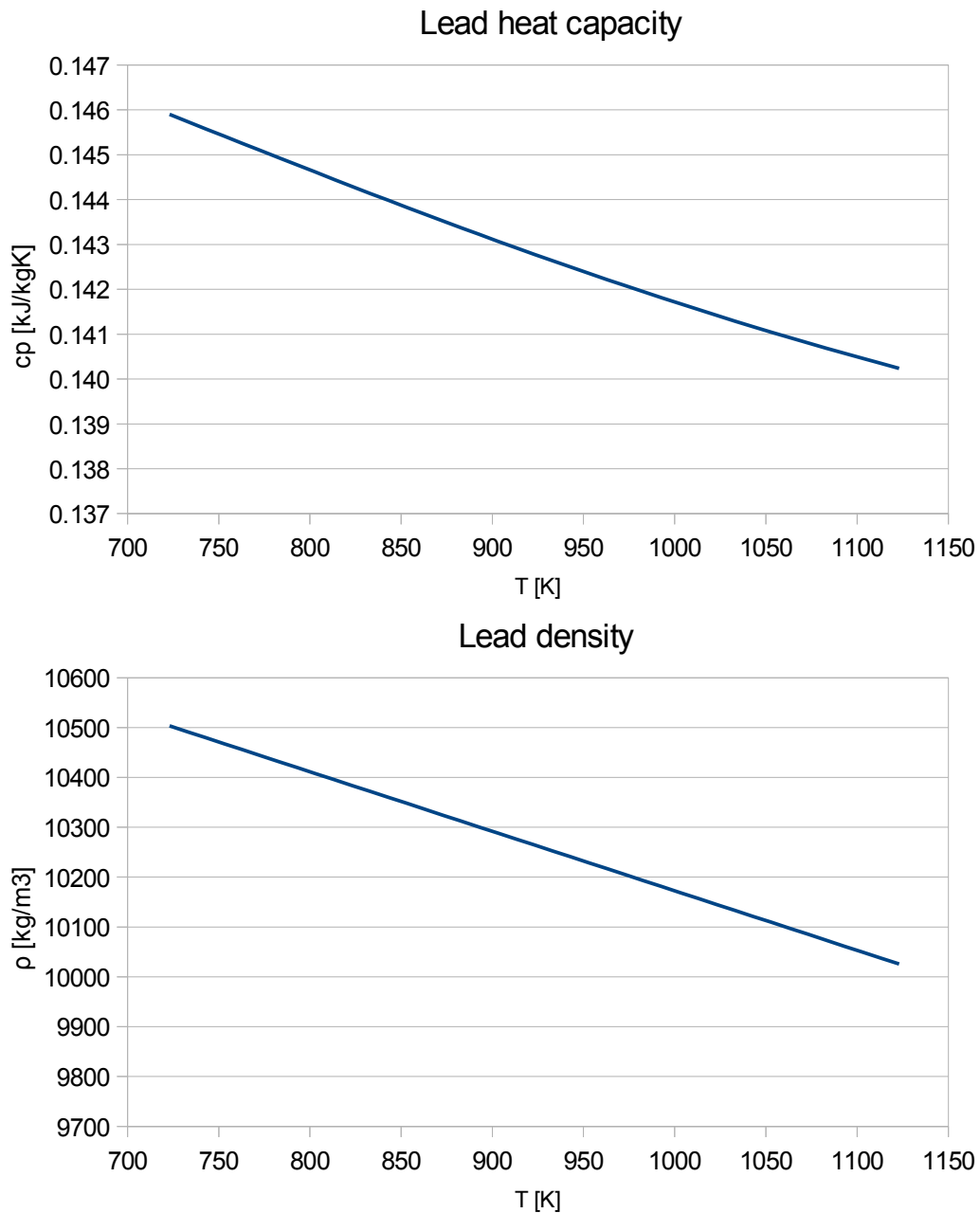
Where:

- k is the thermal conductivity (W/mK)
- c_p is the heat capacity at constant pressure (J/kgK)
- ρ is the density (kg/m³)
- T is the temperature expressed in Kelvin

Results can be seen in figure 4.2.



⁴³ These equations are valid in a temperature range of 327 °C to 1027°C.



4.2: From the top: lead thermal conductivity, heat capacity and density.

The greatest advantage of using liquid lead is its high density, in the order of $10,000 \text{ kg/m}^3$, that is ten times higher than the sodium density.

However, this advantage is neutralized by the low specific heat, in the order of 0.1 kJ/kgK , resulting in a volumetric heat capacity comparable to the liquid sodium one.

The high thermal conductivity of liquid lead (about 20 W/mK) and the possibility to reach high working temperatures make it a good heat transfer fluid.

Unlike the liquid sodium, lead is inert when in contact with air (there's no risk of fire), but it is a highly poisonous metal, affecting almost every organ and system in the body. Moreover, if lead is in contact with air, the formation of black oxides, which have a higher melting temperature, could happen, so it's required the use of inert gases and the installation of a monitoring system that detects the presence of oxygen, caused by the rupture of a pipe in which the air flow.

Another problem is that the lead could corrode the metallic pipes in which the air flows.

In more detail, most Fe-Cr and Fe-Cr-Ni steels form oxides (for example PbO) that are protective below temperatures in the range 500-550 °C, specially for an oxygen concentration above 10^{-6} wt.% for short to medium-term applications, while austenitic steels show thinner oxide layers. For oxygen concentrations lower than 10^{-6} wt.%, dissolution takes place in most of the steels, especially austenitic steels, due to the high solubility of nickel in lead. For operating temperatures higher than 550 °C, the formation and protectiveness of oxides is uncertain, and protection usually fails due to dissolution for long times[62].

Another disadvantage of the liquid lead is its high melting temperature (327 °C), because, during long periods of inactivity of the plant, the storage could solidify. A solution of this problem is the use of a lead-bismuth eutectic (LBE), composed of 44.5 wt.% of lead and 55.5 wt.% of bismuth, instead of liquid lead. With LBE the melting temperature is lowered at 124 °C, moreover the corrosion rates are lowered too, reducing the maintenance costs.

As for liquid lead, the thermal properties of liquid LBE can be calculated in function of the temperature[62]:

$$k = 3.61 + 0.01571 \cdot T - 1.741 \cdot 10^{-6} \cdot T^2 \quad (4.8)$$

$$c_p = 159 - 0.0272 \cdot T + 7.12 \cdot 10^{-6} \cdot T^2 \quad (4.9)$$

$$\rho = 11096 - 1.3236 \cdot T \quad (4.10)$$

Where:

- k is the thermal conductivity (W/mK)
- c_p is the heat capacity at constant pressure (J/kgK)
- ρ is the density (kg/m³)
- T is the temperature expressed in Kelvin

Figure 4.3 shows the results.

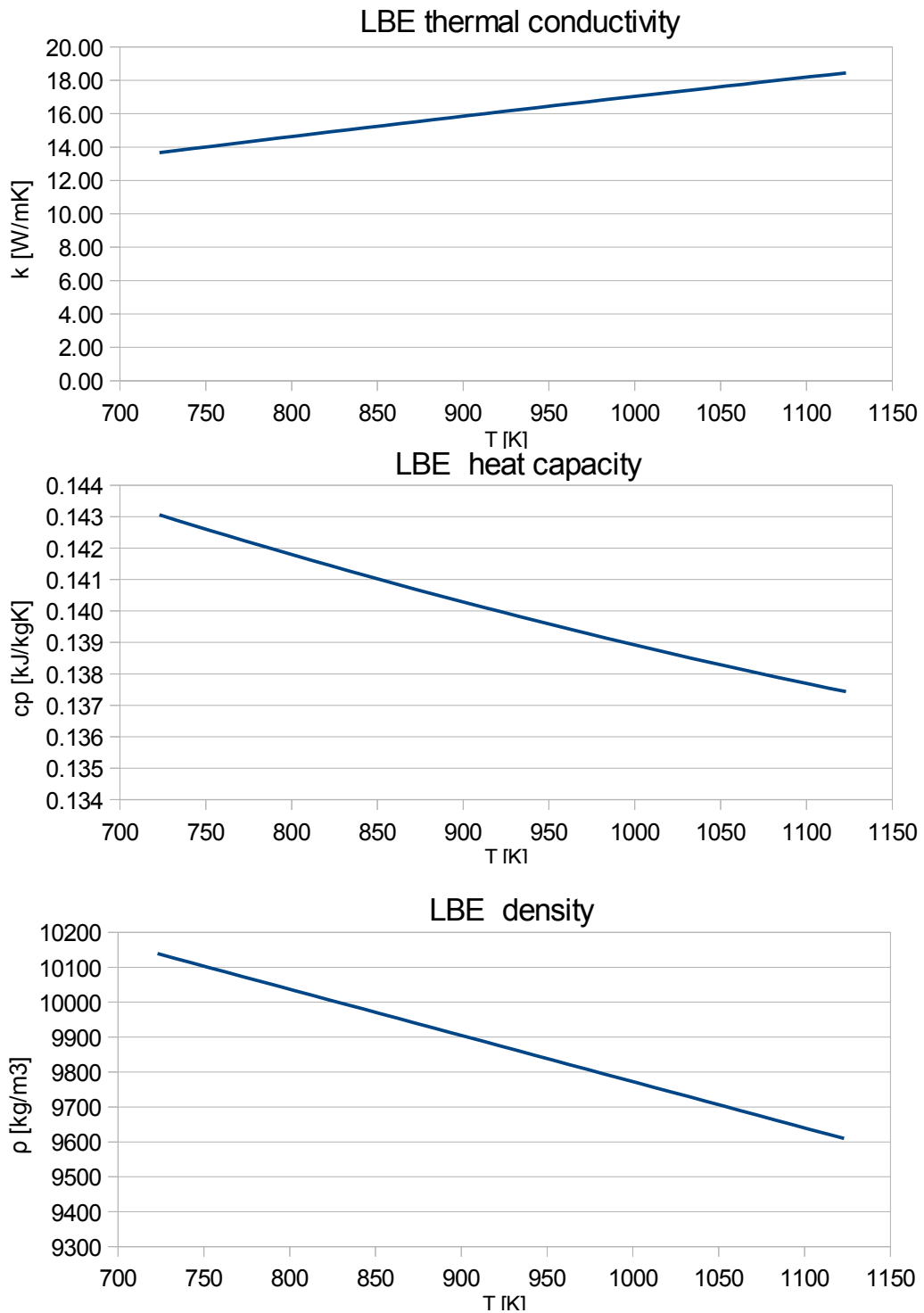


Figure 4.3: From the top: LBE thermal conductivity, heat capacity and density.

As can be seen from the graphs, the density and the heat capacity of LBE are approximately equal to those of lead, while the thermal conductivity is slightly lower.

In conclusion, both liquid lead and LBE are suitable for working as storage medium, but precautions must be taken due to the toxicity and the corrosivity of the lead. Moreover, the high melting temperature, especially if black oxides are formed, requires the installation of additional heaters, in order to avoid its solidification.

4.2.4 Ceramic materials

Ceramic materials are generally used in applications that include heat exchangers for high temperature and aggressive environments, seals, bearings and wear resistant components. In particular, a ceramic storage is installed at the Jülich solar power station.

One of the most attractive ceramic materials is the sintered silicon carbide (α -SiC), since it can reach temperature up to 1100 °C. In air, SiC forms a protective silicon oxide coating at 1200°C and is able to be used up to 1600°C. Its thermal properties vary with the temperature and are calculated with formulae (4.11), (4.12) and (4.13)[63]⁴⁴.

$$k = \frac{52000 \cdot e^{(-1.24 \cdot 10^{-5} \cdot T)}}{(T + 437)} \quad (4.11)$$

$$c_p = 1110 + 0.15 \cdot T - 425 \cdot e^{(-0.003 \cdot T)} \quad (4.12)$$

$$\rho = \frac{k}{c_p} \left(\frac{12,1 \cdot e^{-6.98 \cdot 10^{-5} \cdot T}}{T + 219} \right)^{-1} \quad (4.13)$$

Where:

- k is the thermal conductivity (W/mK)
- c_p is the heat capacity (J/kgK)
- ρ is the density (kg/m³)
- T is the temperature expressed in Celsius degree.

Figure 4.3 shows the results.

⁴⁴ The temperature must be between 0 °C and 2000 °C.

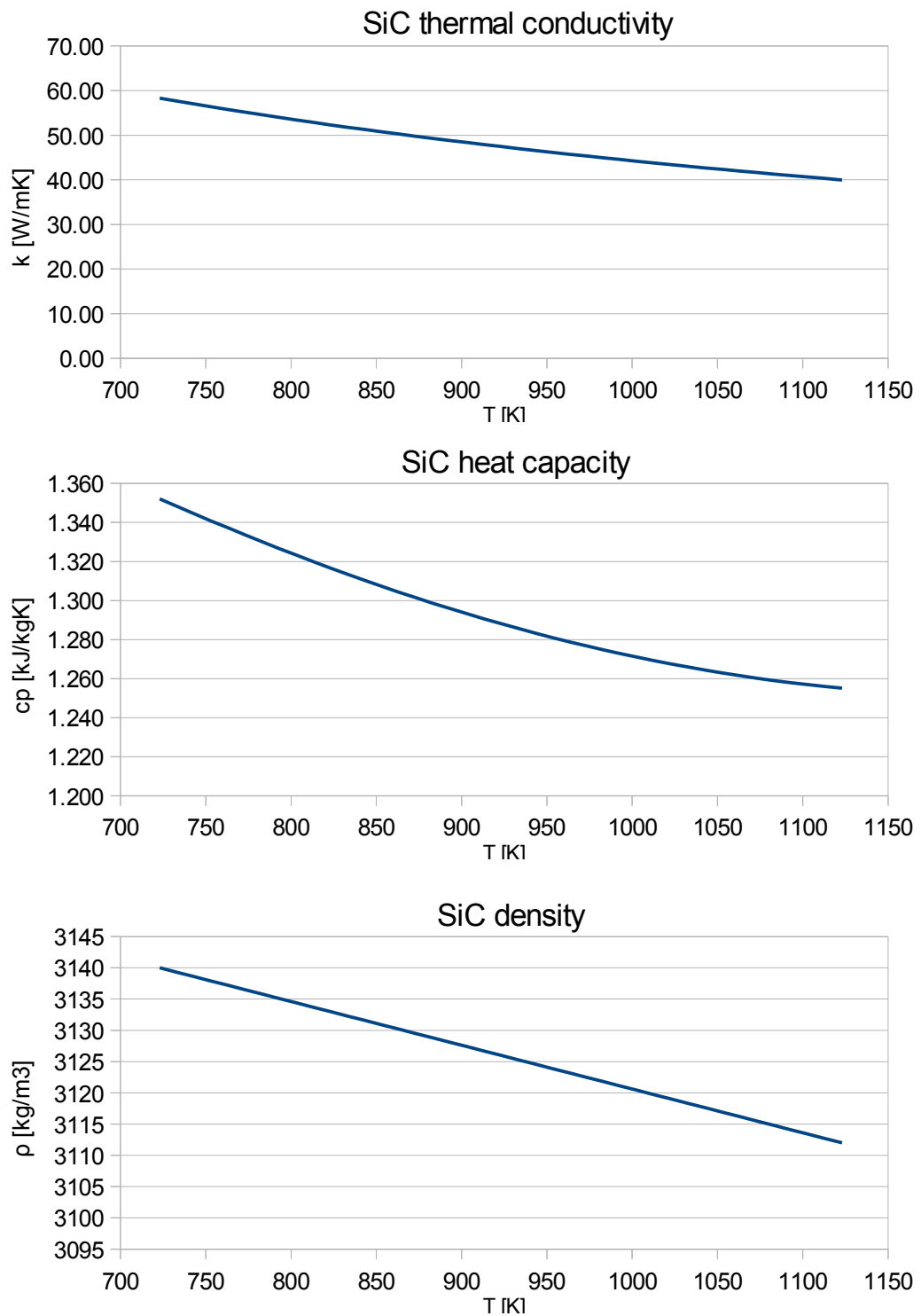


Figure 4.4: From the top: SiC thermal conductivity, heat capacity and density.

The greatest advantage of the SiC is that it combines a high density, like the liquid lead, with a high heat capacity, like the liquid sodium, resulting in a high volumetric heat capacity and in a lower storage volume.

Unlike the previous storage media, in this case it's possible to use a direct contact storage, so the air is directly in contact with the ceramic walls and there's no need for installing metallic pipes. In this way the storage is less expensive, since the expensive pipes made of high temperature resistant steel are not necessary, and the temperature difference at the storage outlet between air and storage medium is reduced. Moreover, the heat exchange is improved because the thermal resistance of the pipe is absent.

In more detail, the storage can be seen as the one used in the Jülich solar power plant (figure 4.5).



Figure 4.5: Storage unit used at the Jülich solar plant[64].

The thermal conductivity of the SiC varies from 40 to 70 W/mK, which is an intermediate value between the sodium and the lead.

Another advantage of the SiC is its low thermal expansion ($4 \cdot 10^{-6}$ 1/K).

However, the storage could break due to the low impact resistance and the low fracture toughness of the SiC. If this happens, some little debris could be transported by the air into the turbine, damaging the turbine blades.

Another material that can be used as medium for a direct contact storage is the magnesium oxide (MgO), also known as magnesia.

The thermal conductivity of magnesia is almost the same of the SiC (it vary in the range of 45-60 W/mK), while the density is higher (3580 kg/m^3), but the

heat capacity is slightly lower (0.96 kJ/kgK), resulting in a lower volumetric heat capacity.

A reason to use magnesia instead of SiC consists in the lower price of magnesia. If magnesia is used as storage medium the layout of the storage is different. In this case the channels in which the air flows are not within the ceramic material, but are created by placing the magnesia bricks in alternate positions, as is shown in figure 4.6.

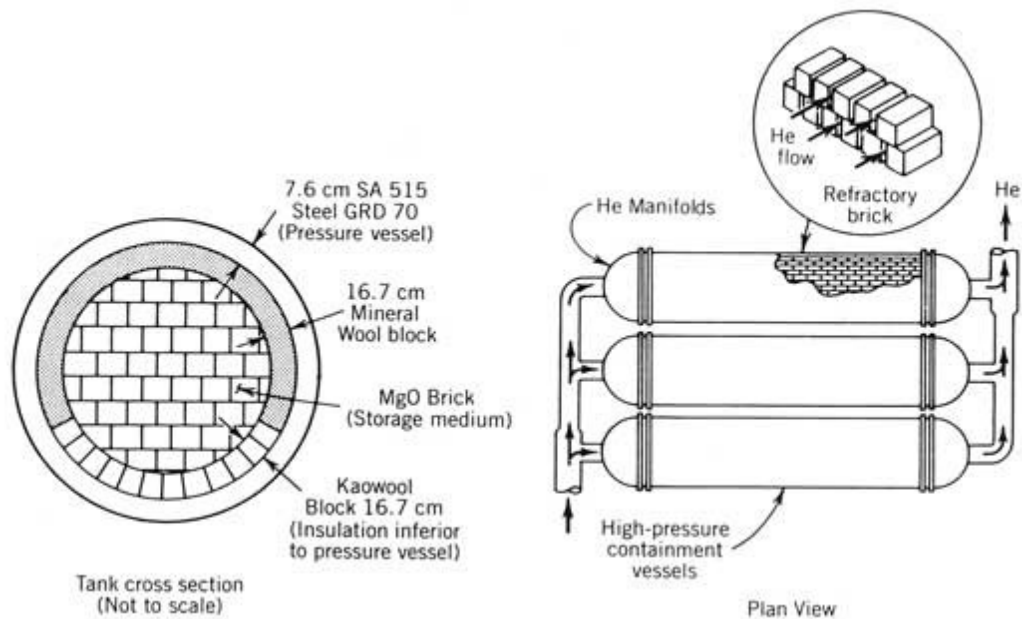


Figure 4.6: Example of a TES using magnesia as storage medium. In this figure helium is used instead of air[6].

To conclude, we can say that both magnesia and SiC are suitable for working as storage medium, but SiC is preferable thanks to its better thermal properties and the more reliable storage design.

4.3 Comparison between the storage media proposed

Now, after having analyzed in detail all the possible storage media, it's necessary to choose one material of which the TES of our solar power plant will be made. First of all, the materials that can't work at 850 °C must be discarded, so nitrate salts and thermal oil aren't considered.

The carbonate salts are discarded too, since they change phase during the charging and discharging phase, moreover their low thermal conductivity makes difficult to exchange heat with the air when they are in solid state.

The NaK isn't taken into account since it has the same advantages and

disadvantages of the liquid sodium, but with worse thermal properties. The same reasoning applies to the magnesia, to which the silicon carbide is preferred. The first comparison criterion is the thermal conductivity of the materials. Figure 4.7 shows the thermal conductivity in function of the temperature.

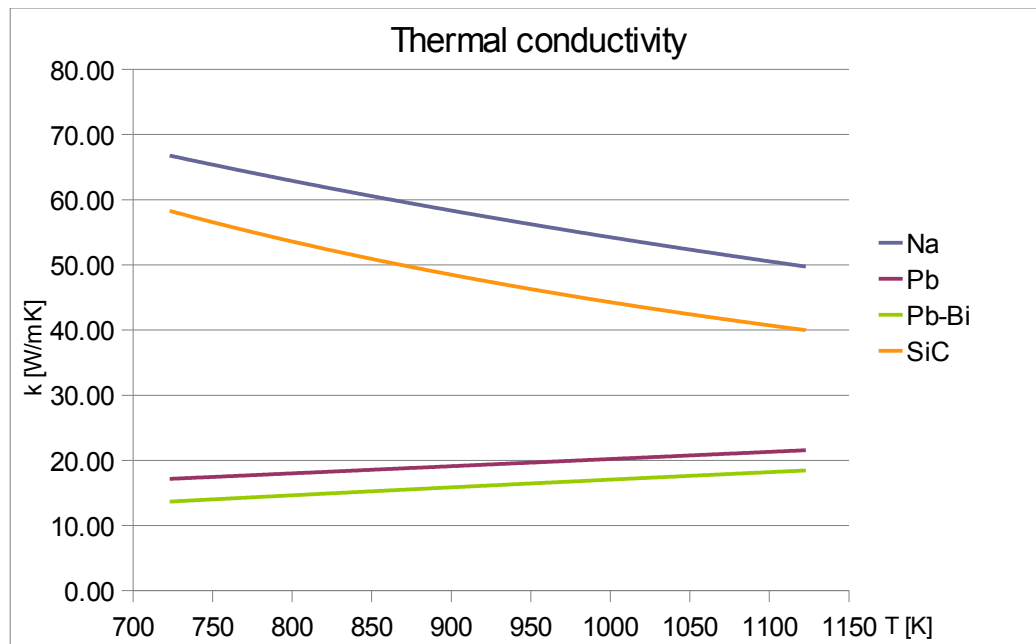


Figure 4.7: Thermal conductivity of the materials in function of the temperature.

The thermal conductivity of the liquid sodium is the highest, while the one of SiC is slightly lower. The thermal conductivities of lead and LBE are similar, but they are also 3-4 times lower than the sodium one.

From this comparison it's clear that the liquid sodium is the primary choice followed by SiC.

Another important criterion of comparison is the thermal diffusivity. In fact, a material with a higher thermal diffusivity requires shorter time for propagating the heat into it. Figure 4.8 shows the thermal diffusivity in function of the temperature.

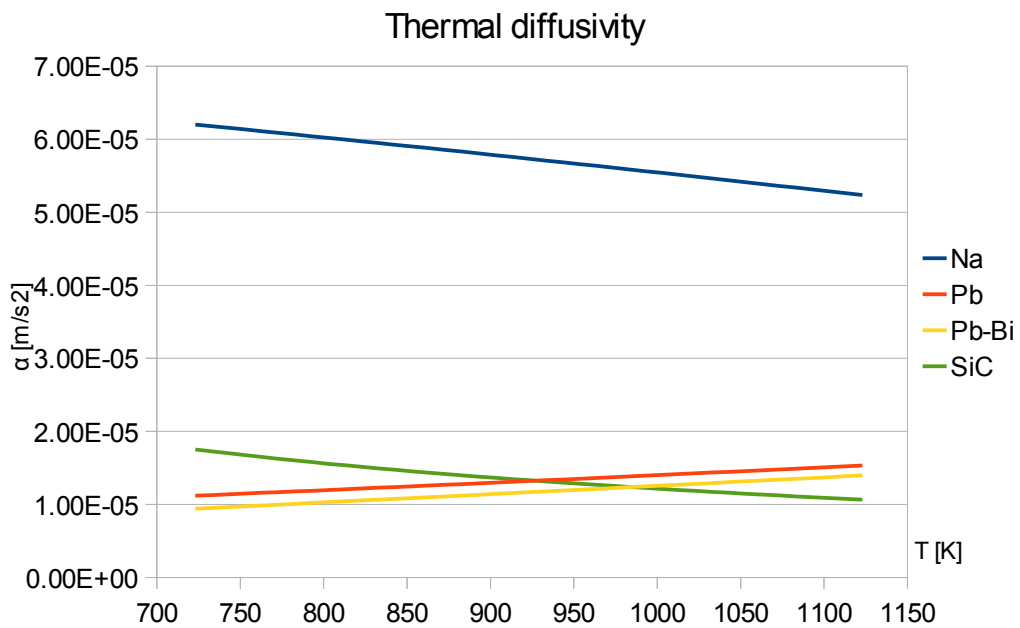


Figure 4.8: Thermal diffusivity of the materials in function of the temperature.

Even in this case the liquid sodium is the best choice, since it has by far the highest thermal diffusivity of all the materials. The thermal diffusivity of lead, LBE and SiC are approximately similar.

From the comparisons made until now it's possible to state that the liquid sodium is the best storage medium, thanks to its good attitude to heat transfer.

Another important parameter of choice is the volumetric heat capacity of the material, since the volume of the storage is in inverse proportion to it. Figure 4.9 shows the volumetric heat capacity in function of the temperature.

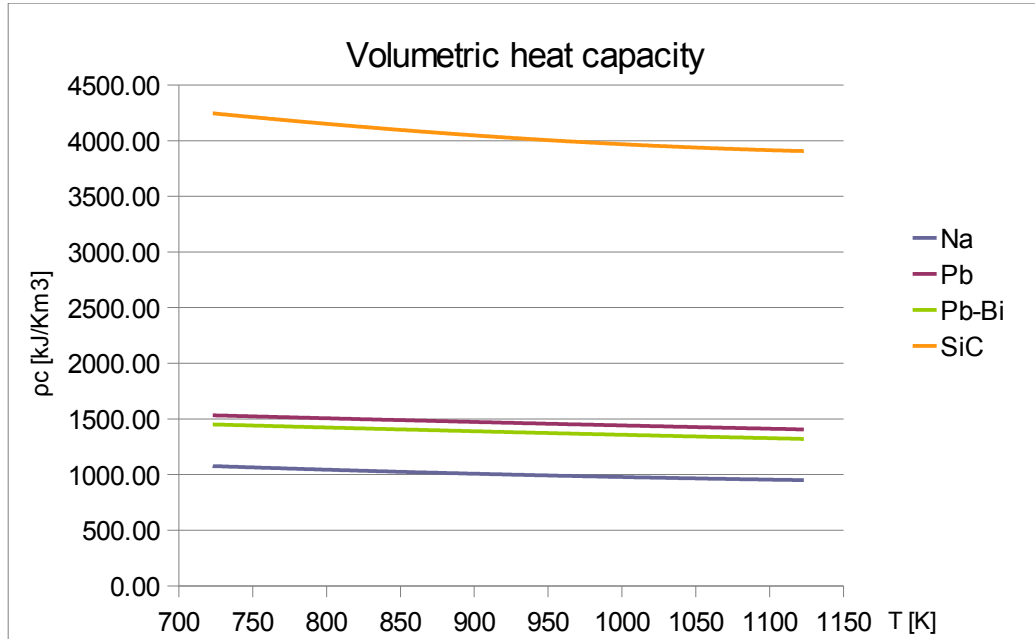


Figure 4.9: Volumetric heat capacity of the materials in function of the temperature.

Unlike the previous comparisons, in this case the silicon carbide is the favorite material, since its volumetric heat capacity is 2-3 times higher than the others. The liquid sodium, which is the storage medium with the higher thermal conductivity and diffusivity, is the worst material, since, to store the same energy, it requires a storage volume of about 4 times larger than one made of silicon carbide.

More in detail, the specific volume of the TES is calculated with formula (4.14).

$$\frac{V}{Q} = \frac{1}{\rho \cdot c_p \cdot \Delta T} \quad (4.14)$$

Where:

- V/Q is the specific volume of the TES (m^3/kJ)
- ρ is the average density (kg/m^3)
- c_p is the average heat capacity (kJ/kgK)
- ΔT is the temperature difference between the beginning and the end of the discharge phase (or the charging phase) of the TES.

In other words, V/Q is the volume required by the material to store 1 kJ of thermal energy.

Figure 4.10 shows the results for the four types of storage medium.

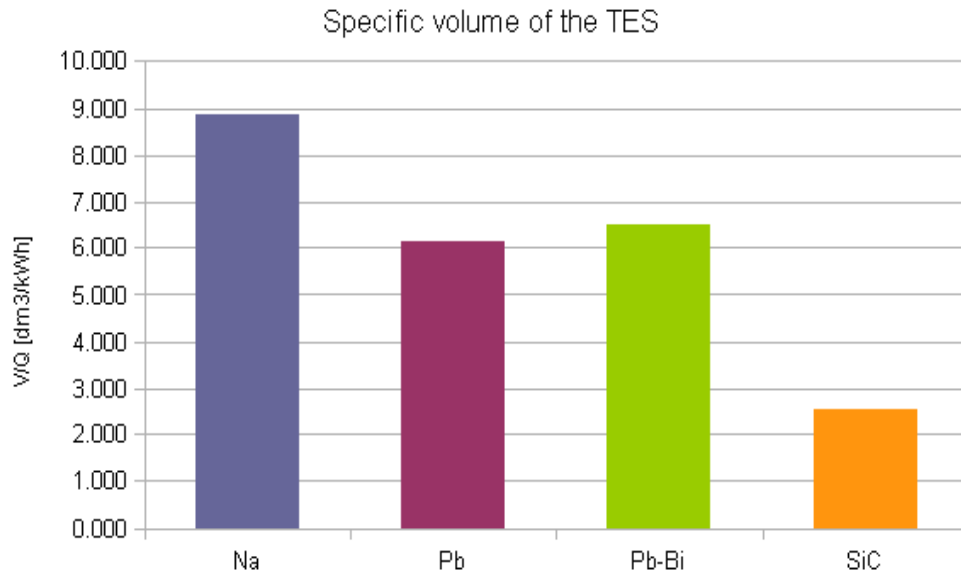


Figure 4.10: Specific volume of the materials.

4.3.1 Results of the comparison

After all the comparisons made it's now possible to decide what is the storage medium that will be used in the TES.

The silicon carbide is the first choice thanks to its good thermal properties and, especially, to the low volume required to store thermal energy. Moreover it's a non-hazardous material, since it isn't toxic or flammable.

In more detail, a direct contact storage scheme is adopted, in order to contain cost and improve the heat exchange.

The liquid sodium is a suitable material too, despite it requires a storage volume 3.5 times larger to store the same amount of energy, thanks to its good heat transfer properties. However it remains as a second option, since it is highly flammable and has a solidification point at 98 °C, and won't be discussed in the following chapters.

The lead and the LBE have thermal properties inferior to both sodium and silicon carbide, while their volumetric heat capacity is slightly higher than the one of the sodium, but it's lower by far than the one of the silicon carbide. The high solidification point and the toxicity and corrosivity of the lead are additional reason to discard them.

Table 4.2 summarizes the characteristics of the storage media proposed.

Table 4.2: Characteristics of the proposed storage media.

	ρ [kg/m ³]	c_p [kJ/kgK]	k [W/mK]	α [m ² /s]	V/Q [dm ³ /kWh]	T _{melt} [K]
Na	798.57	1.269	58,251	5.72E-05	8.882	97.82
Pb	10264.39	0.143	19.355	1.33E-05	6.129	327
LBE	9874.12	0.140	16.061	1.17E-05	6.499	124
SiC	3132	1.126	49.139	1.41E-05	2.552	-

Chapter 5

Design of the thermal energy storage

After having selected the storage medium, it's now necessary to optimize the storage dimensions in order to obtain a good heat exchange with low pressure drop. This chapter introduces the software used to simulate the behavior of the storage during charging and discharging process. After a primary selection, various storage configurations are simulated and the most suitable is selected. At the end a brief description of the storage thermal insulation is given.

5.1 Description of the software used

In the field of real time power plant dynamic simulation, RSE developed an integrated software environment, named “Lego Plant Simulation Tools” (LegoPST), able to model the whole plant, from the field (plant process and machinery) to the Human Machine Interface.

LegoPST was successfully used to build dynamic plant simulators both in nuclear (LWR) and conventional field, in order to verify plant control and automation system, and to perform plant operation transient analysis and plant operators training.

LegoPST suite consists in:

- A master solver for non-linear differential and algebraic equation systems.
- An expandable library of mathematical models of plant components.
- Integrated tools covering all plant simulator building steps, from the design to the final simulator including debugging, monitoring and configuration.

Specifically Lego Process CAD (LegoPC) is useful to develop and test process models; Lego Automation CAD (LegoAC) allows full graphic editing of automation schemes; LegoHMI is specific for Plant Display and Operating Window building and configuration; Lego Simulation Manager (legoSM) runs the whole simulator, managing multiple link among process, automation and HMI models.

To model the storage and the reference plant only LegoPC tool is requested[65].

5.1.1 Process CAD (LegoPC)

The process model builder LegoPC covers and sequences all the phases of the process model building and testing: models topology build-up, input assignment, steady state and transient calculation, as well as output analysis. The plant model is built by selecting the plant components from the models library, placing it on a graphical page (figure 5.1) and linking the components input-output terminals to draw the plant section.

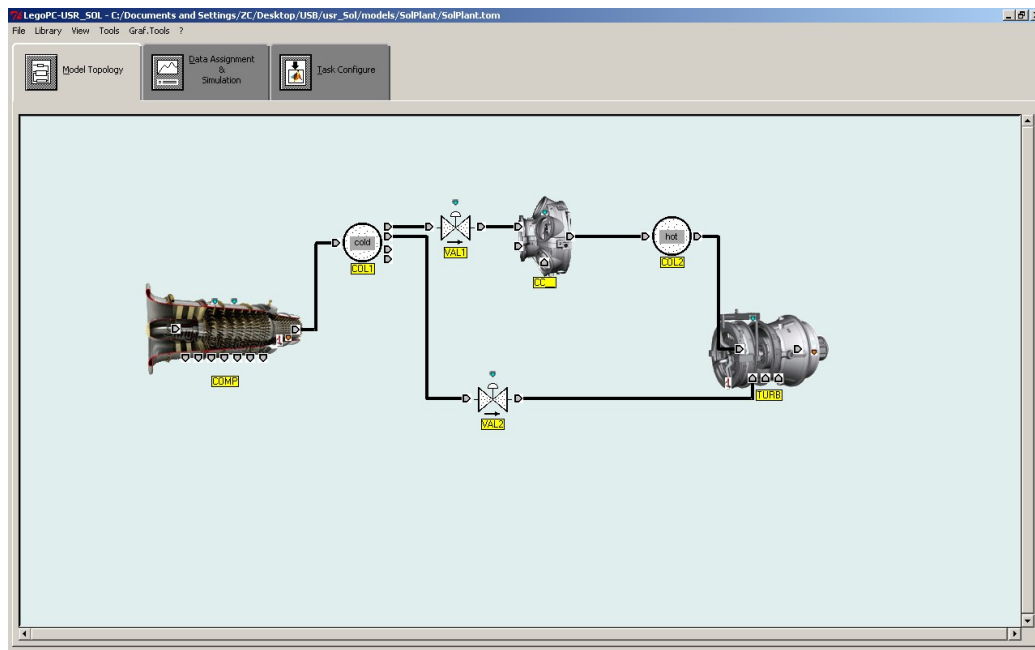


Figure 5.1: LegoPC graphic interface.

The plant drawing is translated into a global non-linear algebraic and differential equations system (Figure 5.2) solved via a Newton–Raphson iterative method, based on system linearization. It requires for each components:

- *The Jacobian matrix J* : it is composed of the partial derivatives values of each equations with respect to all the variables.
- *The residual vector RN* : it is composed of the values of $f(.)$ for differential equations or of $g(.)$ for algebraic equations.

The global matrix J and the global vector RN are created by means of topological vectors and the linearized system (5.1) is solved:

$$J \cdot \Delta x = RN \quad (5.1)$$

An iterative process repeats calculation till a stop condition is satisfied (generally when the module of the residual vector is lower than a given ϵ).

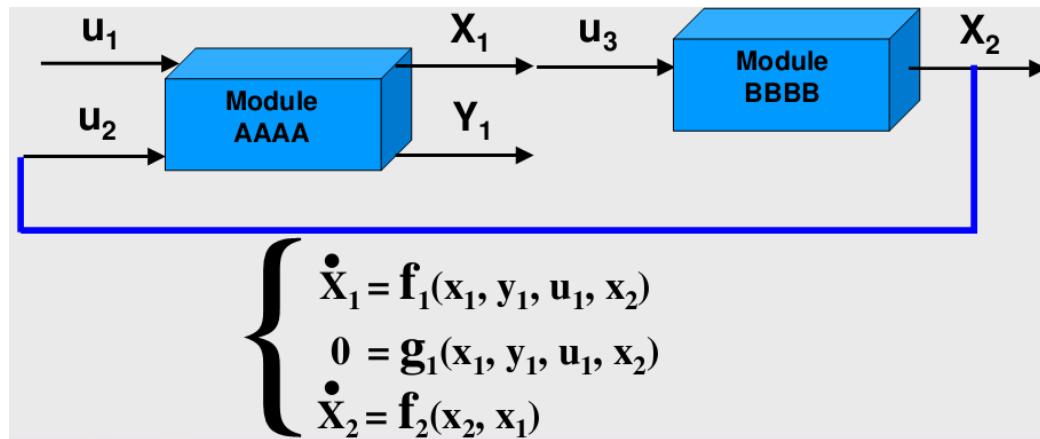


Figure 5.2: Translation of the component link into a non-linear equation system[65].

Dynamic simulation and transient analysis can be performed interactively by the embedded LegoSM, which allows to set simulation speed (real, accelerated or step by step) and time step integration, to freeze and restart simulation from a “snapshot” previously recorded, to perturb boundary conditions (with a step or a ramp perturbation) and show variables trend[65].

5.2 General parameters of the TES

In Chapter 4 the silicon carbide was chosen as storage medium thanks to its volumetric heat capacity. Now it's necessary to choose the characteristics of the TES, in particular its volume and the air flow that is used to heat it.

5.2.1 TES volume

The primary function of the storage is to maintain a constant electricity production during solar transient and to extend solar operations after the sunset. In particular, a larger storage can store more thermal energy, so the solar plant produces at nominal power for a longer period without increasing the fuel consumption, resulting in a reduction of the levelized cost of electricity. On the other hand, it requires a higher installation cost.

Since the plant is designed to work in nominal condition at the vernal equinox, when the sun sets at 18:00, the storage is designed to ensure the operation of the solar plant for two hours after the sunset, in order to produce electricity when the grid demand is still high.

During these two hours the air flow at the compressor outlet is heated by the storage from a temperature of 450 °C to 850 °C, so the air temperature at the inlet of the combustion chamber remains constant, even if the solar receiver doesn't work. The thermal energy required by the air flow is calculated with formula (5.2).

$$E_{th} = \dot{m} \cdot \bar{c}_p \cdot \Delta T \cdot \Delta t \quad (5.2)$$

Where:

- E_{th} is the thermal energy required (379.685 GJ).
- \dot{m} is the air flow at the compressor outlet (117.5 kg/s).
- \bar{c}_p is the average air heat capacity (1.122 kJ/kgK).
- ΔT is the temperature difference between the compressor outlet and the combustion chamber inlet (400 °C).
- Δt is the operating time of the storage.

The mass of ceramic material necessary to store this thermal energy is calculated with formula (5.3).

$$m = \frac{E_{th}}{c \cdot \Delta T} \quad (5.3)$$

Where:

- m is the mass of ceramic material required (842,994 kg).
- E_{th} is the thermal energy stored (379.685 GJ).
- c is the heat capacity of the ceramic material (1.126 kJ/kgK).
- ΔT is the storage temperature difference between the start and the end of the discharging process (400 °C).

Now it's possible to calculate the storage volume with formula (5.4).

$$V = \frac{m}{\rho} \quad (5.4)$$

Where:

- V is the volume of the storage (265.09 m³).
- m is the mass of ceramic material used as storage (842,994 kg).
- ρ is the ceramic material density (3132 kg/m³).

Despite a volume of ceramic material equal to 265 m³ seems too large, the

ceramic regenerative thermal oxidizer (RTO) produced by KBA, which is the company that has built the ceramic storage for the Jülich solar power plant basing on the RTO concept, have a typical volume of up to 600 m³[66].

5.2.2 Charging process

Once the storage is discharged, or at the start of the plant's operation, it's necessary to recharge it in order to increase its temperature up to 850 °C. To do that part of the air at the solar receiver outlet is sent to the cold storage and, after having heated the storage, re-injected into the solar tower.

To maintain the turbine inlet constant, the solar field must be expanded in order to concentrate more energy towards the solar receiver. In this way, during the most sunny hours of the day, the solar radiation in excess is used for heating the recirculated air.

Another solution consists in charging the storage during the morning, when the grid demand is low, with the air coming from the solar receiver. After having heated the storage, the air flows into the combustion chamber at a temperature of about 450 °C. When the storage is fully charged, it is bypassed by the air, which flows directly into the combustion chamber at a temperature of about 850 °C. Unlike the first solution in this case there's no fuel saving, since the storage is used only to shift the solar production when the grid demand is higher. For this reason this solution is discarded in favor of the first one.

The air flow recirculated, that is necessary to heat the storage, is calculated with formula (5.5).

$$\dot{m}_{RIC} = \frac{m_{STOR} \cdot c \cdot \Delta T}{c_p \cdot \Delta T \cdot t} \quad (5.5)$$

Where:

- m_{RIC} is the air flow recirculated.
- c is the heat capacity of the storage (1.126 kJ/kgK).
- ΔT is the temperature difference of the storage between the start and the end of the charging process (400 °C).
- c_p is the average heat capacity of the air (1.122 kJ/kgK).
- ΔT is the temperature difference of the air between the inlet and the outlet of the storage (400 °C).
- t is the time required to complete the charging process.

Figure 5.3 shows the variation of the air flow recirculated in function of the time required for the charging process.

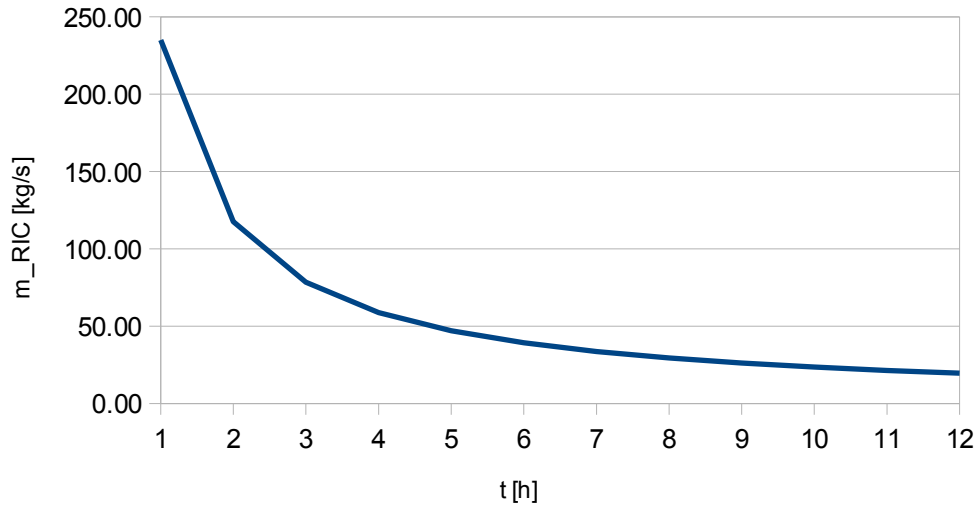


Figure 5.3: Variation of the air flow recirculated in function of the time required for the charging process.

As it can be seen from the chart, a high air flow allows to reduce the time required for charging the storage. In particular, it's recommended to use an air flow rate greater than 30 kg/s because, with a small increase of air flow, the charging time can be drastically reduced.

However, a fan must be installed in order to overcome the pressure drop of the solar tower and of the storage. The electrical power consumed by the fan is calculated with formula (5.6).

$$W_{FAN} = \dot{m}_{RIC} \cdot \frac{\Delta p}{\rho \cdot \eta_{FAN}} \quad (5.6)$$

Where:

- W_{FAN} is the electrical power consumed by the fan.
- \dot{m}_{RIC} is the air flow recirculated.
- Δp is the total pressure increase in the fan.
- ρ is the air density at 450 °C (10.21 kg/s).
- η_{FAN} is the fan efficiency (about 0.8).

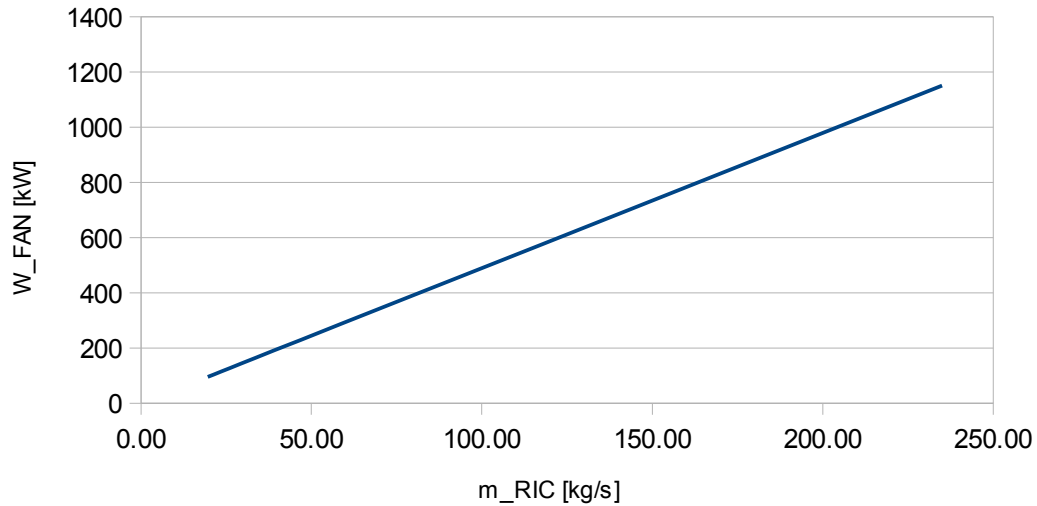


Figure 5.4: Variation of the power required by the fan in function of the air flow rate.

As can be seen in figure 5.4, the power consumed by the fan is directly proportional to the air flow and, for air flows above 100 kg/s, the power consumption becomes significant.

The pressure increase used in formula (5.6) is equal to 0.4 bar, since the pressure drop of the solar tower is equal to 0.2 bar, as calculated in Chapter 2, and the pressure drop of the storage is expected to be less than 0.2 bar.

To decide the air flow that charge the storage it's necessary to make a trade-off between the charging time and the power consumed by the fan, since choosing a higher air flow results in a lower charging time, but also in a higher power consumption, while choosing a lower air flow results in a lower power consumption, but also in a higher charging time.

In conclusion, an air flow equal to 39.16 kg/s (33% of the air flow at the compressor outlet) is chosen, which correspond to a charging time of 6 hours and to a power consumption of 192 kW.

5.3 Design of the storage parameters

Since the storage is made of a ceramic material, the air can be in direct contact with the storage medium. The storage is composed of several parallel channels, in which the air flows, passing through, as is shown in figure 5.5.

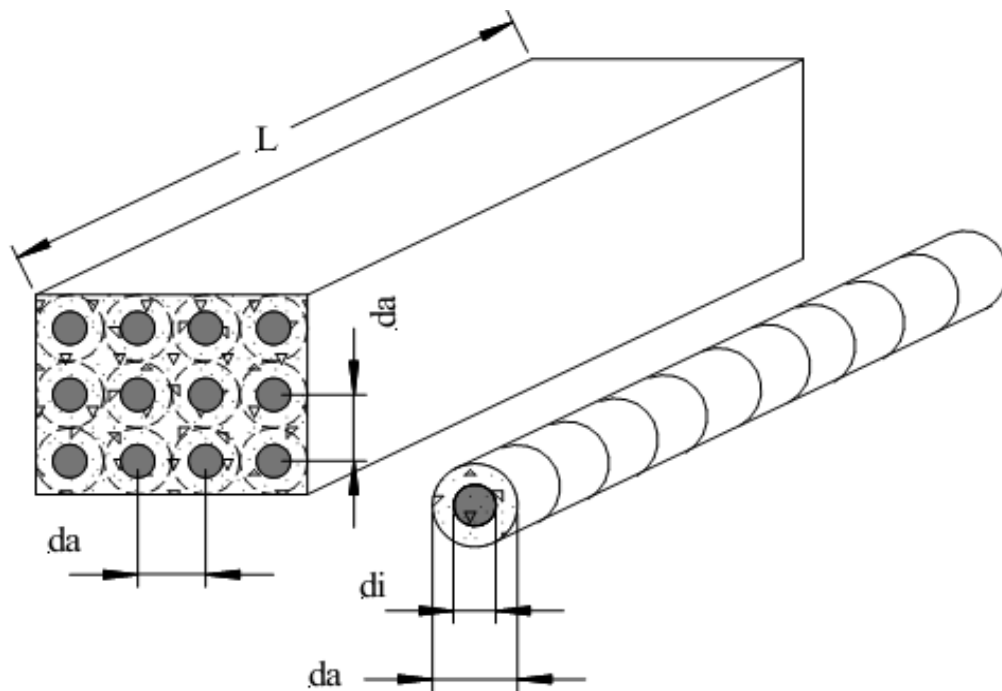


Figure 5.5: Scheme of the thermal storage and parameters describing the geometry[67].

Referring to figure 5.5, L is the length of the storage, d_i is the diameter of a single channel in which the air flows and d_a is the distance between the centers of two channels. The half of the difference between d_a and d_i is the thickness of ceramic associated to each channel.

Each parameter must be optimized in order to ensure a good thermal exchange with a low pressure drop. In particular, the storage parameters are chosen for the discharging process, when the air flow is the highest.

5.3.1 Number of channels and their diameter

The number of channels and the diameter of them are correlated, since the air flow rate is fixed at the nominal value. Formula (5.7) expresses this correlation.

$$N_c = \frac{4 \cdot \dot{m}}{\pi \cdot \rho \cdot v \cdot D_i^2} \quad (5.7)$$

Where:

- N_c is the number of channels.
- \dot{m} is the nominal air flow (117.5 kg/s).
- ρ is the air density at 850 °C (6.57 kg/m³)

- v is the air velocity.
- D_i is the channels diameter.

The air velocity is an important parameter because a higher value increase the heat exchange coefficient, while a lower value decrease the pressure drop. However it has not yet been determined, so it changes with the channels diameter and the channels number. The results of formula (5.7) are shown in figure 5.6.

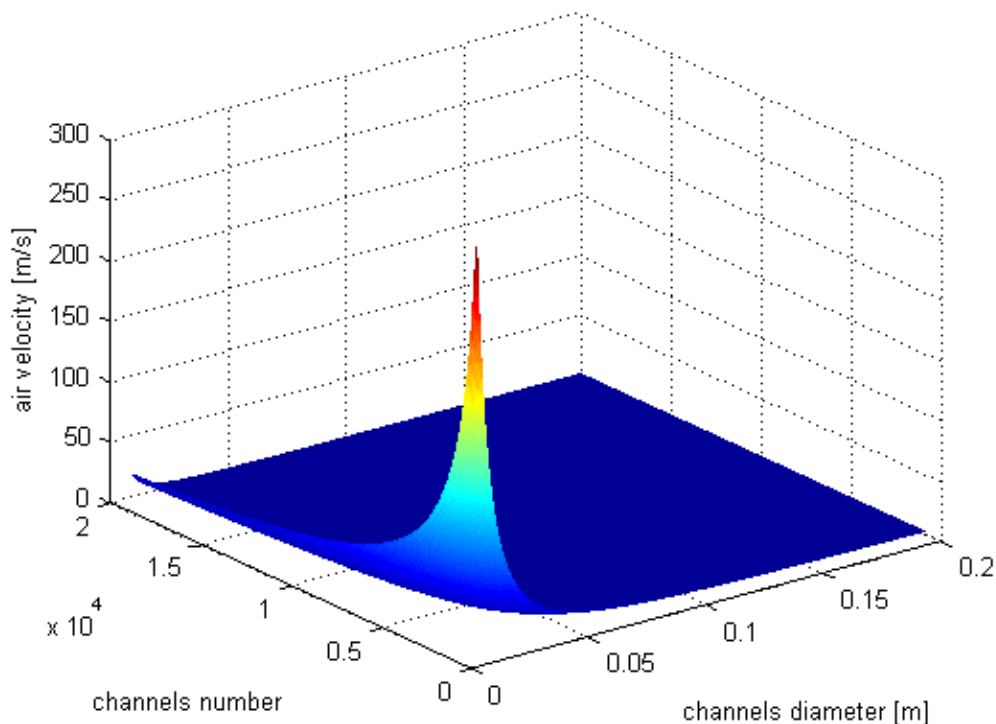


Figure 5.6: Air velocity in function of channels number and of channels diameter.

It's possible to infer from the chart that a low number of channels with a small diameter is a solution to discard, because the air velocity is too high, resulting in high pressure drop.

Acceptable values of the air velocity vary from 5 m/s (to avoid high pressure losses) to 20 m/s (to ensure a good heat exchange coefficient).

It's possible to extract from the chart of figure 5.6 the area delimited by these velocity values and the result can be seen in figure 5.7.

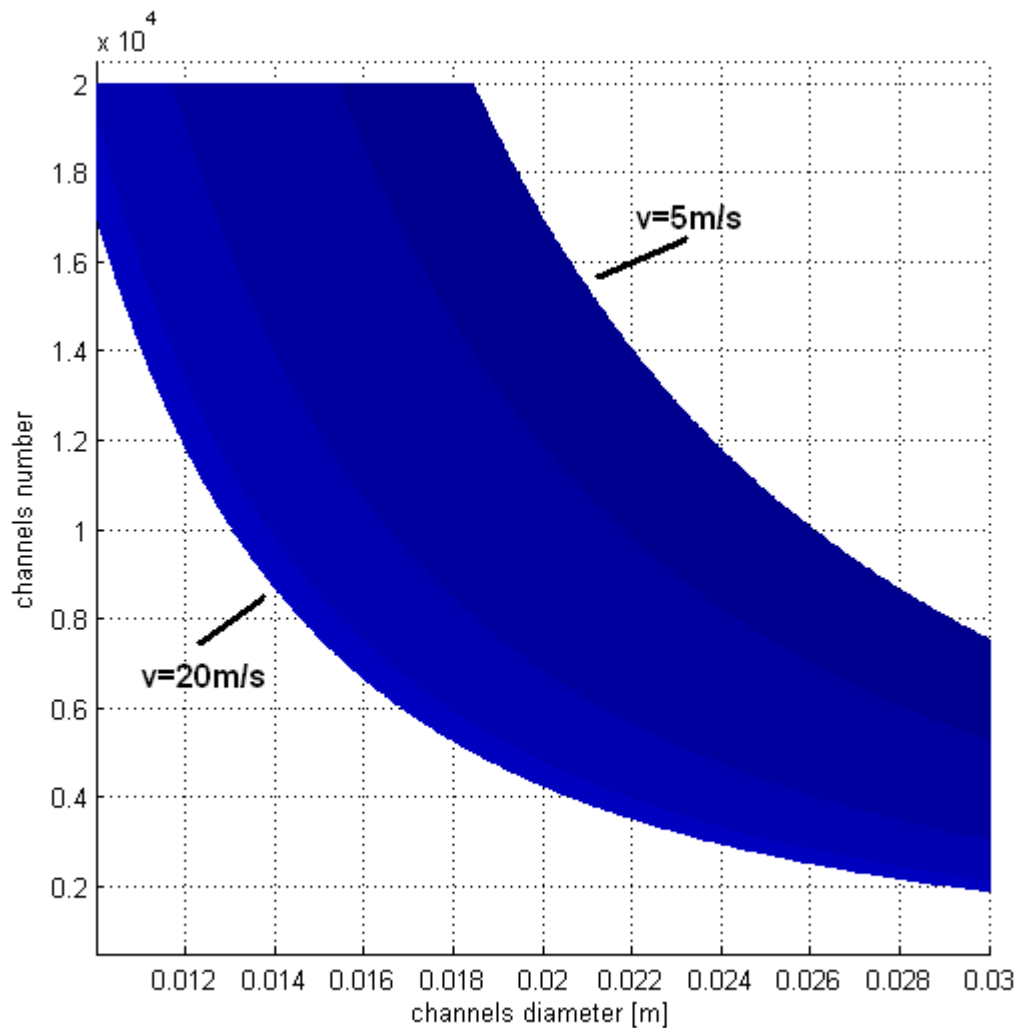


Figure 5.7: Channels number in function of channels diameter. The darker the color, the lower is the air velocity.

As it can be seen from the chart, the most suitable diameters are comprised between 0.01 m and 0.03 m. However, diameters between 0.01 m and 0.015 m are discarded due to the high number of channels required.

After this first selection, it's possible to compare the heat transfer coefficient and the pressure drop of each configuration.

The coefficient of heat transfer is calculated from the Nusselt number.

$$Nu = \frac{h \cdot D_i}{k} \quad (5.8)$$

Where:

- Nu is the Nusselt number.
- h is the coefficient of heat transfer.
- D_i is the channels diameter.
- k is the air thermal conductivity at 850 °C (0.074 W/mK).

For heat exchange in forced convection in a circular pipe, the most commonly used correlation for predicting the Nusselt number is the Dittus-Boelter equation, which can be seen in formula (5.9).

$$Nu = 0.023 \cdot Re^{0.8} \cdot Pr^{0.4} \quad (5.9)$$

Where:

- Nu is the Nusselt number.
- Re is the Reynolds number (formula 5.10).
- Pr is the air Prandtl number (0.7).

The Reynolds number gives a measure of the ratio of inertial forces to viscous forces and characterizes different flow regimes, such as laminar or turbulent flow.

$$Re = \frac{\rho \cdot v \cdot D_H}{\mu} \quad (5.10)$$

Where:

- Re is the Reynolds number.
- ρ is the air density at 850 °C (6.57 kg/m³).
- D_H is the hydraulic diameter (for a circular pipe it coincides with the internal diameter d_i).
- μ is the air viscosity at 850 °C (4.7*10⁻⁵ Pas).

The distributed pressure drop caused by friction of each channel is calculated with formula (5.11).

$$\frac{\Delta p}{L} = 0.05 \cdot \frac{1}{2} \cdot \frac{\rho \cdot v^2}{D} \quad (5.11)$$

Where:

- $\Delta p/L$ is the distributed pressure drop.
- ρ is the air density at 850 °C (6.57 kg/m³).

- v is the air velocity.
- D is the channel diameter.

Table 5.1 shows the results for four values of diameter.

Table 5.1: Channels parameters in function of the air velocity and channels diameter.

d_i 0.015 m				
v [m/s]	N_channels	Re	h [W/m ² K]	$\Delta p/L$ [bar/m]
5	20399	1.04E+04	161.41	0.0027
8	12749	1.67E+04	235.09	0.0070
11	9272	2.30E+04	303.30	0.0132
14	7286	2.92E+04	367.84	0.0213
17	6000	3.55E+04	429.65	0.0314
20	5100	4.18E+04	489.30	0.0435

d_i 0.02 m				
v [m/s]	N_channels	Re	h [W/m ² K]	$\Delta p/L$ [bar/m]
5	11474	1.39E+04	152.39	0.0020
8	7172	2.23E+04	221.94	0.0052
11	5216	3.06E+04	286.34	0.0099
14	4098	3.90E+04	347.27	0.0160
17	3375	4.73E+04	405.63	0.0236
20	2869	5.57E+04	461.95	0.0326

d_i 0.025 m				
v [m/s]	N_channels	Re	h [W/m ² K]	$\Delta p/L$ [bar/m]
5	7344	1.74E+04	145.73	0.0016
8	4590	2.78E+04	212.25	0.0042
11	3338	3.83E+04	273.84	0.0079
14	2623	4.87E+04	332.11	0.0128
17	2160	5.92E+04	387.92	0.0189
20	1836	6.96E+04	441.78	0.0261

d_i 0.03 m				
v [m/s]	N_channels	Re	h [W/m ² K]	$\Delta p/L$ [bar/m]
5	7344	1.74E+04	145.73	0.0016
8	4590	2.78E+04	212.25	0.0042
11	3338	3.83E+04	273.84	0.0079
14	2623	4.87E+04	332.11	0.0128
17	2160	5.92E+04	387.92	0.0189
20	1836	6.96E+004	441,78	0.0261

To determine a precise value of the channels number and their diameter, it's necessary to consider another parameter: the storage length.

5.3.2 Storage length

The storage length is a fundamental parameter for the storage design, since the storage pressure drop is proportional to it and the temperature difference between the ceramic and the air flow at the storage outlet is lower if the storage is longer.

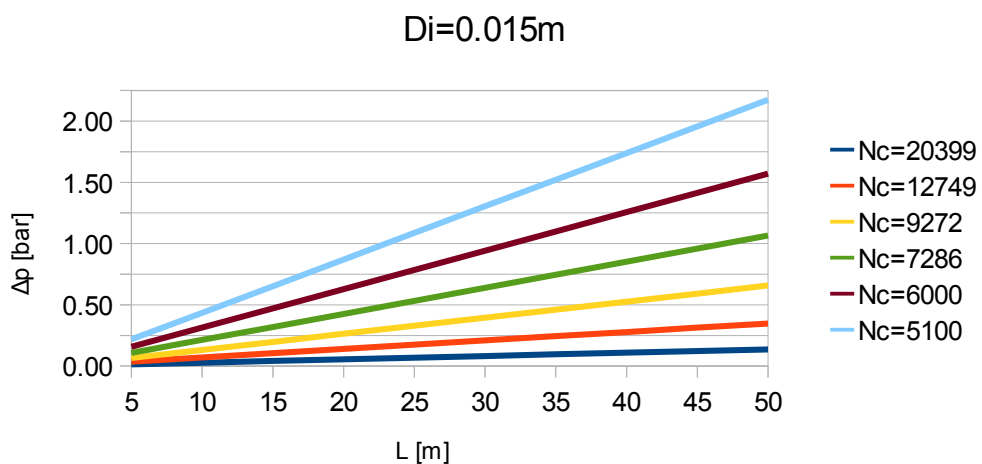
Moreover, the storage length is related to its volume and to the channels number, as is shown in formula (5.12).

$$V = N_c \cdot \frac{\pi \cdot (D_a^2 - D_i^2)}{4} \cdot L \quad (5.12)$$

Where:

- V is the volume of ceramic material of which the storage is made (265.09 m³).
- N_c is the number of channels.
- D_a is the equivalent external diameter of a single channel.
- D_i is the channels diameter.
- L is the storage length.

Due to space problems, the maximum storage length is set equal to 50 m, and the storage pressure drop, which is calculated with formula (5.11), is reported on the chart of figure 5.8.



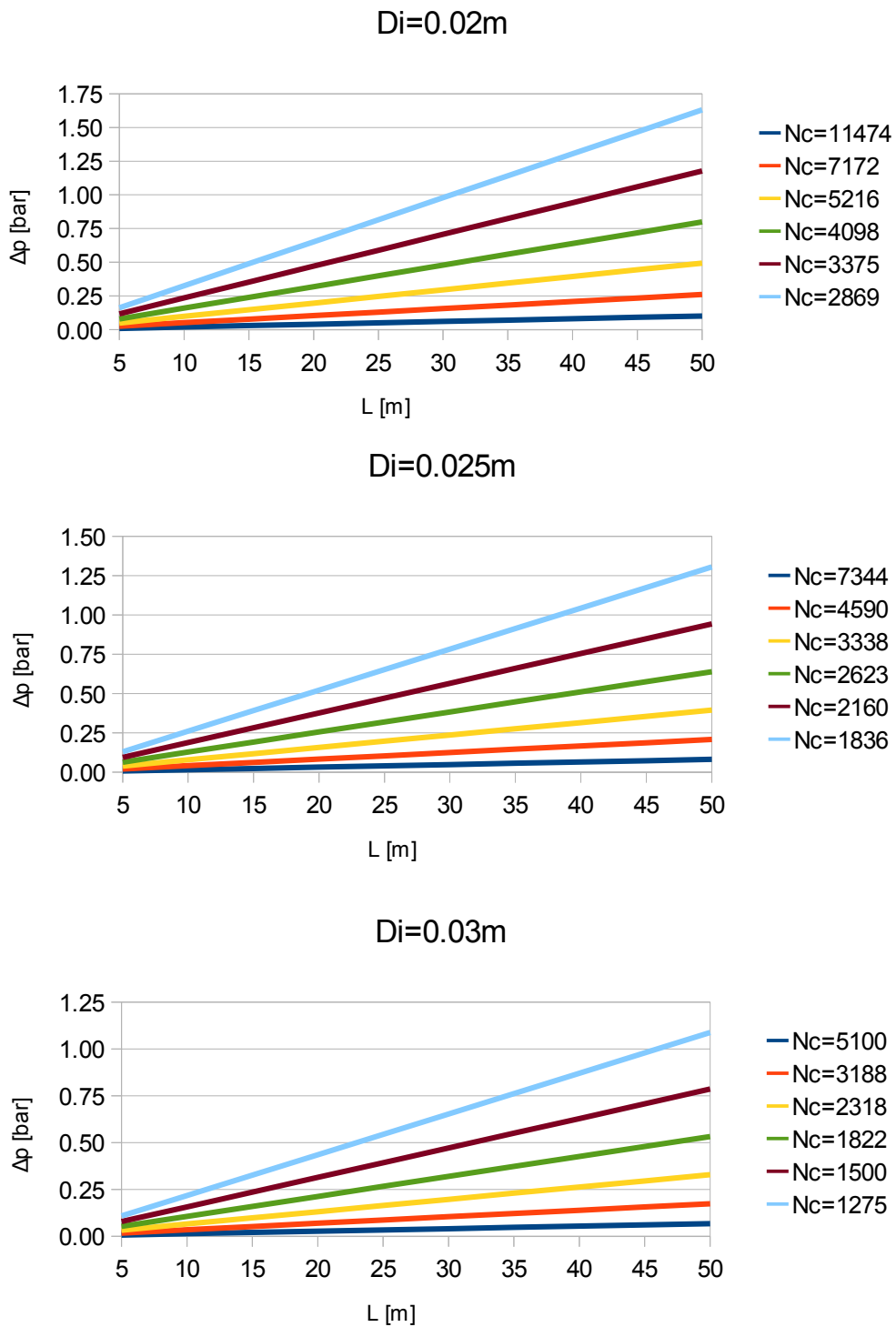


Figure 5.8: Storage pressure drop for four channel diameter.

The air temperature at the storage outlet depends on the channels length too. In fact, the longer are the channels, the higher is the outlet temperature because the heat exchange surface is larger.

To correlate the outlet air temperature with the channels length and the other parameters (channels number and diameter), it's necessary to make one simplification.

Since the air transit time inside the storage channels is of the order of a few seconds while the storage operating time is about two hours, it's possible to neglect the energy variation of the storage and consider the wall temperature constant during the air heating process.

The energy balance of the system is written in formula (5.13).

$$\dot{m} \cdot c_p \cdot (T_{a,in} - T_{a,out}) = h \cdot \pi \cdot D_i \cdot L \cdot \frac{T_{a,in} - T_{a,out}}{\ln \frac{T_w - T_{a,in}}{T_w - T_{a,out}}} \quad (5.13)$$

The first term is the heat transferred to the air, while the second term is the heat transferred from the storage.

The parameters involved in the equation are:

- m is the air flow in a single channel (it's obtained by dividing the total air flow for the number of channels).
- $T_{a,in}$ and $T_{a,out}$ are the air temperature at the inlet and at the outlet of the storage.
- h is the heat transfer coefficient.
- D_i is the channels diameter.
- L is the length of the channels.
- T_w is the wall temperature of the storage (850 °C at the beginning of the discharging process).

The heat transfer coefficient can be calculated with the Dittus-Boelter equation, formula (5.9), since in any case the flow is turbulent ($Re > 10000$) and fully developed ($L/D_i > 60$).

During the discharge process, the air temperature at the storage inlet is equal to 450 °C and the temperature difference between the storage wall and the air flow at the outlet is about 5 °C.

Combining all the constant, the formula (5.13) can be rewritten in this way.

$$L = \frac{816.81}{N_c} \cdot \frac{1}{\frac{1}{(N_c \cdot D_i)^{0.8}}} \quad (5.14)$$

Where:

- L is the storage length (measured in meters).
- N_c is the channels number.
- D_i is the channels diameter (measured in meters).
- The constant dimension is $m^{0.2}$.

The results are shown in figure 5.9.

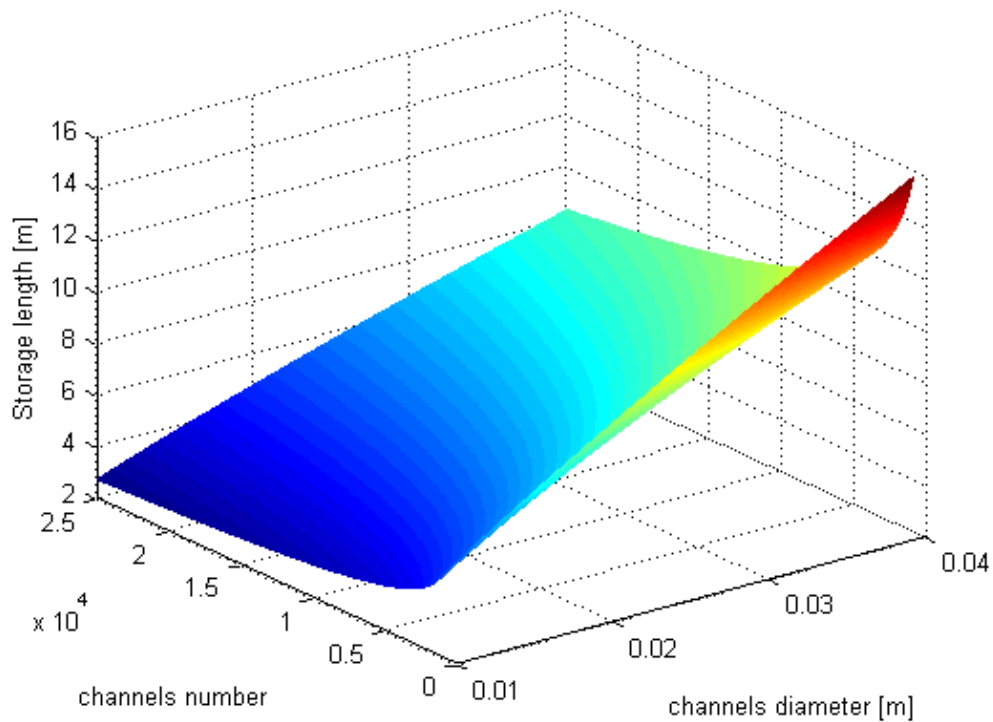


Figure 5.9: Storage length in function of the channels number and of their diameter.

In more detail, the calculated minimum storage length, in order to ensure a temperature difference at the outlet equal to 5 °C, is shown in table 5.2 for different channels configurations.

Table 5.2: Minimum storage length and pressure drop for different channels configurations.

d_i 0.015 m			d_i 0.020 m		
N_channels	L [m]	Δp [bar]	N_channels	L [m]	Δp [bar]
20399	3.90	0.0106	11474	5.51	0.0112
12749	4.28	0.0298	7172	6.05	0.0316
9272	4.57	0.0601	5216	6.45	0.0636
7286	4.79	0.1021	4098	6.77	0.1081
6000	4.98	0.1565	3375	7.04	0.1658
5100	5.15	0.2238	2869	7.27	0.2370

d_i 0.025 m			d_i 0.030 m		
N_channels	L [m]	Δp [bar]	N_channels	L [m]	Δp [bar]
7344	7.20	0.0117	5100	8.96	0.0122
4590	7.91	0.0330	3188	9.84	0.0342
3338	8.43	0.0665	2318	10.49	0.0690
2623	8.85	0.1131	1822	11.01	0.1173
2160	9.20	0.1733	1500	11.44	0.1798
1836	9.50	0.2478	1275	11.82	0.2571

However, the channels could be longer than the minimum length required, in order to obtain a lower temperature difference at the storage outlet and, above all, to keep constant the air outlet temperature during the discharging process, thanks to the formation of a thermocline inside the storage.

So, it's necessary to simulate the storage behavior during thermal transients for different channels length.

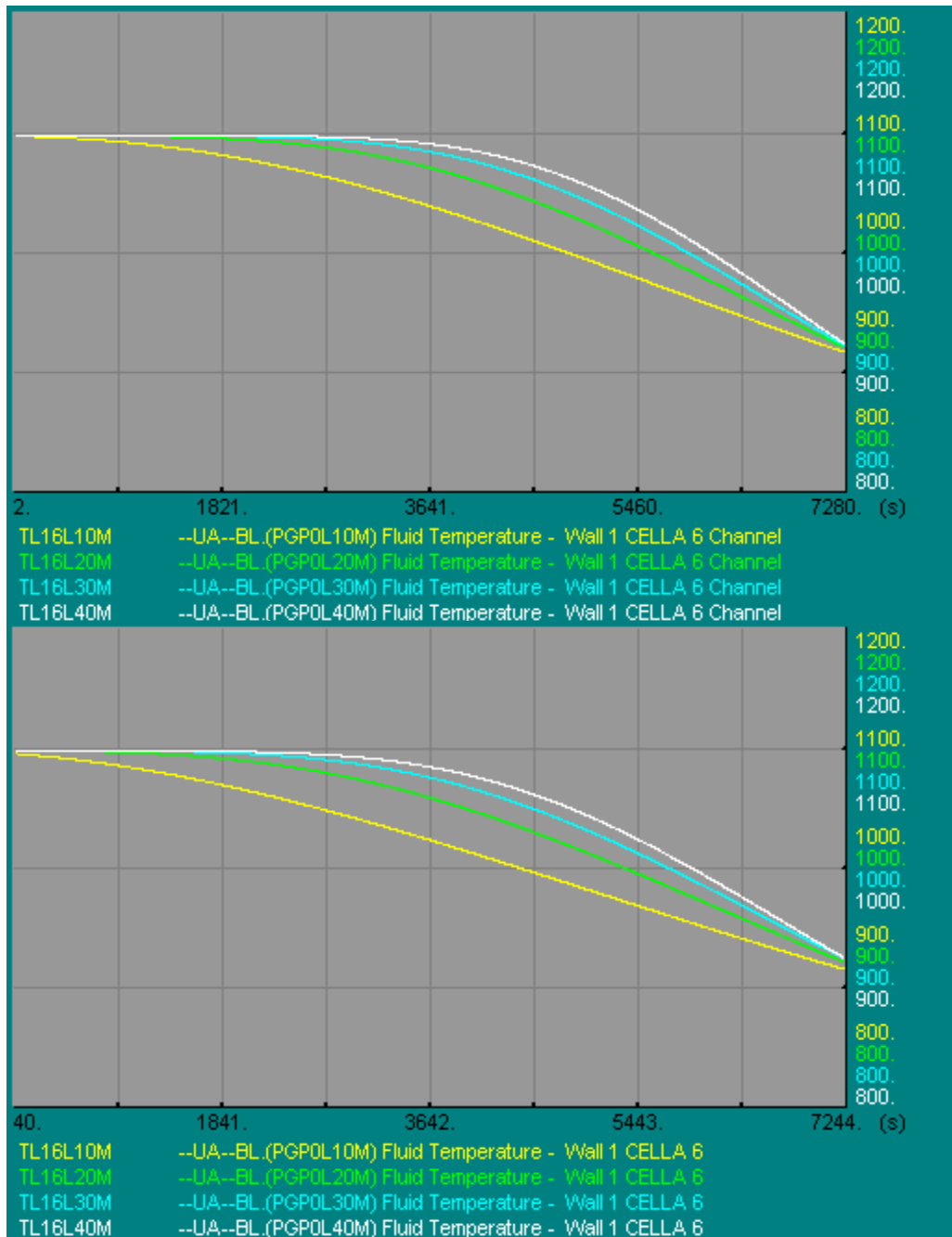
5.3.3 Storage response to thermal transients

The software used for this operation is the LegoPC, which was described at the beginning of this chapter. More in detail, the storage is modeled with two modules: the PGP0 module, which simulate the air flow behavior, and the META module, which simulate the ceramic behavior.

To obtain comparable results, it's necessary to confront storage configurations with different length and channels diameter, but with the same air velocity, set equal to 11 m/s, so that the air heat exchange into the channels is almost the same. As is shown in formula (5.12), the equivalent thickness associated at each channel varies with the storage length, since it is calculated with formula (5.15).

$$s_e = \frac{D_a - D_i}{2} \tag{5.15}$$

During the discharging process, the 117.5 kg/s air flow enters into the storage with a temperature equal to 450 °C, while the ceramic temperature is about 850 °C. The process lasts two hours and the temporal trend of the air outlet temperature for different storage configurations is shown in figure 5.10.



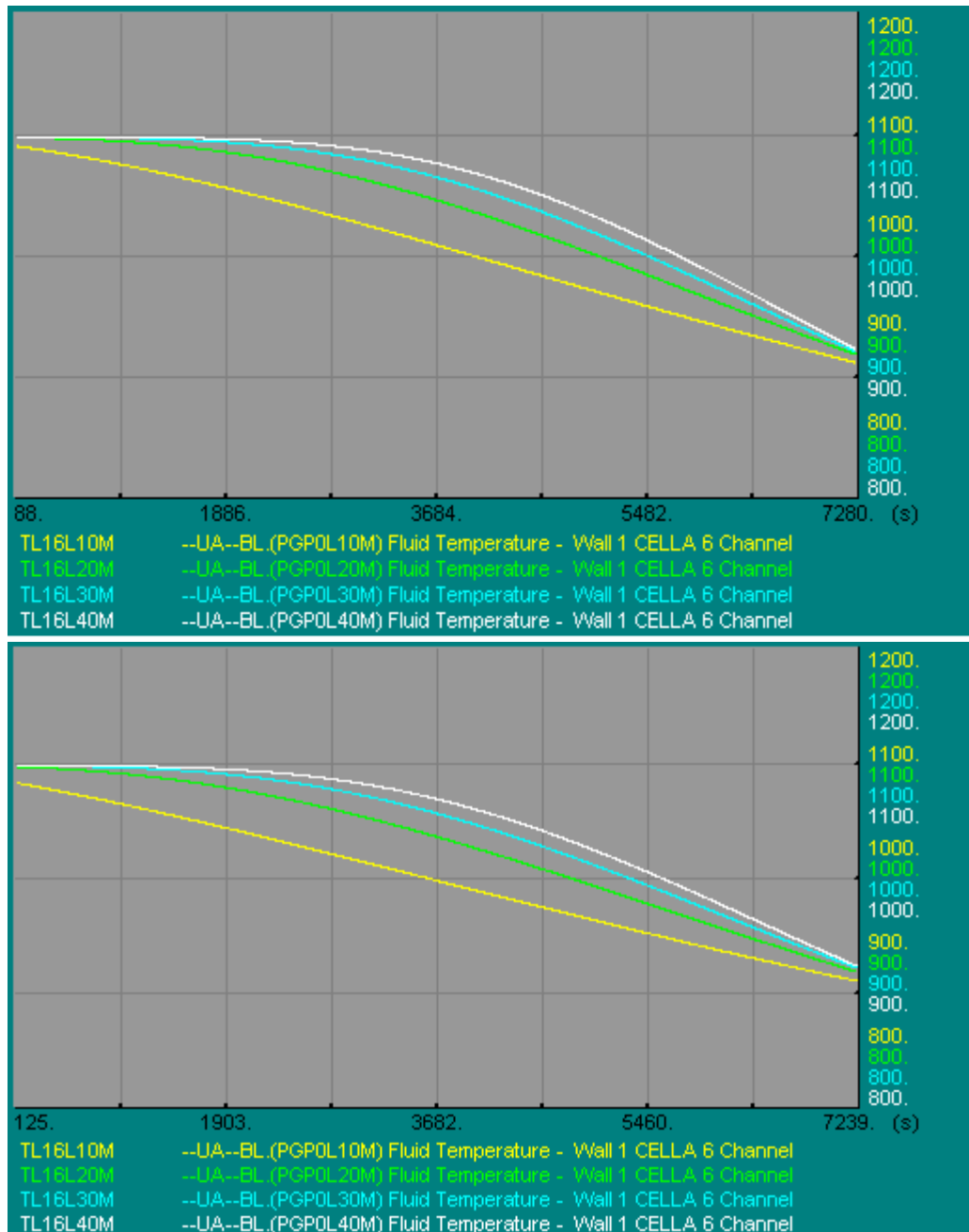
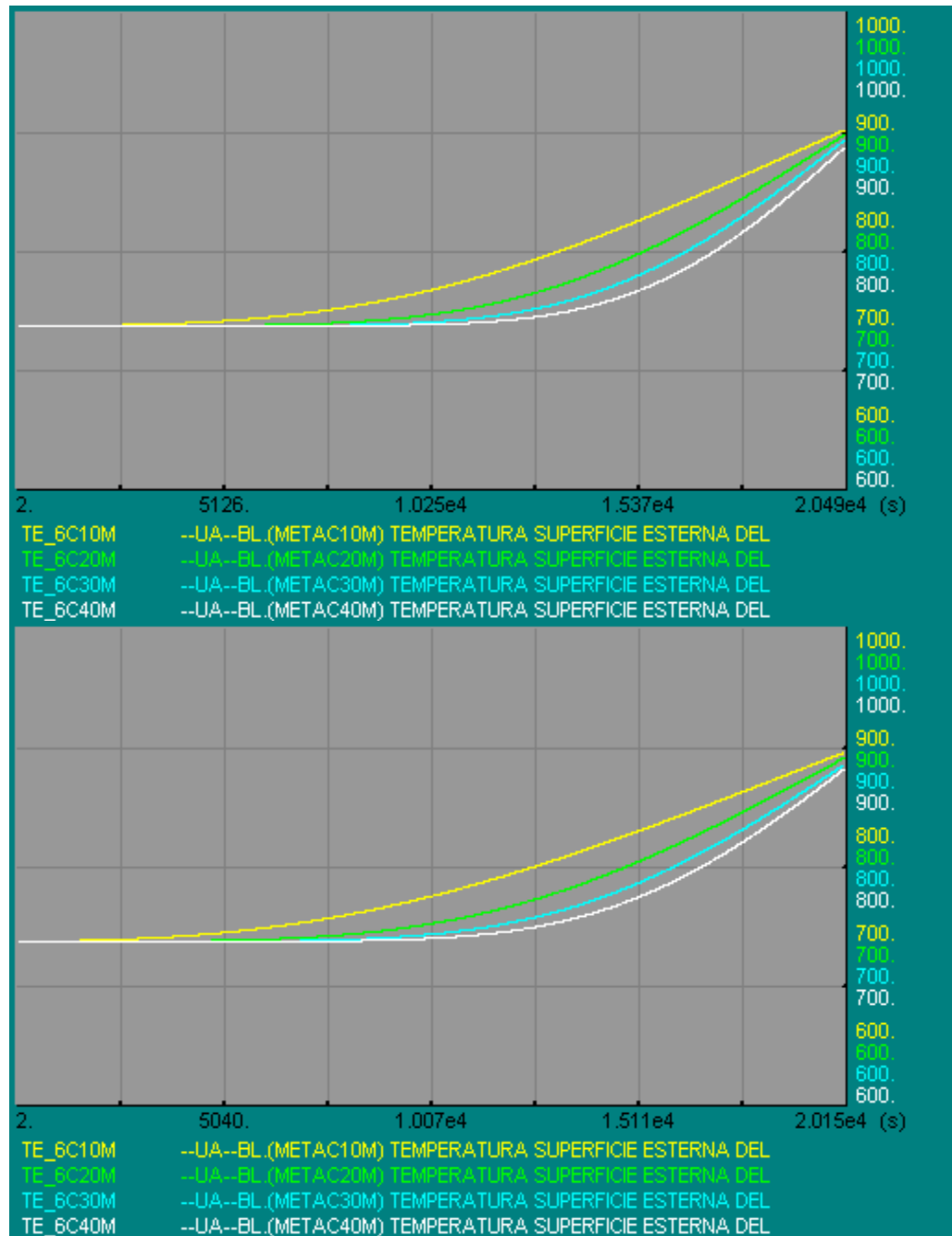


Figure 5.10: From the top: profile of the air temperature (in Kelvin) at the storage outlet during the discharging process for a storage with a 0.015 m, 0.02 m, 0.025 m, 0.03 m diameter channels. The yellow line is for a 10 m channels length, the green line is for a 20 m, the blue line is for a 30 m and the white line is for a 40 m.

In order to have a complete view of the storage operations, it's necessary to simulate the charging process too. In this case the air flow is lower (39.17 kg/s), but the process duration is longer (6 hours) and the temperatures are inverted, since the air flow enters at 850 °C while the storage is at about 450 °C. The temporal trend of the ceramic temperature measured at the storage outlet is shown in figure 5.11 for different storage configurations.



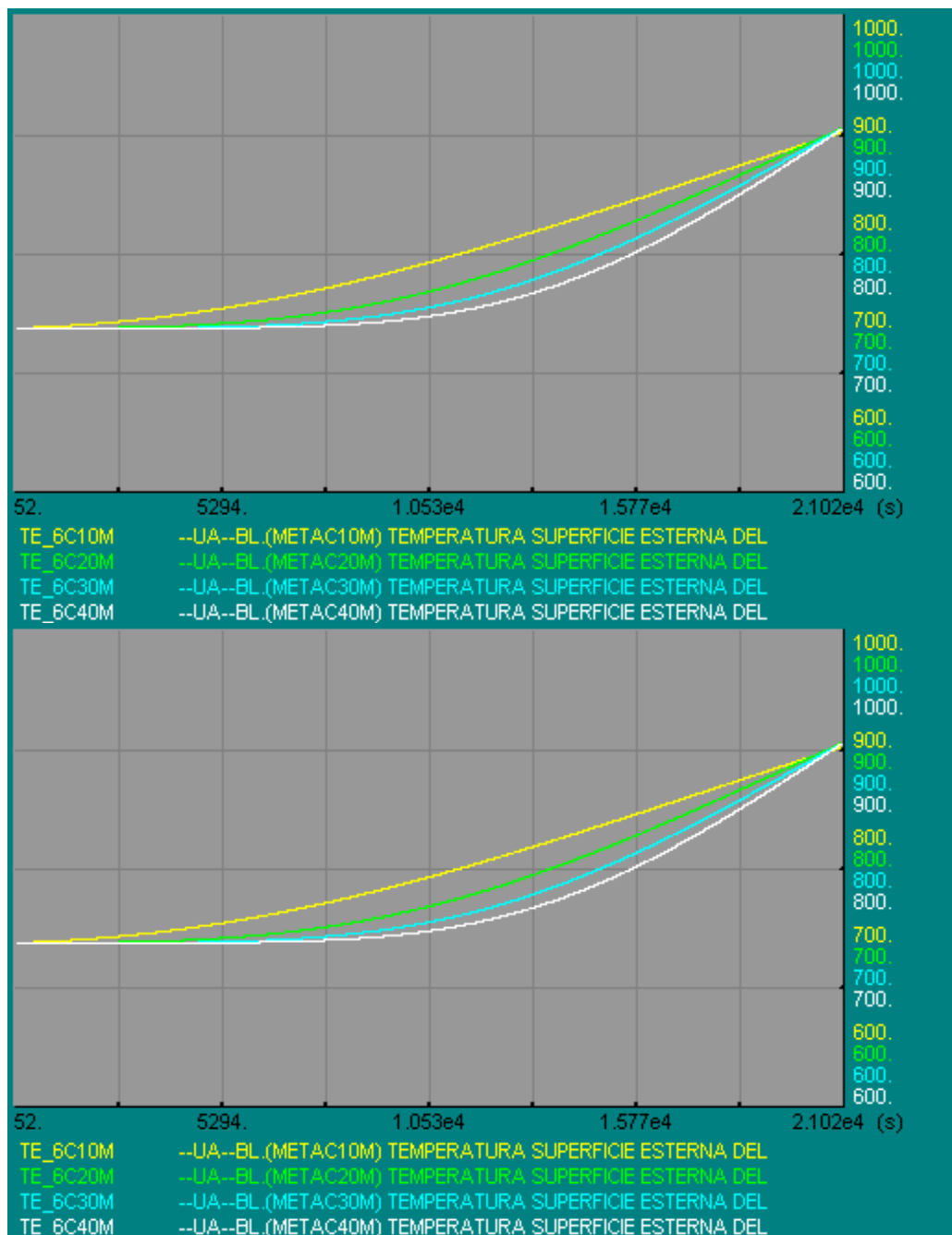


Figure 5.11: From the top: profile of the wall temperature (in Kelvin) at the storage outlet during the discharging process for a storage with a 0.015 m, 0.02 m, 0.025 m, 0.03 m diameter channels. The yellow line is for a 10 m channels length, the green line is for a 20 m, the blue line is for a 30 m and the white line is for a 40 m.

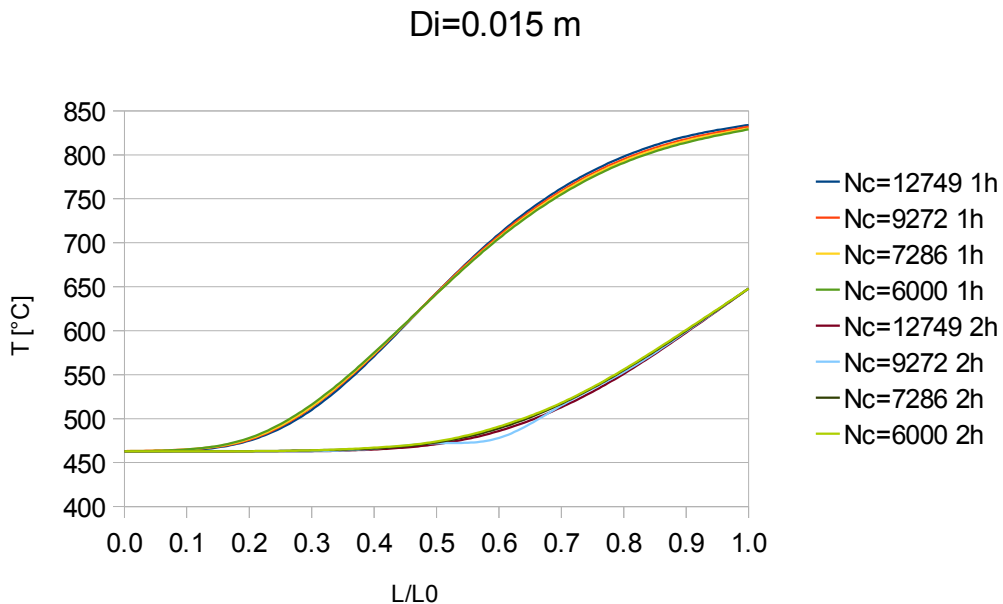
As can be seen from the charts of figure 5.10 and 5.11, longer channels allow a more constant air outlet temperature during the storage discharge, resulting in a steady air flow into the combustion chamber inlet.

For the charging process, the outlet wall temperature increases more rapidly for the shorter channels, but, if the wall temperature is measured at the same point (for example at 10 m), it results equal for each configuration. However, after six hours, all the storage configurations have reached the same wall outlet temperature (900 K).

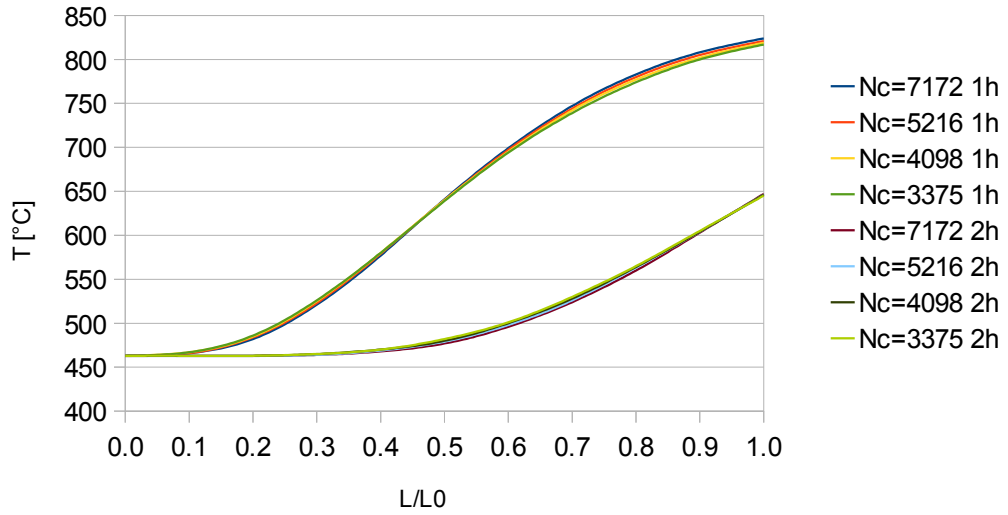
Comparing the various configurations, it's possible to state that the solution consisting in a length of 10 m must be discarded, since it has the worst performance. On the other hand, the best storage behavior during thermal transients owns to the 40 m solution, which keep the air outlet temperature constant for the longest time, while the 30 m solution has a similar temperature trend. A length of 20 m is a good solution too, but the 30 m solution is better because it's closer to the 40 m solution than the 20 m. So, the channels length chosen is equal to 30 m.

Now it's possible to decide the other two parameters of the storage (number of channels and their diameter).

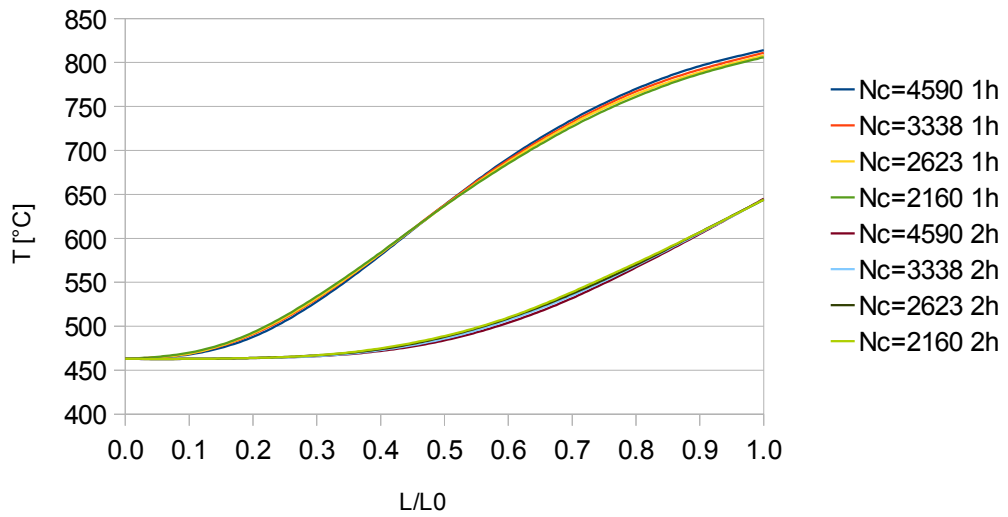
First, it's necessary to study the air temperature distribution inside the storage with the variation of the two parameters at two determinate instants. These instants are set equal to one hour and two hours after the beginning of the storage discharge. Results are shown in figure 5.12.



Di=0.02 m



Di=0.025 m



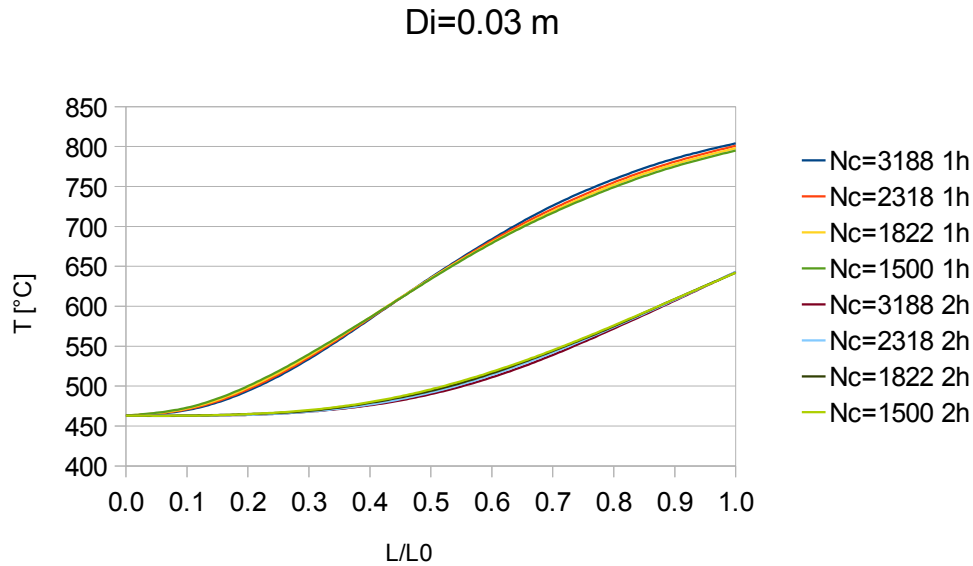


Figure 5.12: Air temperature profile inside the storage at 1 hour and 2 hours after the beginning of the discharging process. The profiles vary in function of the channels number and of their diameter.

As can be seen from the charts, the number of channels, which is related to the air flow velocity, is almost non influential in the development of the air temperature profile. On the other hand, the channels diameter is more important, since the air temperature at the storage outlet is higher when the channels are more narrow, so a channels diameter of 0.015 is chosen.

The number of channels is chosen in order to have a pressure drop not exceeding 0.2 bar. Using formulae (5.7) and (5.11), the calculated value of the channels number is equal to 12749, with an air flow velocity of 8 m/s. Table 5.3 summarizes the calculated values for the geometrical parameters of the storage.

Table 5.3: Parameters of the TES.

Parameter	Value
Channels length	30 m
Channels number	12479
Channels diameter	0.015 m
Air flow during the charge	117.5 kg/s
Air flow velocity during the charge	8 m/s
Pressure drop during the charge	0.2087 bar
Air flow during the discharge	39.17 kg/s
Air flow velocity during the discharge	1.75 m/s
Pressure drop during the discharge	0.015 bar

5.4 Storage thermal insulation

In order to increase the storage efficiency, thermal losses are limited thanks to the storage insulation. It consists of a inner insulation made of ceramic fiber blankets and of a mild steel containment, whose outer surface temperature is kept below 60 °C, like the thermal insulation used for the ceramic storage of the Jülich solar power plant[66].

5.4.1 Storage thermal losses

Before calculating the storage losses, it's necessary to make some assumptions, in order to simplify the problem. First, the thermal losses are calculated for the worst possible scenario, that is when the storage is fully charged and isn't used for 24 hours.

Secondly, the heat exchange with the external air is approximated as a one-dimensional steady state conduction, so the storage temperature, which is supposed uniform, and the air temperature don't change during the 24 hours.

Furthermore, thermal bridges of the edges of the storage containment and the heat exchange through the ground are neglected. These limitations are balanced by the absence of the solar irradiation, which is neglected too.

The thermal losses are calculated with formula (5.16)

$$Q_l = h_{cr} \cdot S \cdot (T_{w,e} - T_a) \cdot \Delta t \quad (5.16)$$

Where:

- Q_l is the total thermal loss of the storage.
- h_{cr} is the heat transfer coefficient, which takes into account both the convective heat exchange and the radiative heat exchange.
- S is the heat exchange surface area.
- $T_{w,e}$ is the temperature of the storage outer surface (60 °C).
- T_a is the average air temperature during the 24 hours (10 °C).
- Δt is the duration of inactivity of the storage (24 hours).

The radiative heat transfer coefficient is calculated with formula (5.17).

$$h_r = \sigma \cdot \varepsilon_{w,e} \cdot (T_{w,e} + T_a) \cdot (T_{w,e}^2 + T_a^2) \quad (5.17)$$

Where:

- h_r is the radiative heat transfer coefficient.
- σ is the Stefan–Boltzmann coefficient ($5.67 \cdot 10^{-8} \text{ W/m}^2\text{K}^4$).
- $\varepsilon_{w,e}$ is the emissivity of the storage containment (0.1).

For the free convection on a horizontal surface, the convective heat transfer coefficient is calculated with the Fishenden-Saunders equation (5.18).

$$h_c = 0.15 \cdot \frac{k}{x} \cdot Ra^{\frac{1}{3}} \quad (5.18)$$

Where:

- h_c is the free convection heat transfer coefficient.
- k is the air thermal conductivity (0.025 W/m²K).
- x is the characteristic length.
- Ra is the Rayleigh number, which is calculated with formula (5.19).

The Rayleigh number, which can be viewed as the ratio of buoyancy and viscosity forces times the ratio of momentum and thermal diffusivity, is calculated with formula (5.19).

$$Ra = Gr \cdot Pr = \frac{g \cdot \beta}{\nu \cdot \alpha} \cdot (T_{w,e} - T_a) \cdot x^3 \quad (5.19)$$

Where:

- Ra is the Rayleigh number.
- g is the gravity acceleration (9.81 m/s²).

- β is the air thermal expansion coefficient (0.0035 K^{-1}).
- ν is the air kinematic viscosity ($1.44 \cdot 10^{-5} \text{ m}^2/\text{s}$).
- α is the air thermal diffusivity ($2.01 \cdot 10^{-5} \text{ m}^2/\text{s}$).
- x is the characteristic length.

The global heat transfer coefficient is the sum of the radiative and conductive term. The thermal losses calculated are reported in table 5.4.

Table 5.4: Storage thermal losses.

	Surface area [m^2]	Thermal power loss [kW]	Thermal energy loss [MWh]
Lateral surfaces	450	168.15	4.04
Storage inlet surface	25	9.34	0.22
Storage outlet surface	25	9.34	0.22
Global	500	186.83	4.48

Since the thermal energy stored is equal to 105.47 MWh, in the worst possible conditions the efficiency of the storage is equal to 96%.

Chapter 6

Thermal energy storage integration into the plant

Now that the thermal storage is designed it's necessary to insert it into the solar power plant. Moreover, in this chapter are calculated the benefits of adopting a TES system in terms of fuel saving, increasing of solar share and CO₂ avoided in comparison to a traditional gas turbine power plant and to a HSGTPP without a TES system.

Lastly, in this chapter is simulated the storage behavior during solar transients when the storage isn't fully charged, like in a real solar power plant.

6.1 Plant configuration

The TES is placed in parallel to the solar receiver, so it may be excluded from the plant when it's not used. Moreover, a bypass line is added in order to make the air flows directly into the combustion chamber.

The solar power plant can work in four different configurations, depending on the solar irradiance and on the storage charging condition.

6.1.1 Power plant operation at nominal power

In this condition the air at the compressor outlet flows through the solar receiver and is heated up to 850 °C. Part of the air flow enters into the storage and, after having charged it, is recirculated thanks to a fan that increases the air pressure at the storage outlet, in order to overcome the pressure drops of the solar tower and of the storage.

Typical periods of operation in this condition happen during the summer season, when the solar radiation is the highest of the year. A scheme of the solar power plant working on this condition is shown in figure 6.1.

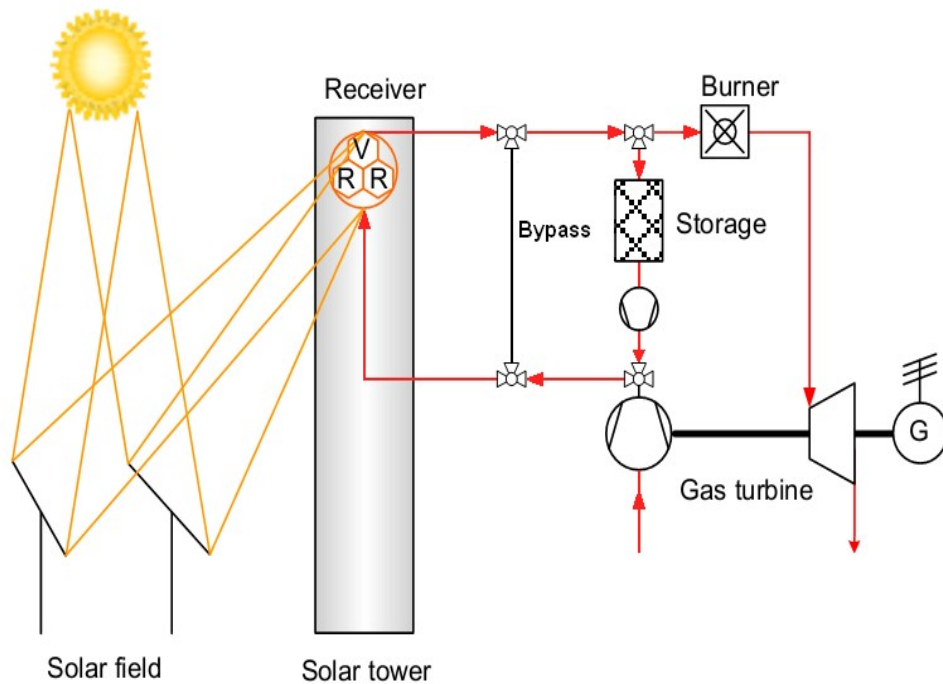


Figure 6.1: Scheme of the solar power plant operating at nominal power.

6.1.2 Power plant operation without storage charging

When the solar radiation is lower than the nominal value (800 W/m^2), the solar receiver doesn't collect enough thermal energy to charge the storage, so the fan is turned off and the inlet and outlet storage valves are closed. This happens especially during the first hours of the day or during the colder months. Another particular case where the storage is inactive is when the solar radiation is higher than 800 W/m^2 , but the storage is completely charged, so some mirrors of the solar field must be unfocused in order to avoid the overheating of the solar receiver.

If the solar radiation is slightly lower than the nominal one the air flow at the receiver inlet is reduced, since there's no air recirculation, so the air outlet temperature could be equal to $850 \text{ }^\circ\text{C}$ or a bit less. Figure 6.2 shows the scheme of the solar power plant in this condition.

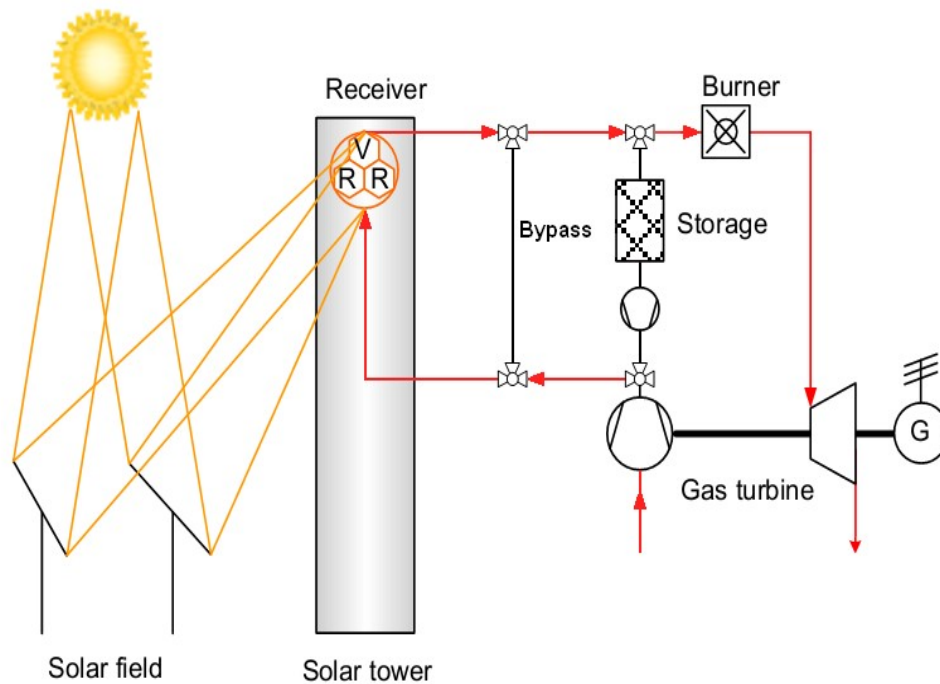


Figure 6.2: Scheme of the solar power plant without storage charge.

6.1.3 Power plant operation with storage discharge

After the sunset, or when the solar radiation is very low, the air flow cannot be heated by the solar receiver, so it's necessary to deploy the thermal energy previously collected into the storage. As in the first case, the storage inlet and outlet valves are opened, but there's no need to turn on the fan because the air flow is moved thanks to the pressure difference. In this way, the air temperature at the combustion chamber inlet remains constant and the electricity is produced with solar contribution for a longer period.

The solar tower is bypassed, but the storage causes a pressure drop equal to the one of the solar tower (0.2 bar), so the cycle efficiency remains unchanged compared to the previous case. Figure 6.3 shows the air path on the solar power plant when the storage is discharged.

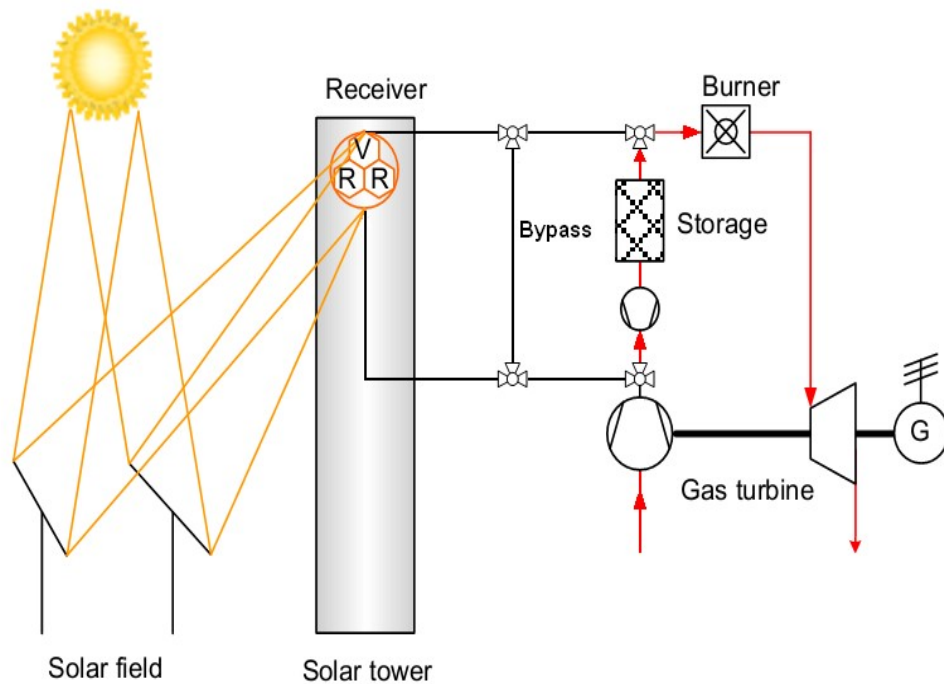


Figure 6.3: Scheme of the solar power plant operation with storage discharge.

6.1.4 Power plant operation with bypass line

In this last case the storage and the solar tower are bypassed and the air flow enters directly into the combustion chamber, so the thermodynamic cycle is the same of a conventional gas turbine power plant. It's necessary to do that when the solar radiation is absent and the storage doesn't ensure a minimum air temperature at the storage outlet. The cycle efficiency is the highest of the four cases, since there isn't any relevant pressure loss between the compressor outlet and the combustion chamber inlet, but the fuel consumption is the highest too because the solar contribution is equal to zero. A scheme of the solar power plant working on this condition is shown in figure 6.4.

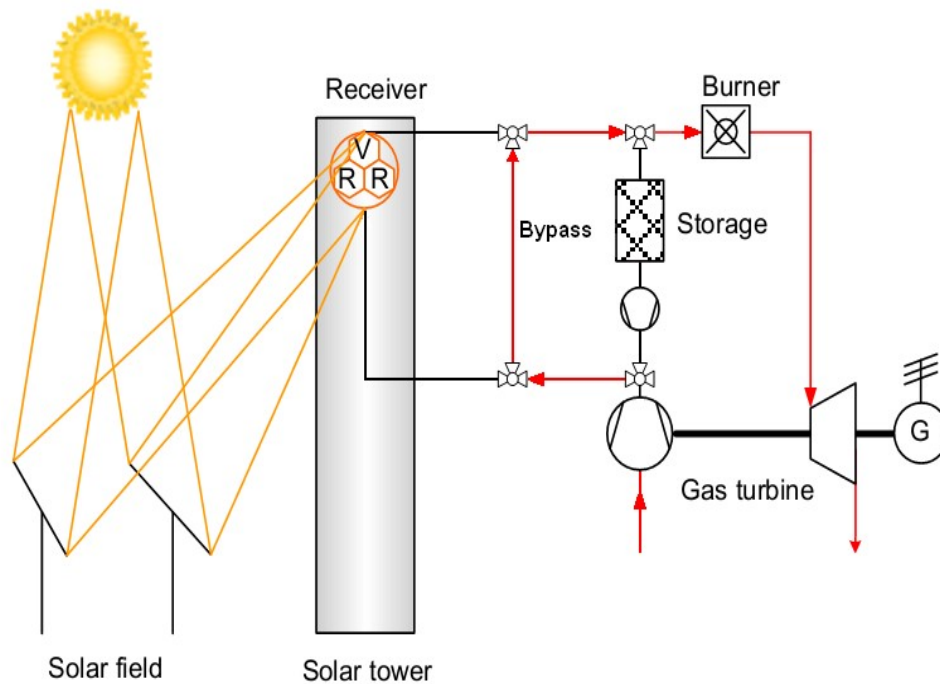


Figure 6.4: Scheme of the solar power plant operation with bypass line activated.

6.1.5 Choice of the solar power plant operation mode

During a typical sunny day, the solar power plant works in each of the four configurations presented, depending on the value of the solar radiation and on the condition of the storage. A scheme of the selection of the proper mode of operation is shown on figure 6.5.

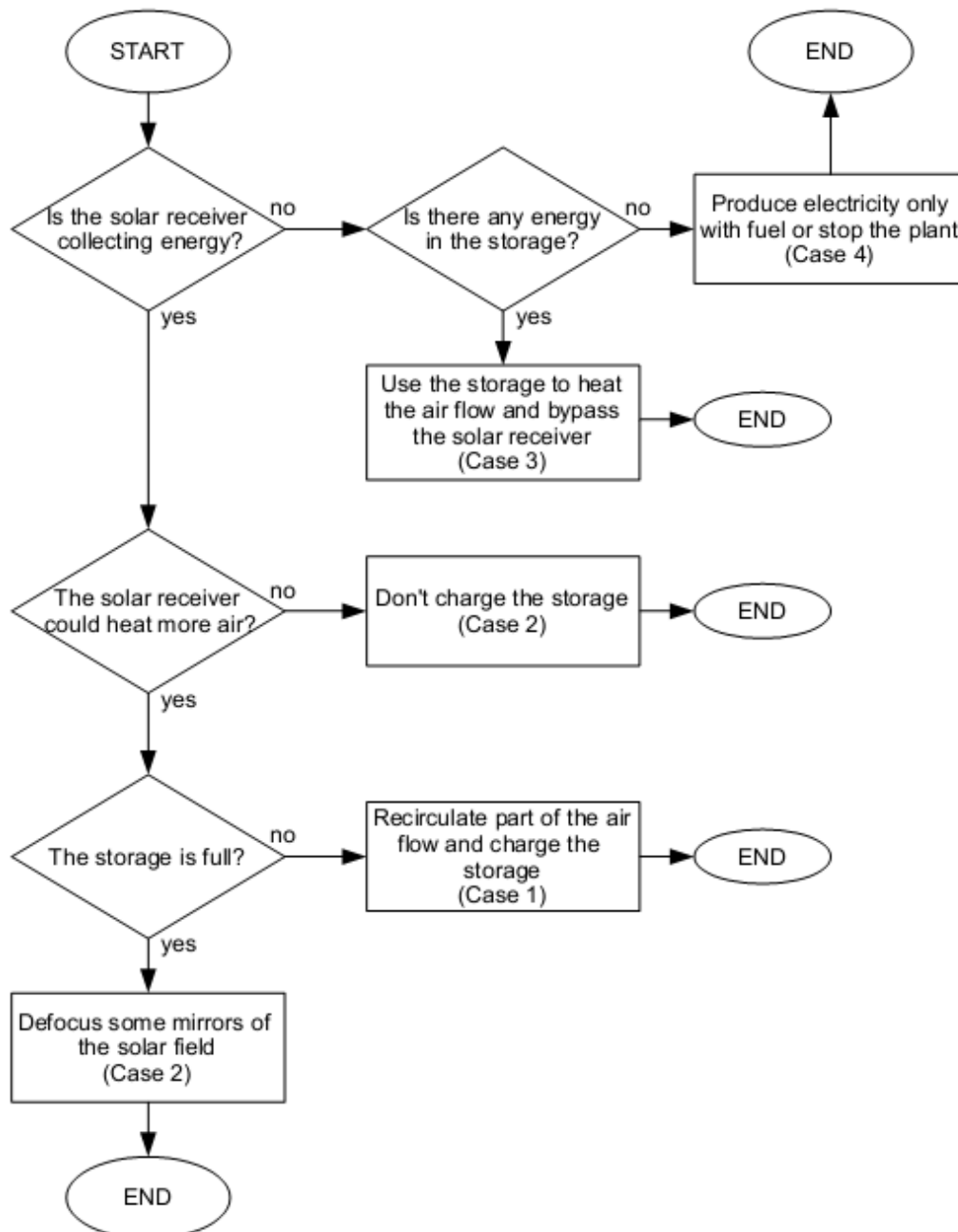


Figure 6.5: Control logic scheme that determines the proper mode of operation of the solar power plant.

6.2 Power plant performance improvements

The major advantages due to the implementation of a TES storage system into

the power plant are the increase of solar share and the reduction of fuel consumption and of CO₂ emissions. Now, since the storage parameters have been designed, it's possible to evaluate these advantages. In particular, the calculated values for the reference solar power plant are compared to those of a solar power plant of the same size but unprovided of a TES system and those of a conventional gas turbine power plant.

The values of solar share, fuel consumption and CO₂ emissions are calculated for the selected power plants if they work in mid load operation (from 0-24h) or in base load operation (from 6-22h).

6.2.1 Increase of solar share

The solar share is defined as the ratio between the average heat collected from the solar field (Q_{SF}) and the total heat supplied into the power process (Q_{tot}), as is shown in formula (6.1).

$$Solar\ Share = \frac{Q_{SF}}{Q_{tot}} \quad (6.1)$$

At design point conditions, the solar share of the plant is equal to 47%, but this value can be increased with an increase of the receiver outlet temperature or a reduction of the turbine inlet temperature.

Since the power plant is designed to work in nominal conditions at the noon of the vernal equinox, during the summer the solar share increases thanks to the increase of the solar irradiation and decreases during the winter, so, the annual average solar share is lower than the one calculated at design point conditions.

The addition of a thermal energy storage system increase the solar energy collected from the solar field, but the power production is increased too, resulting in an increase of fuel consumption. The annual average solar share for the solar power plant without the storage system and the plant with the storage system is shown in figure 6.6.

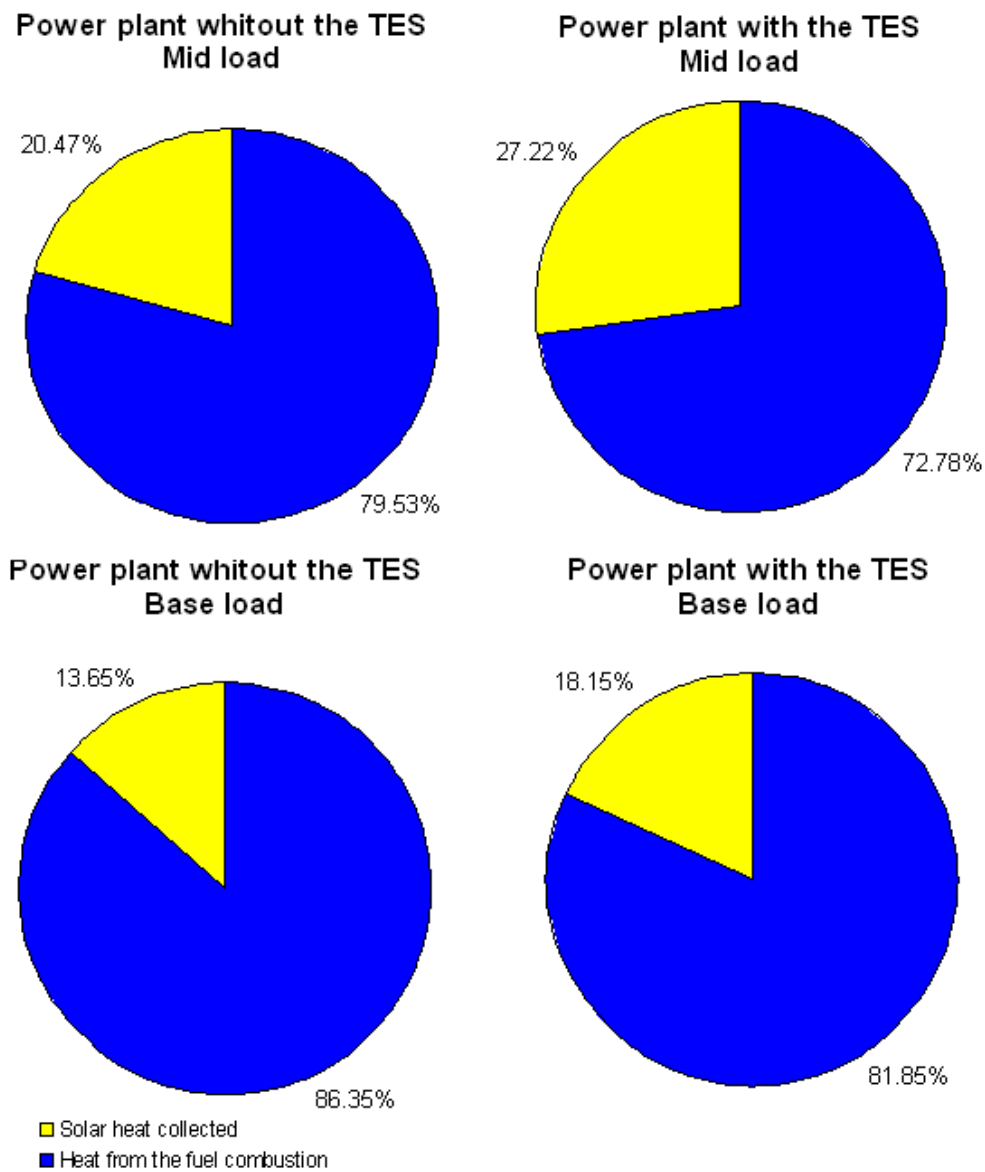


Figure 6.6: Average annual solar share for the power plant with and without TES.

As can be seen in the chart, with the addition of the storage, if the plant is operated as a mid load plant, the annual average solar share increases of 32%, passing from 20.47% to 27.22%. Instead, in case of operating the plant in base load, the increase of solar share is equal to 33%, passing from 13.65% to 18.15%.

6.2.2 Fuel saving

In order to make more attractive the hybrid solar-gas technology, it's necessary to reduce the fuel consumption so the operating cost are reduced too, resulting in a lower LCOE.

The parameter that is used to describe the fuel saving is the specific fuel consumption, which is the amount of fuel necessary to produce one kWh_{el}, as is shown in formula (6.2).

$$m_{fuel} = \frac{\dot{Q}_{tot} - \dot{Q}_{SF}}{P.C.I._{fuel} \cdot P_{el} \cdot \Delta t} \quad (6.2)$$

Where:

- \dot{Q}_{tot} is the thermal power required from the solar power plant.
- \dot{Q}_{SF} is the heat collected from the solar field.
- $P.C.I._{fuel}$ is the lower heating value of the fuel.
- P_{el} is the power output of the solar power plant.
- Δt is the operating time of the solar power plant.

In order to have a more precise value, the specific fuel consumption is calculated on a monthly basis, since, during the summer months, the air temperature is higher, resulting in a lower efficiency. The results are shown in figure 6.7.

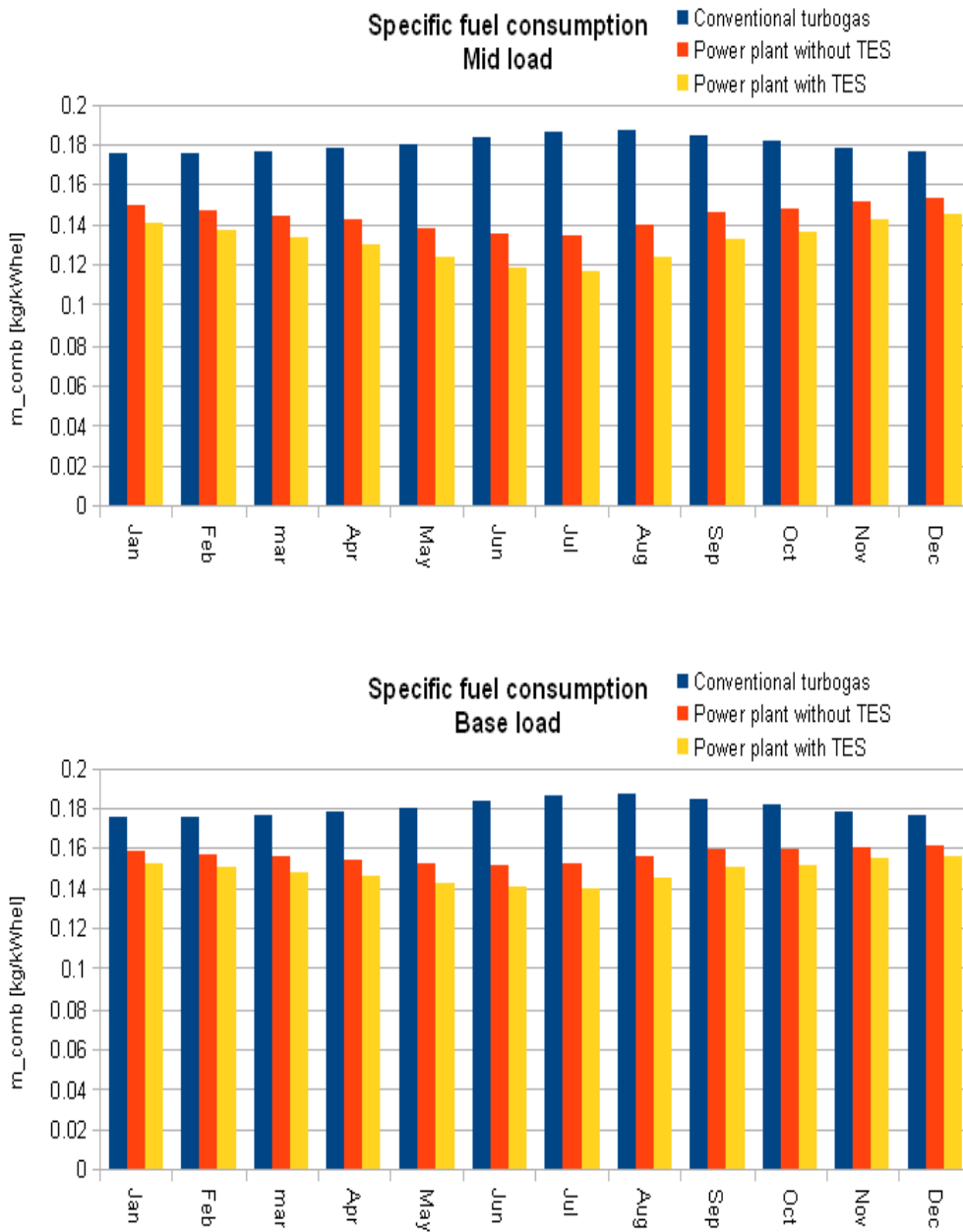


Figure 6.7: Specific fuel consumption in mid load and base load operations for the three reference plants.

As can be seen in the chart above, the implementation of the storage system results in a decrease of the specific fuel consumption, in particular during the summer months, when the solar irradiation is higher.

In more detail, if the plant is operated in mid load, a reduction of fuel consumption equal to 29% is achieved passing from a conventional turbogas power plant to hybrid solar-gas power plant and an additional 4% of reduction is added if a TES system is installed into the power plant, resulting in a total fuel consumption reduction of 33%.

If the power plant is operated in base load, the fuel consumption reduction is lower, since during the night the electrical power is produced only from the fuel combustion. In this case the fuel consumption reduction, in comparison to the conventional gas turbine power plant, is equal to 13.5% for the solar power plant without the TES system and to 18% for the solar power plant with the TES system.

6.2.3 Carbon dioxide emissions reduction

A reduction of fuel consumption allows another advantage that is the reduction of carbon dioxide emissions, since a lower quantity of natural gas is burned.

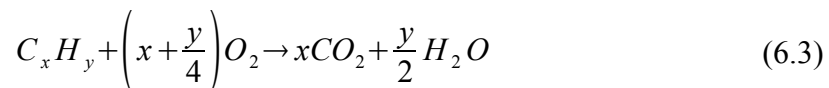
Generally, natural gas is composed of hydrocarbons (for example methane, ethane, propane) and inert gases such as nitrogen and carbon dioxide.

The typical molar composition of natural gas is given in table 6.1.

Table 6.1: Composition of natural gas[68].

Component	mol. %
Methane (CH ₄)	95.0
Ethane (C ₂ H ₆)	2.5
Propane (C ₃ H ₈)	0.5
Nitrogen (N ₂)	1.3
Carbon dioxide (CO ₂)	0.7

Assuming that the natural gas combustion is complete and that the production of nitrogen oxides is neglected, the equation of natural gas combustion can be written as formula (6.3).



The specific carbon dioxide emissions are calculated as the quantity of CO₂ emitted for producing one MWh_{el} and the results are reported on figure 6.8.

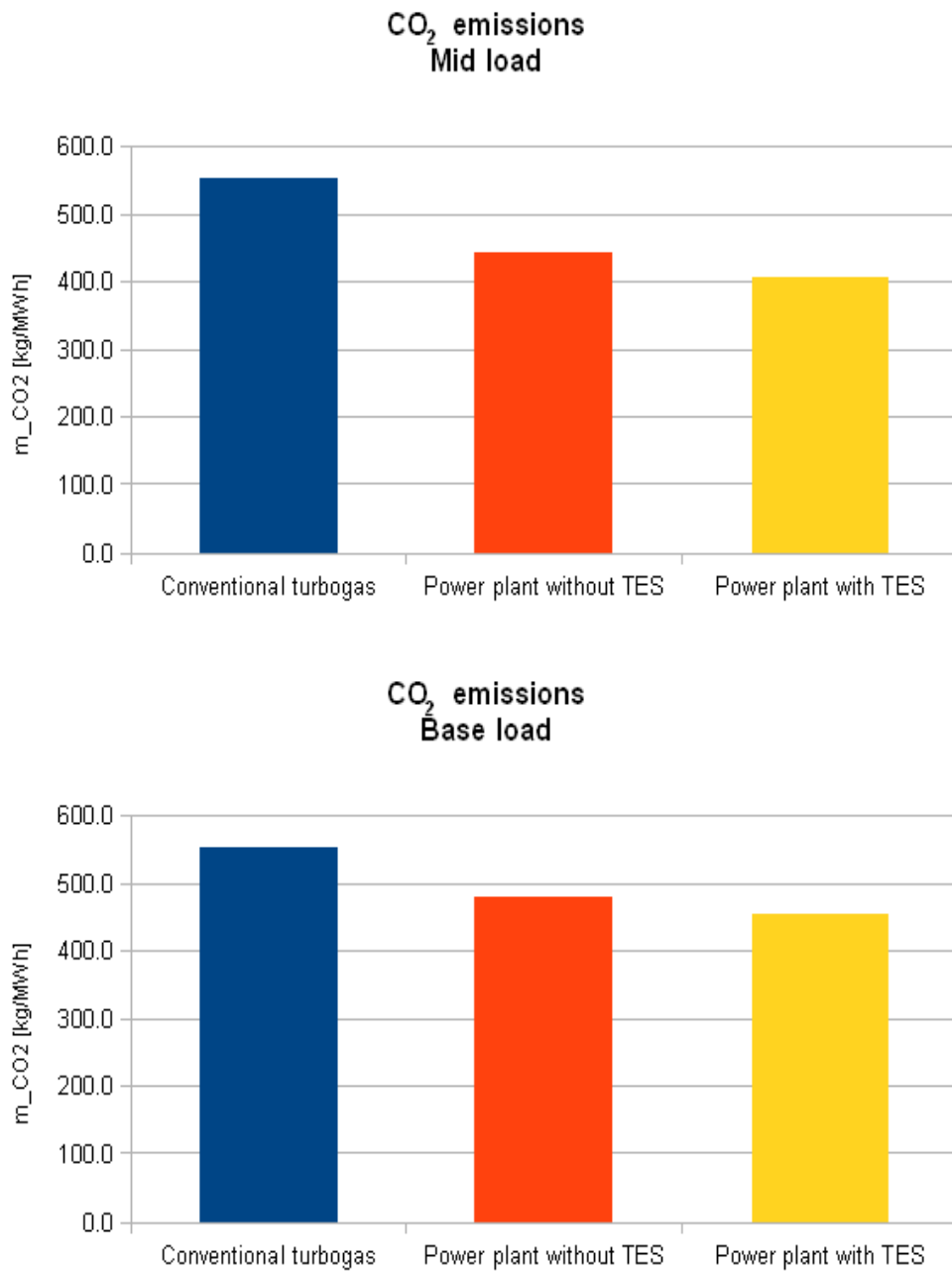


Figure 6.8: Specific CO₂ emissions in mid load and base load operations for the three reference plants.

For a conventional gas turbine power plant the carbon dioxide emissions are equal to 553 kg/MWh_{el} in both mid load and base load operations. Instead, for a hybrid solar-gas power plant, the carbon dioxide emissions are equal to 442

kg/MWh_{el} in mid load operations and 480 kg/MWh_{el} in base load operations, with a reduction equal to 20% and 13% respectively. If the designed thermal energy storage is added to the hybrid solar-gas power plant the carbon dioxide emissions are reduced to 404 kg/MWh_{el} in mid load operations and 454 kg/MWh_{el} in base load operations, which means a reduction of about 27% and 18% in comparison to the conventional gas turbine power plant. However, the carbon dioxide emissions may be further reduced if sustainably derived biogas or syngas are used instead of natural gas as fuel.

6.3 Storage behavior during solar transients

The solar power plant is designed to work at nominal conditions with a clear sky, but it might suddenly become cloudy, so the solar irradiation may be lower than expected and the solar receiver may not be able to heat the air flow.

In this case the air flow may bypass the solar tower and enter into the combustion chamber or enter into the TES where is heated at a temperature of about 850 °C thanks to the thermal energy previously stored. This last case is preferable because the combustion process is more stable (since the air temperature at the combustion chamber inlet is constant) and the fuel consumption doesn't increase.

Since the reduction of solar radiation could happen at any time of the day, it's necessary to study the storage response to solar transients that happen after different charging time. To do that it's necessary to simulate the charging and discharging processes on the LegoPC, which scheme is shown in figure 6.9.

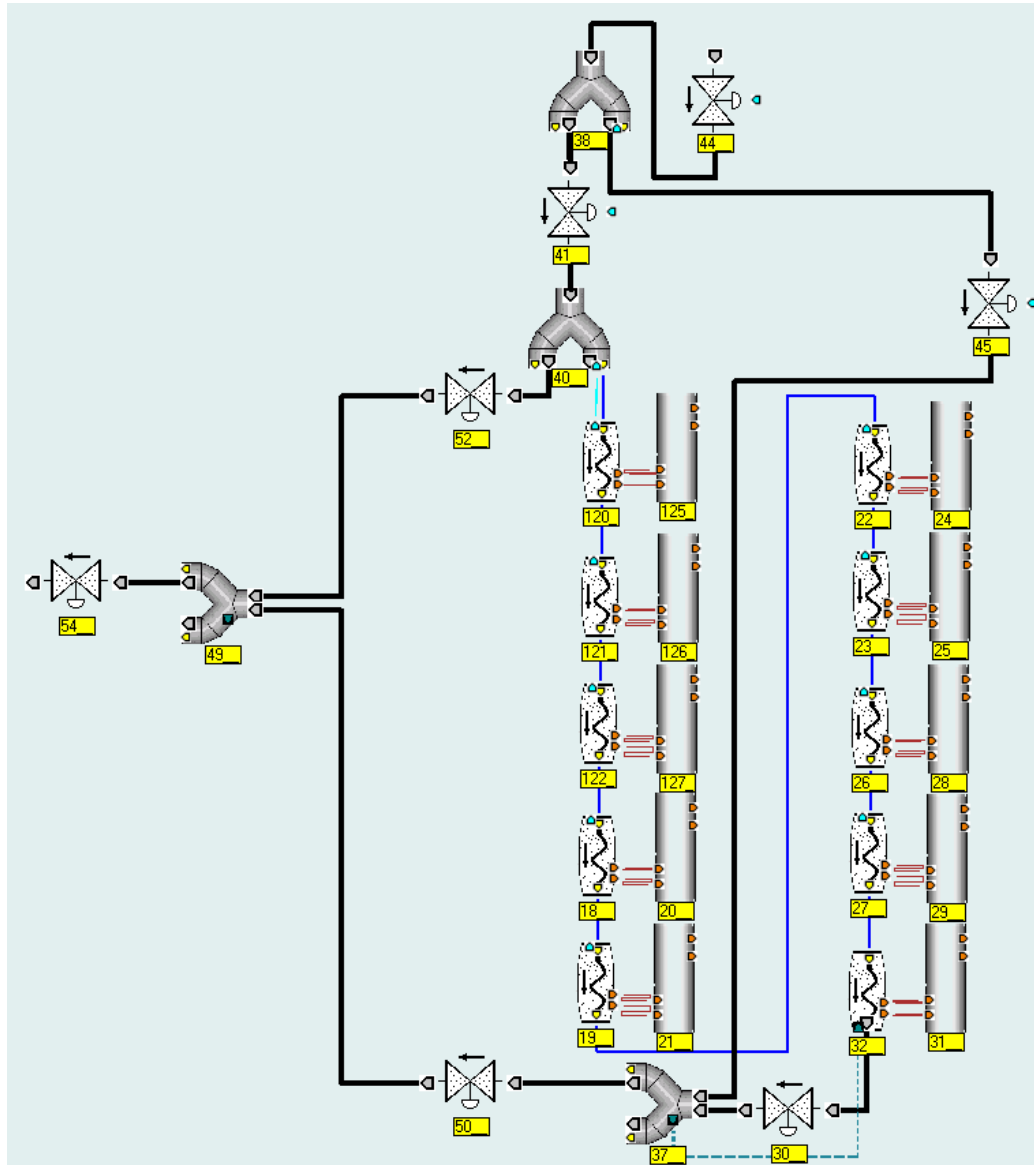


Figure 6.9: Scheme of the storage configuration used on the LegoPC software for simulating the charging and discharging processes.

Referring to the scheme of figure 6.9, on the LegoPC model the storage consists of ten PGP0 modules connected in series which simulate the air behavior through the storage channels and ten META modules, which simulates the behavior of the ceramic material, each linked to its corresponding PGP0 module. The air flow enters into the system through valve44 and, when the storage is operated in charging mode, valve45 and valve52 are closed while valve50 and valve41 are open, so the air flows into the storage through block120 and exit from the storage from block32. In this case the air flow at the inlet is equal to

39.16 kg/s with a temperature of 850 °C. The ceramic material temperature is equal to 450 °C, because it's assumed that the storage has been completely deployed the day before.

When the solar radiation is reduced, the storage, which is not completely charged, is used to heat the air at the compressor outlet. The air flow must be inverted, so, at the storage inlet, the cold air is in contact with the cold zone of the storage and, at the storage outlet, the hot air is in contact with the hot zone of the storage, otherwise, if there's no flow inversion, the air flow is heated by the hot inlet zone, but it's chilled by the cold outlet zone, so the air temperature at the storage outlet is lower. Moreover, if the air flow is inverted, in each section of the storage the temperature difference between the air flow and the ceramic material is reduced, resulting in an increase of the thermal exchange efficiency.

To invert the air flow on the LegoPC scheme, it's necessary to close valve41 and valve50 and open valve45 and valve52, so the air flows into the storage through block32 and exit from the storage from block120. The valves are opened and closed at the same time, in order to maintain the storage pressurized, with an opening/closing time of about five seconds. The air temperature at the storage outlet is detected at the outlet of valve52.

The simulation test consists in starting the charging process, stopping it after a certain time interval, inverting the air flow circulation and starting the discharging process. This test is made four times, with a start of the discharging process after the complete charging process and after one hour and a half, after three hours and after four hours and a half from the beginning of the discharging process.

6.3.1 Storage discharge after a complete charge

This is the most common case, since it happens when the storage is used to extend the solar operation of the power plant beyond the sunny hours or when the solar transient happens after 15 o'clock.

After six hours from the beginning of the charging process the air flow is inverted and the inlet conditions are changed. The air temperature at the storage outlet in function of the discharging time is shown in figure 6.10.

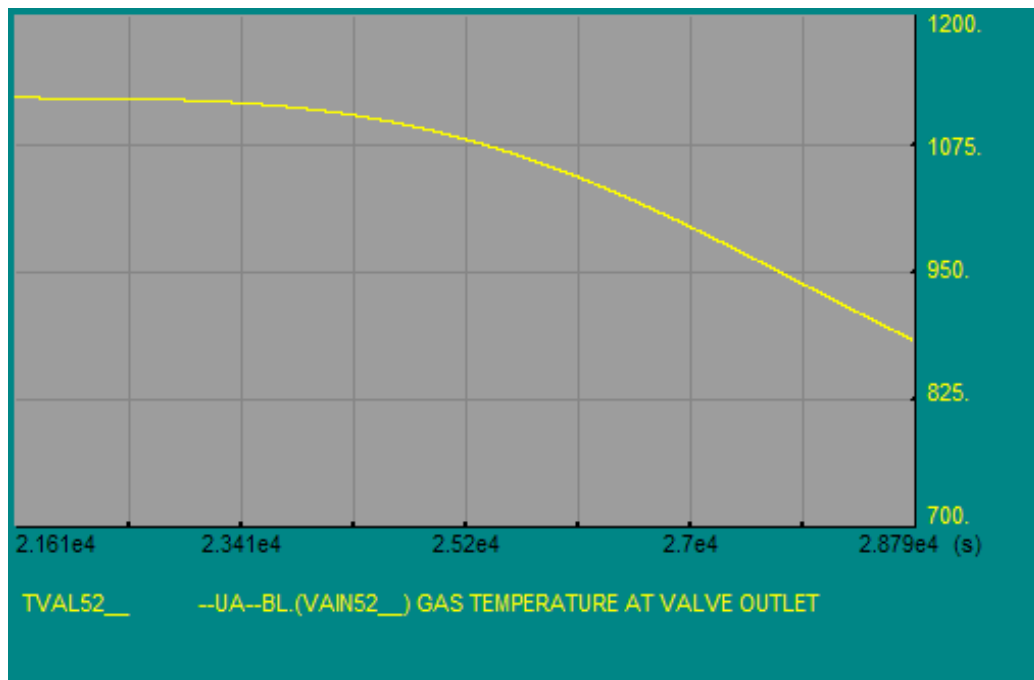


Figure 6.10: Air temperature (measured in Kelvin) at the storage outlet during the discharging process, starting from a completely charged storage.

As can be seen from the chart, an air outlet temperature of about 850 °C is ensured for half an hour, which means that the temperature at the combustion chamber inlet doesn't change significantly during this period.

After one hour from the beginning of the discharging process the air temperature at the storage outlet is decreased to 800 °C. This means that the combustion chamber must increase the fuel injected in order to maintain the air temperature at the turbine inlet steady, but the storage is still used since the solar contribution is high.

Finally, after two hours, the air temperature at the storage outlet is about 600 °C, since the storage is almost completely deployed. Now the solar contribution to the electricity production is very low and the air may bypass the storage and the solar tower and enter directly into the combustion chamber. In this case the solar contribution is zero, but the cycle efficiency is higher since the pressure drop of the storage channels are avoided.

6.3.2 Storage discharge after three quarters of the charge

In this case the solar transient happens between 13:30 and 15 o'clock, when the storage charging process is almost finished.

After four hours and a half from the beginning of the charging process the air flow is inverted and the inlet conditions are changed. The air temperature at the

storage outlet in function of the discharging time is shown in figure 6.11.

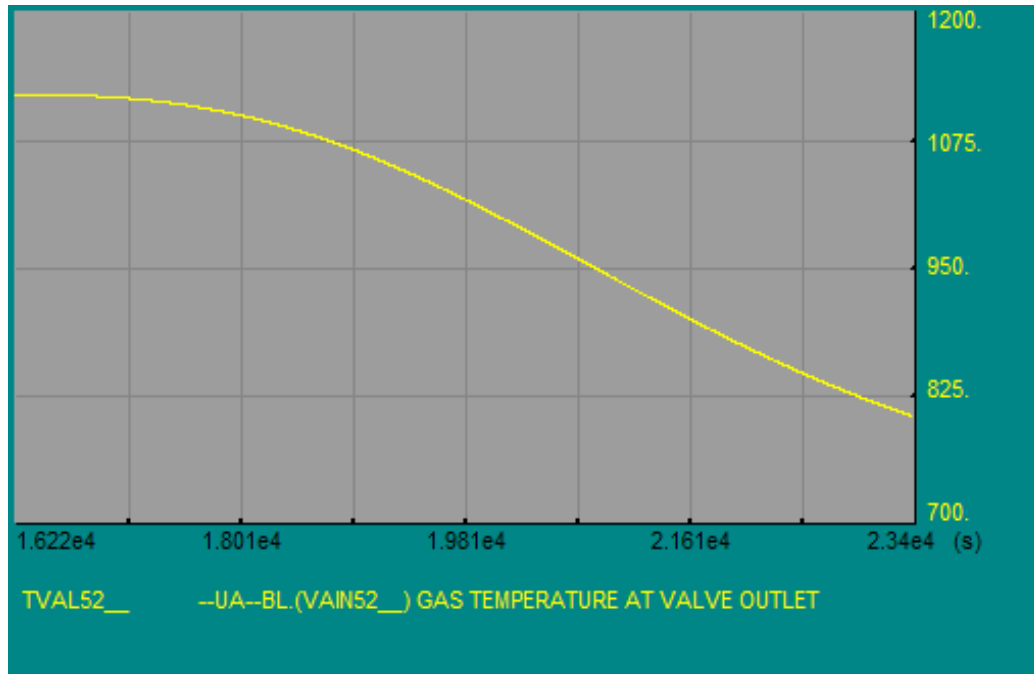


Figure 6.11: Air temperature (measured in Kelvin) at the storage outlet during the discharging process, starting from a storage that has been charged for three quarters of the nominal charging time.

In comparison to the previous case, now the period in which the air outlet temperature is about 850 °C is reduced. More in particular, an air outlet temperature of 850 °C is ensured only for 900 seconds, which is half of duration of the previous case.

Moreover, in this case the temperature reduction during the time is quicker and, after one hour from the beginning of the discharging process, the air temperature at the storage outlet is equal to 750 °C, so the fuel consumption is increased for maintaining the turbine inlet temperature steady, but the solar contribution is still significant.

The air temperature, after two hours of discharging, is about 550 °C, which is a low temperature for the combustion chamber inlet, but still allows to deploy the thermal energy previously stored. Otherwise, as in the previous case, the air flow may bypass the storage and the solar tower and enter directly into the combustion chamber. In this last option the increase of the cycle efficiency could result in a reduction of fuel consumption since the temperature increase due to the storage is quite low.

6.3.3 Storage discharge after half of the charge

Another critical case is when the solar transient happens after noon, which is the time of day when the grid demand is the highest.

After three hours from the beginning of the charging process the air flow is inverted and the inlet conditions are changed. The air temperature at the storage outlet in function of the discharging time is shown in figure 6.12.

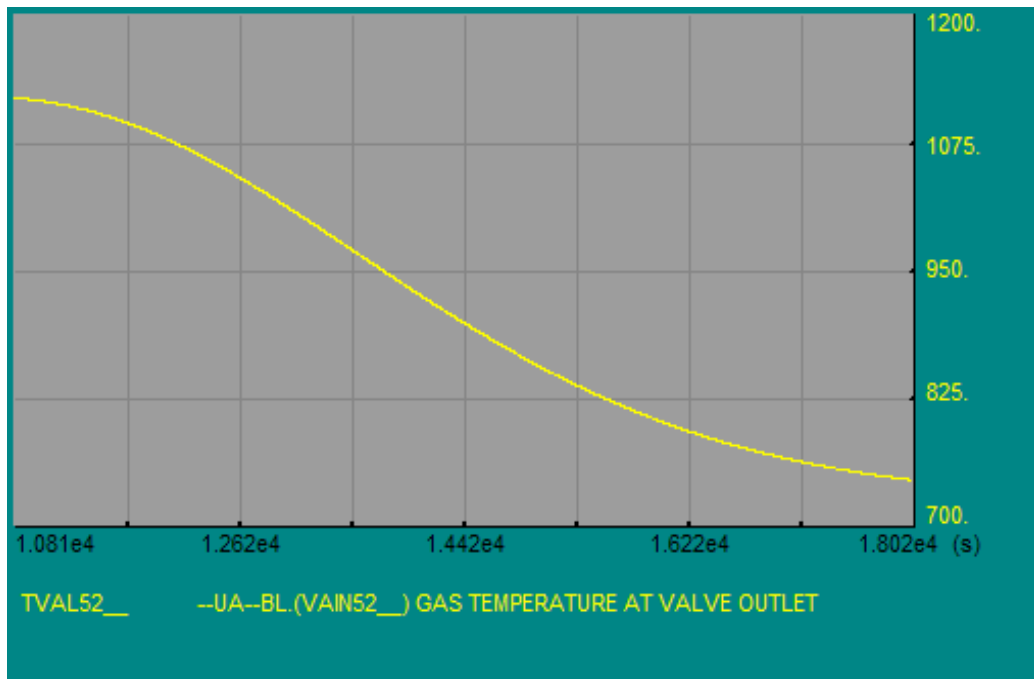


Figure 6.12: Air temperature (measured in Kelvin) at the storage outlet during the discharging process, starting from a storage that has been charged for half of the nominal charging time.

In this case the charging process is interrupted in the middle, so there's not enough thermal energy stored to ensure the heating of the air flow for two hours. In particular, the air temperature at the storage outlet is equal to 850 °C for few minutes, so the storage may cover only brief solar transients, for example in case of clouds moving.

In comparison to the other cases, here the air outlet temperature reduction during the time is quicker and, after one hour from the beginning of the discharging process, the air temperature at the storage outlet is equal to 620 °C, and the solar contribution starts to become negligible.

After two hours from the beginning of the discharging process, the air temperature is slightly higher than 450 °C, which is the air temperature at the compressor outlet, so there's no reason to sent the air into the storage, since it

cannot heat the air, but the pressure drop along the channels decreases the cycle efficiency. In this case it's compulsory to bypass the storage and the solar tower and make the air flow enter directly into the combustion chamber, so the solar power plant works like a conventional gas turbine power plant.

6.3.4 Storage discharge after a quarter of the charge

This is the most critical case, since the charging process is just begun and the solar transient happens one hour and a half before noon.

The charging process is stopped after one hour and a half from its beginning and, as in the other cases, the air flow is inverted with a change of the inlet conditions. The air temperature at the storage outlet in function of the discharging time is shown in figure 6.13.

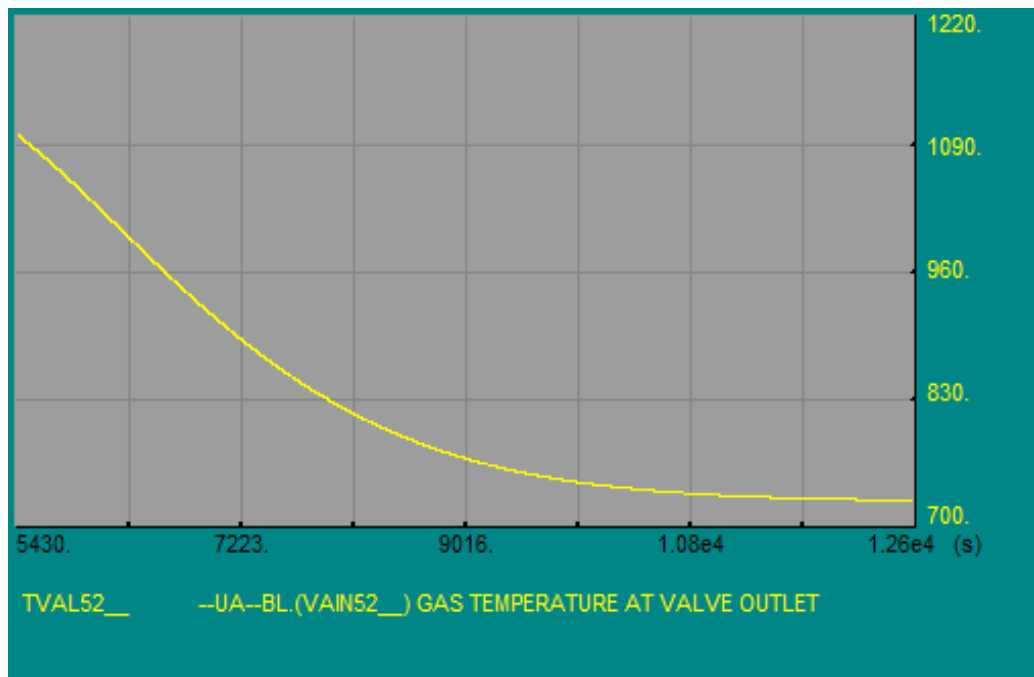


Figure 6.13: Air temperature (measured in Kelvin) at the storage outlet during the discharging process, starting from a storage that has been charged for half of the nominal charging time.

As can be seen from the chart, the charging process isn't long enough to heat the ceramic material, of which the storage is composed of, at a temperature equal to 850 °C. This fact limits the air outlet temperature, that, at the beginning of the discharging process, is equal to 820 °C and decreases rapidly.

In particular, after one hour from the beginning of the discharging process, the air outlet temperature is almost equal to its temperature at the compressor outlet

so the storage is unable to heat the air and must be bypassed.

In this case the storage performance is the worst, since the air outlet temperature decreases rapidly during the first minutes of storage operation, so, if the charging process is just begun and a solar transient lowers the solar radiation, it's preferable to bypass the storage, unless the solar transient is really quick or there's thermal energy into the storage that wasn't used the previous day.

Conclusions and future developments

Purpose of this master thesis work is the design of a high temperature thermal energy storage for a hybrid solar-gas power plant that is installed at latitude 35°N. To verify the dynamic behavior of the designed TES system, a model of the storage has been created with LegoPC software and the transient analysis has been carried out for different operating conditions.

After having introduced all the various technologies for producing electricity from the sun and the existing solar power plant, the advantages and drawbacks of using a solar driven Brayton cycle have been analyzed. In particular the advantages consist in a high cycle efficiency, in reduced start-up and load ramping times, in the possibility of cover solar transients with an addition of fuel combustion and in a low water consumption, so this kind of power plant can be installed in arid zones where the solar irradiation is the highest. Since air must be used as heat transfer medium, there's no limit on the maximum temperature that can be reached on the solar receiver, but, because of the air low density, it's required the use of volumetric receivers where the air temperature exceeds 600 °C, in order to contain the receiver surface and its cost. Moreover, this technology is quite unreliable, since only few projects have been made operative.

In order to have a scenario in which the thermal energy storage should work, the reference plant has been designed. The Siemens SGT-800 has been chosen as gas turbine, for a power output of 47 MWel and an air temperature at the compressor outlet equal to 450 °C. The solar receiver chosen is the REFOS receiver, which has been tested on the SOLGATE project in Almeria, and, supposed an air temperature at the receiver outlet equal to 850 °C, it consists of 84 tubular low temperature modules that are connected in series to 84 volumetric high temperature modules. About the solar field, a surrounding field configuration has been chosen, in order to contain the atmospheric losses, and a reflecting area of 110,250 m² has been calculated, which consists of 782 heliostates each with a reflecting surface area equal to 141 m².

Once established the boundary conditions in which the storage will work, the technologies that are currently used or studied to store thermal energy in concentrated solar power plant have been analyzed. The most common heat storage media are the molten salts, especially a mixture composed of 40% by weight KNO₃ and 60% by weight NaNO₃, thanks to their low price and their maximum temperature that they can reach. Other existing storage media are the thermal oil, whose use is limited by its low maximum operating temperature and

Conclusions and future developments

its high flammability, and steam, but it requires high storage volume due to its low density. Storage media that have been tested or studied, but which are not yet operational, are phase change materials (PCMs), but they are more suited to work with a Rankine cycle since the heat exchange is isothermal, concrete, whose low thermal conductivity implies long charging time, and thermochemical storage, which consists in a chemical reaction that absorbs thermal energy and releases it with the reverse reaction, but the rapid degradation of the storage materials, caused by poisoning and sintering of the catalysts, doesn't allow its application. However, the maximum operating temperature of all these technologies is limited to 550 °C or less, so they aren't suitable for the storage under consideration.

So, it was necessary to consider new storage media that can reach temperatures above 850 °C. In particular, carbonate salts could be a feasible option, but their high melting point implies that the heat is transferred when they're in solid phase or phase changing, so they have been discarded. Liquid metals are further options, for example liquid sodium, which has a high thermal conductivity and a low melting point (98 °C) but it's also highly flammable, liquid lead, which has a high density and a high heat capacity but it has a high melting point (327 °C) and black oxides could be created, and a lead bismuth eutectic (LBE), which has the same thermal properties of the liquid lead, but with a low melting temperature (124 °C). The last option considered was the use of a direct-contact regenerative storage made of ceramic material, such as silicon carbide, so the expensive pipes made of high temperature resistant steel are not necessary, resulting in a cost reduction and in an improvement of the heat exchange, since the thermal resistance of the pipe is absent. A comparison between these materials resulted in the choice of silicon carbide as storage material, thanks to its high volumetric heat capacity (2-3 times higher than the others candidate materials), which results in a low specific volume, and its good thermal conductivity, which is slightly lower than the sodium one.

Finally, a model of the storage has been created with the LegoPC software, in order to optimize the geometrical parameters of the storage. To extend the operation of the solar plant for two hours after the sunset, in order to produce electricity when the grid demand is still high, a storage volume of 265.09 m³ has been selected, which correspond to a mass of ceramic material equal to 842,994 kg. An air flow of 39.16 kg/s is used to heat the storage and, at the storage outlet, it's recirculated into the solar receiver, resulting in a charging time of six hours and in a 192 kW of fan power consumption, which is required for overcoming the pressure drops on the storage and on the solar tower. After that, the geometrical parameters of the storage have been analyzed, in particular the number of channels in which the air flows, their diameter and their length. All these parameters have been correlated and optimized, in order to have a good

heat exchange coefficient and a low pressure drop, so the storage is made of 12479 channels, each with a 0.015 m of diameter and a length equal to 30 m. Moreover, a scheme of the thermal insulation has been made and, in the worst possible scenario (storage fully charged, inactive for 24 hours and absence of solar radiation) a thermal efficiency of 96% has been calculated, which is consistent with the data of the existing TES systems.

Lastly, the performances of the solar power plant with the TES system have been calculated. In particular, the addition of the TES system increases the solar share of the solar power plant (from 20.47% to 27.22% in mid load operation and from 13.65% to 18.15% in base load operation) reduces the specific fuel consumption (from 0.144 kg/kWh_{el} to 0.132 kg/kWh_{el} in mid load operation and from 0.156 kg/kWh_{el} to 0.148 kg/kWh_{el} in base load operation) and holds the CO₂ emissions (from 442 kg/kWh_{el} to 404 kg/kWh_{el} in mid load operation and from 480 kg/kWh_{el} to 454 kg/kWh_{el} in base load operation, which is a reduction of 27% and 18% in comparison to a conventional gas turbine power plant). Moreover it's been simulated the storage behavior during solar transients. In particular, if the solar transient happens after a full cycle of charge, it's ensured an air outlet temperature equal to 850 °C for half an hour, but, if the solar transient happens at the beginning of the charge cycle, the air outlet temperature is considerably lower, so it may be appropriate to bypass both the solar receiver and the storage and make the air flow enter directly into the combustion chamber.

For the future it's expected an increase of the maximum receiver operating temperature (the SOLGATE project achieved a temperature of 959 °C), so the annual solar share can be further increased and the fuel consumption reduced, and the development of more reliable solar receivers, consisting of a cavity with several tubular receiver panels. Moreover, the development of dry cooling systems will allow the installation of a recuperative steam cycle that will increase the efficiency of the solar power plant, resulting in a reduction of the electricity cost. The adoption of sustainable fuels, such as biogas, will help the reduction of the carbon dioxide emissions. About the TES system, it's expected an extension of its operating time and the adoption of cheaper storage materials in order to contain its cost despite the increase of its volume.

List of acronyms

CLFR	Concentrated Linear Fresnel Reflector
CSP	Concentrating Solar Power
DISS	Direct Solar Steam
DNI	Direct Normal Irradiation
DSG	Direct Steam Generation
EPIA	European Photovoltaic Industry Association
FLOX	Flameless Oxidation
HPC	High Performance Concrete
HSGTTP	Hybrid Solar-Gas Turbine Power Plant
HTF	Heat Transfer Fluid
IEA	International Energy Agency
LBE	Lead Bismuth Eutectic
LCOE	Levelized Cost of Electricity
LPC	Lean Premixed Combustion
MENA	Middle East and North Africa
PCM	Phase Change Material
PEGASE	Production of Electricity with Gas Turbine and Solar Energy
PSA	Plataforma Solar de Almeria
RES	Renewable Energy Sources
RTO	Regenerative Thermal Oxidizer
SCOT	Solar Concentrator Off Tower
SEGS	Solar Electric Generating system
SOLGATE	Solar Hybrid Gas Turbine Electric Power System
SOLUGAS	Solar Up-Scale Gas Turbine System
STPP	Solar Thermal Power Plant
TES	Thermal Energy Storage

Bibliography and references

- [1] “Advantages and Disadvantages of Wind Energy” Wind & Hydropower Technologies Program. 30 Aug. 2005 U.S. Department of Energy. 19 Dec. 2005.
- [2] International Energy Agency (IEA), “Key World Energy Statistics”, 2011.
- [3] International Energy Agency (IEA), “World Energy Outlook”, 2011.
- [4] B. Sills, “Solar may produce most of World's power by 2060, IEA says”, Bloomberg, 29 August 2011.
- [5] European Photovoltaic Industry Association, “Global Market Outlook for Photovoltaics until 2016”, May 2012.
- [6] W. B. Stine, M. Geyer, “Power from the Sun”, 2001.
- [7] A. Akbarzadeh, J. Andrews, P. Golding, “Solar Pond Technologies: a Review and Future Directions”, 2005.
- [8] J. Schlaic, R. Bergermann, W. Schiel, G. Weinrebe, “Design of Commercial Solar Updraft Tower Systems—Utilization of Solar Induced Convective Flows for Power Generation”, Journal of Solar Energy Engineering, 2005.
- [9] European Commission, “European Research on Concentrated Solar Thermal Energy”, 2004.
- [10] Estela Solar “Solar Thermal Electricity 2025”, A.T. Kearney, June 2010.
- [11] H. Mitavachan, J. Srinivasan “Is land really a constraint for the utilization of solar energy in India?”, Current Science, Vol. 103, No. 2, 25 July 2012.
- [12] Estela Solar, “Solar Power from Europe's Sun Belt”, June 2009.
- [13] International Energy Agency (IEA), “Concentrating Solar Power, Technology Roadmap”, 2010.
- [14] P. Schwarzbozl, R. Buck, C. Sugarmen, A. Ring, M. J. M. Crespo, P. Altwegg, J. Enrille, “Solar Gas Turbine Systems: Design, Cost and Perspectives”, ScienceDirect, November 2005.
- [15] C. Björkqvist, “Hybrid Gas Turbine for the Efficient Use of Concentrated Solar Energy”, 21 October 2011.
- [16] C. Belli, P. Chizzolini, “Conversione dell'Energia”, 2009.
- [17] European Commission -Directorate-General for Research, “SOLGATE Solar Hybrid Gas Turbine Electric Power System”, 2005.
- [18] E. Hanson, “New Landmark Solar Flower Tower by Haim Dotan Shapes New Vision for Solar Energy”, 22 June 2009.
- [19] Z. Rosenzweig, “AORA: Hybrid Tulip tower system to be switched on in Spain”, Concentrated Solar Power Today, 27 January 2012.
- [20] A. Ferrière, “The PEGASE Project”, International Scientific Journal for Alternative Energy and Ecology N.6, 2008.
- [21] Siemens, “SGT-800 Industrial Gas Turbine Brochure”.

- [22] J. Sinai, C. Sugarmen, U. Fisher, “Adaptation and Modification of Gas Turbines for Solar Energy Applications”, Volume 5: Turbo Expo 2005 p. 87-94, 2005.
- [23] B. Hoffschmidt, “Vergleichende Bewertung Verschiedener Konzepte Volumetrischer Strahlungsempfänger”, DLR Forschungsbericht pp. 97–35, 1997.
- [24] T. Fend, “High Porosity Materials as volumetric receivers for solar energetics”, *Optica Applicata*, Vol.XL, No. 2, 2010.
- [25] J. S. Estrada, “Solar Application of TopSpool Gas Turbine Concept”, Master of Science Thesis, 2011
- [26] L. Crespo, F. Ramos, F. Martinez, “Question and Answers on Solar Central Receiver Plant Design by NSPOC”, *Solar Paces*, 2011.
- [27] “Assessment of Parabolic Through and Power Tower Solar Technology Cost and Performance Forecasts”, Sargent & Lundy LLC Subcontractor Report, NREL/SR-550 -34440, October 2003.
- [28] G. J. Kolb, S. A. Jones, M. W. Donnelly, D. Gorman, R. Thomas, R. Davenport, R. Lumia, “Heliostat Cost Reduction Study”, Sandia Report, June 2007.
- [29] A. Kribus, R. Zaibel, D. Carey, A. Segal, J. Karni, “A Solar-Driven Combined Cycle Power Plant”, *Solar Energy* Vol. 62, No. 2, pp. 121–129, 1998.
- [30] S. Giuliano, R. Buck, S. Eguiguren, “Analysis of Solar-Thermal Power Plants With Thermal Energy Storage and Solar-Hybrid Operation Strategy”, *Journal of Solar Energy Engineering*, August 2011.
- [31] R. Dracker, K. Riffelmann, “Integrated Thermal Storage for Concentrating Solar Power”, *Integrated Energy Policy Report Workshop*, July 2008.
- [32] D. Laing, W. D. Steinmann, M. Fib, R. Tamme, T. Brand, C. Bahl, “Solid Media Thermal Storage Development and Analysis of Modular Storage Operation Concepts for Parabolic Trough Power Plants”, *Journal of Solar Energy Engineering*, February 2008.
- [33] Pilkington Solar International GmbH, “Survey of Thermal Storage for Parabolic Trough Power Plants”, September 2000.
- [34] M. Romero, R. Buck, J. E. Pacheco, “An Update on Solar Central Receiver Systems, Projects, and Technologies”, *Journal of Solar Energy Engineering*, May 2002.
- [35] Department of Energy San Francisco Operations Office Accident Report, “Report of the Committee Investigating the Thermal Storage Tank Fire at Solar One Generating Station August 30, 1986”, SAN-86-03, 1986.
- [36] M.A. Geyer, “Thermal Storage for Solar Power Plants”, Ch. 6 of C.-J. Winter, R.L. Sizmann, L.L. Vant-Hull (Eds.), “Solar Power Plants”, Springer-Verlag, New York, 1991.

- [37] J. E. Pacheco, R. Gilbert, “Overview of Recent Results of the Solar Two Test and Evaluations Program, Renewable and Advanced Energy Systems for the 21st Century”, Proceedings of the 1999 ASME International Solar Energy Conference, Maui, HI, April 11-14, 1999.
- [38] Pilkington Solar International GmbH, “Survey of Thermal Storage for Parabolic Trough Power Plants”, September 2000.
- [39] S. St. Laurent, “Thermocline Storage Test for Large Scale Solar Thermal Power Plants”, September 2000.
- [40] O. Ercan Ataer, (2006), STORAGE OF THERMAL ENERGY, in Energy Storage Systems, [Ed. Yalcin Abdullah Gogus], in Encyclopedia of Life Support Systems (EOLSS), Developed under the Auspices of the UNESCO, Eolss Publishers, Oxford, UK, [<http://www.eolss.net>].
- [41] G. Glatzmaier, “Summary Report for Concentrating Solar Power Thermal Storage Workshop”, May 2011.
- [42] Deutsches Zentrum für Luft und Raumfahrt, “MENA Regional Water Outlook; Part II: Desalination Using Renewable Energy”, February 2011.
- [43] Solúcar, “10 MW Solar Thermal Power Plant for Southern Spain, Final Technical Progress Report”, November 2006.
- [44] H. Michels, E. Hahne, “Cascaded Latent Heat Storage Process Heat, Proc. 8th Int. Symp. Solar Thermal Concentrating Technologies”, Köln, Germany, 1996.
- [45] W. D. Steinmann, D. Laing, R. Tamme, “Latent Heat Storage Systems for Solar Thermal Power Plants and Process Heat Applications”, Journal of Solar Energy Engineering, May 2010.
- [46] W. D. Steinmann, R. Tamme, “Latent Heat Storage for Solar Steam Systems”, Journal of Solar Energy Engineering, February 2008.
- [47] T. Bauer, R. Tamme, M. Christ and O. Öttinger, 2006, “PCM—Graphite Composites for High Temperature Thermal Energy Storages”, ECOSTOCK 2006, Stockton, NJ, May 31–June 2.
- [48] A. Steinfeld, R. Palumbo, “Solar Thermochemical Process Technology”, pp.237-256, 2001.
- [49] A. Luzzi, K. Lovegrove, E. Filippi, H. Fricker, M. Schmitz-Goeb and M. Chandapillai, “Base-load solar thermal power using thermochemical energy storage”, 1999.
- [50] D. Laing, W. D. Steinmann, P. Viebahn, F. Gräter, C. Bahl, “Economic Analysis and Life Cycle Assessment of Concrete Thermal Energy Storage for Parabolic Trough Power Plants”, Journal of Solar Energy Engineering, November 2010.
- [51] Solar Millennium AG, “The parabolic trough power plants Andasol 1 to 3”, 2008.
- [52] D. A. Brosseau, P. F. Hlava, M. J. Kelly, “Testing Thermocline Filler Materials and Molten-Salt Heat Transfer Fluids for Thermal Energy Storage Systems Used in Parabolic Trough Solar Power Plant”, July 2004.

- [53] J. I. Ortega, J. I. Burgaleta, F. M. Téllez, “Central Receiver System Solar Power Plant Using Molten Salts as Heat Transfer Fluid”, *Journal of Solar Energy*, May 2008.
- [54] P. K. Falcone, “A Handbook for Solar Central Receiver Design”, December 1986.
- [55] J. Pacheco, S. Showalter, W. Kolb, “Development of a Molten-Salt Thermocline Thermal Storage System for Parabolic Trough Plants”, *Journal of Solar Energy*, Special Issue: Solar Thermal Power, Vol. 124, May 2002.
- [56] Betchel Corporation, “Investigation of Thermal Storage and Steam Generator Issues”, August 1993.
- [57] A. Miliozzi, G. M. Giannuzzi, “Studio e Analisi Critica dei sistemi di accumulo termico a media temperatura”, 2008.
- [58] G. Glatzmaier, “Developing a Cost Model and Methodology to Estimate Capital Costs for Thermal Energy Storage”, December 2011.
- [59] C. Turchi, “Parabolic Through Reference Plant for Cost Modeling with the Solar Advisor Model (SAM)”, NREL Technical Report: NREL/TP-550-47605.
- [60] J. K. Fink, L. Leibowitz, “Thermodynamic and Transport Properties of Sodium Liquid and Vapor”, January 1995.
- [61] J. P. Kotzé, T. W. von Backström, P. J. Erens, “NaK as a primary heat transfer fluid in thermal solar power installations”, 22 May 2012.
- [62] “Handbook on Lead-bismuth Eutectic Alloy and Lead Properties, Materials Compatibility, Thermal-hydraulics and Technologies”, 2007 edition.
- [63] R. G. Munro, “Material Properties of a Sintered α -SiC”, *Journal of Physics and Chemical Reference Data*, Vol. 26, No. 5, 1997.
- [64] R. Tamme, “German Contribution to the Implementation of CSP Technology”, CSP Conference, London 7 July 2009.
- [65] V. Casamassima, F. Parozzi, “Thermal-Hydraulic Models for Liquid Metal Cooling Circuits of Gen. IV Reactors”.
- [66] S. Zunft, M. Hänel, M. Krüger, V. Dreißigacker, F. Göhring, E. Wahl, “Jülich Solar Power Tower – Experimental Evaluation of the Storage Subsystem and Performance Calculation”, *SolarPaces 2010*.
- [67] R. Tamme, D. Laing, W. D. Steinmann, “Advanced Thermal Energy Storage Technology for Parabolic Trough”, 2003 International Solar Energy Conference Hawaii, 15-18 March 2003.
- [68] J. S. Gudmundsson, “Produced and Processed Natural Gas”, Department of Petroleum Engineering and Applied Geophysics – NTNU, 2010.